Coenzyme engineering of NAD(P)$^+$-dependent dehydrogenases

Rui Huang

Dissertation submitted to the faculty of

the Virginia Polytechnic Institute and State University

in partial fulfillment of the requirements for the degree of

Doctor of Philosophy

In

Biological Systems Engineering

Ryan S. Senger, Chair

Chenming Zhang

Jianyong Li

Justin R. Barone

November, 8th 2017

Blacksburg, Virginia

Keywords: coenzyme engineering, NAD(P) dependent dehydrogenases, directed evolution, high-throughput screening, biohydrogen, *in vitro* synthetic biology

Coenzyme engineering of NADP-dependent dehydrogenases

Rui Huang

Abstract

Coenzyme nicotinamide adenine dinucleotide (NAD, including the oxidized form--NAD^+ and reduced form--NADH) and the phosphorylated form--nicotinamide adenine dinucleotide phosphate (NADP, including $NADP^+$ and NADPH) are two of the most important biological electron carriers. Most NAD(P) dependent redox enzymes show a preference of either NADP or NAD as an electron acceptor or donor depending on their unique metabolic roles. In biocatalysis, the low enzymatic activities with unnatural coenzymes have made it difficult to replace costly NADP with economically advantageous NAD or other biomimetic coenzyme for catalysis. This is a significant challenge that must be addressed should *in vitro* biocatalysis be a viable option for the practical production of low-value biocommodities (i.e., biohydrogen). There is a significant need to first address the coenzyme selectivity of the NADP-dependent dehydrogenases and evolve mutated enzymes that accept biomimetic coenzymes. This is a major focus of this dissertation.

Establishment of efficient screening methods to identify beneficial mutants from an enzymatic library is the most challenging task of coenzyme engineering of dehydrogenases. To fine tune the coenzyme preference of dehydrogenases to allow economical hydrogen production, we developed a double-layer Petri-dish based screening method to identify positive mutant of the *Moorella thermoacetica* 6PGDH (*Moth*6PGDH) with a more than 4,278-fold reversal of coenzyme selectivity from $NADP^+$ to NAD^+. This method was also used to screen the

thermostable mutant of a highly active glucose 6-phosphate dehydrogenase from the mesophilic host *Zymomonas mobilis*. The resulting best mutant Mut 4-1 showed a more than 124-fold improvement of half-life times at 60ºC without compromising the specific activity. The screening method was further upgraded for the coenzyme engineering of *Thermotaga maritima* 6PGDH (*Tm*6PGDH) on the biomimetic coenzyme NMN^+. Through six-rounds of directed evolution and screening, the best mutant showed a more than 50-fold improvement in catalytic efficiency on NMN^+ and a more than 6-fold increased hydrogen productivity rate from 6-phosphogluconate and NMN^+ compared to those of wild-type enzyme. Together, these results demonstrated the effectiveness of screening methods developed in this research for coenzyme engineering of NAD(P) dependent dehydrogenase and efficient use of the less costly coenzyme in ivSB based hydrogen production.

Coenzyme engineering of NADP-dependent dehydrogenases

Rui Huang

General Audience Abstract

NADP and NAD are two of the most important electron carriers in cellular metabolism, and they play distinctive roles in anabolism and catabolism, respectively. Most NAD(P)-dependent dehydrogenases exhibit a strong preference for either NADP or NAD. This coenzyme preference, however, make it nearly impossible to replace the costly NADP with less costly NAD or biomimetic coenzymes in the biocatalysis application. How to engineer dehydrogenases through directed evolution and effective screening method to accept NAD or biomimetic coenzymes, is critical and the focus of this dissertation.

The use of *in vitro* synthetic biosystem (ivSB) to produce hydrogen form starch, is one of the most important *in vitro* synthetic biology projects, and it depends on NADP coenzyme. With other issues in this system solved, the efficient use of dehydrogenases along with low cost and stable coenzyme is the last obstacle to hydrogen production through industrial biomanufacturing. However, the 6-phosphogluconate dehydrogenase (6PGDH), one of the rate-limiting enzymes in this biosystem, exhibits a strong coenzyme preference for $NADP^+$. For producing low-cost hydrogen, the coenzyme engineering of this dehydrogenase is urgently required. Its activity with less costly NAD or biomimetic coenzymes must be improved. The establishment of an effective screening method is the most challenging task for coenzyme engineering of dehydrogenases. In this research, we developed a Petri-dish double-layer based screening method for coenzyme engineering of thermophilic 6PGDH for activity for NAD^+. This screening method was also used

to improve the thermostability of a highly active glucose 6-phosphate dehydrogenase from a mesophilic host, where the evolved mutant had a greatly improved thermostability without losing activity. The screening method was further upgraded to develop for coenzyme engineering on biomimetic coenzyme NMN^+. The engineered mutant showing a more than 50-fold increase in catalytic efficiency on NMN^+ was used to develop the first biomimetic coenzyme dependent electron transfer chain for hydrogen production. This screening method is suitable to change the coenzyme selectivity of series of NAD(P)-dependent redox enzymes and show great potential in improving other properties, such as thermostability, substrate scope and optimal pH, of different dehydrogenases. With this method developed, we can efficiently use the low cost stable coenzyme in the biocatalysis, and break the last obstacle to industrial biomanufacturing of hydrogen production.

Acknowledgement

First, I would like to express my sincere thanks to my advisor Professor Y.-H. Percival Zhang. You are the most far-sighted scientist I have met and exhibit incredible self-control ability which really impressed me. I would like to thank you for opening my mind and grading up the taste in research, and for teaching me tremendous knowledge, techniques and skills in experiments and project management. I am proud of being your student and I would try my best to carry forward the techniques we developed in the coenzyme engineering of dehydrogenases.

Secondly, I would like to thank my committee chair, Professor Ryan S. Senger. Your advices on my research and editing of my manuscript are the priceless gifts for me. I would like also thank my current committee members, Professor Justin R. Barone, Professor Jianyong Li and Professor Chenming Zhang, and my previous committee member Professor Xueyang Feng for serving as my committee members, and for give me the brilliant comments and suggestions.

A special thanks to the Department of Biological System Engineering. I would like to say thank you again to our department Head, Professor Mary Leigh Wolfe for the support on my research and graduation. I would like also to thanks for all the smiles given by BSE staffs and other faculty. I would like to acknowledge the financial support I received from Virginia Tech and from graduate research assistantships.

I would like to thanks my family, my mother, father, and especially, my wife. Thank you all for having been still with me and for being with me always. I would like to thank you all my friends, Dr. Hui Chen, Dr. Jae-Eung Kim, Dr. Chao Zhong, Dr. Eui-Jin Kim, Dr. Chun You, Dr. Zhuguang Zhu, Dr. Xiaozhou Zhang, Fangfang Sun and Dr. Hanan Moustafa Abdallah, who supported me in research and writing, and encouraged me to go for my objectives.

Finally, I would like to use my favorite poem from Cheng Gu to end this thesis: I was given dark eyes by the dark night, yet I use them to search for light.

Tables of Contents

List of Figures

Chapter 2

Chapter 3

Chapter 4

Chapter 5

Appendix

Figure S2. Test of background signals from mesophilic redox enzyme and PMS. (a) Test of background signals from mesophilic redox enzymes in the heat-treated colonies. The *E. coli* TOP10 (pET28a-P*tac*) was a negative control while *E. coli* TOP10 (pET28a-P*tac*-*Tm6pgdh*) was a positive control. Colonies were treated at 70 for 1 h and duplicated on the filter paper. The heat-treated cells were then overlaid by the melted agarose solution containing substrates and mediator *Gs*DI followed by incubation at room temperature for 3days for color development. Two control groups with agarose solution excluding coenzyme NMN^+ (6PG only) or both substrates 6PG and NMN^+ (No substrate) were prepared to test background noise resulted from redox dyes and intracellular NAD(P). The pale colony color in negative groups suggested the deactivation of mesophilic redox enzymes, while the strong color change between NMN+6PG group and no substrate group of *Tm*6PGDH indicated that the targeted thermophilic 6PGDH remains active after the heat treatment. (b) Test of background noise of PMS in the colorimetric assay. The colonies of *E. coli* TOP10 (pET28a-P*tac*-*Tm6pgdh*) were heat-treated and operated as described as above. The treated colonies were overlaid by the melted agarose with WST-1 or

List of Tables

Chapter 2

Chapter 3

Chapter 4

Chapter 5

Appendix

Chapter 1. Introduction

Coenzyme nicotinamide adenine dinucleotide (NAD, including the oxidized form--NAD^+ and reduced form--NADH) and the nicotinamide adenine dinucleotide phosphate (NADP, including $NADP^+$ and NADPH) are two of the most important electron carriers in cellular metabolism. These two coenzymes share almost identical dinucleotide structure, except the additional phosphate group esterified at the 2'-hydroxyl group of adenosine monophosphate moiety of NADP. The NAD and NADP play distinctive roles in catabolism and anabolism, respectively. NADH is usually reduced from NAD^+ via glycolysis and the citric acid cycle followed by its oxidation in the oxidative phosphorylation to generate ATP. NADPH can be produced by the pentose phosphate pathway, the one-carbon metabolism pathway and transhydrogenase, and consumed for the synthesis of cell materials (i.e., proteins, lipids, nuclear acids) and biochemicals (i.e., hydrogen, xylitol) (Chin and Cirino 2011; Cracan et al. 2017; Huang et al. 2016). Until now, over 1,800 types of redox enzymes have been characterized to oxidize or reduce NAD(P), and these enzymes always exhibit a strong selectivity of either NADP or NAD (You et al. 2017).

Coenzyme engineering that changes the coenzyme selectivity of NAD(P)-dependent dehydrogenases is of importance to the metabolic engineering, in vivo synthetic biology and biocatalysis. Because of the coenzyme selectivity of NAD(P) dependent dehydrogenases, the mismatch of strictly NAD^+-dependent dehydrogenases and NADPH-dependent reductases can result in the NADPH depletion and NADH accumulation (Wasylenko and Stephanopoulos 2015), followed by the decrease in conversion rate and yield of interested products. Besides the use of transhydrogenase to transfer hydride from NADH to NADPH, coenzyme engineering

matching the coenzyme specificity of dehydrogenases/reductases has been proved as a powerful tool to balance the NADH generation and NAD(P)H consumption, and facilitate the nearly theoretical product yields in the engineered microbe fermentation (Bastian et al. 2011). In the presence of a coenzyme transporter and biomimetic coenzyme, engineered dehydrogenases can be used to insulate the energy-transferring subsystem of interest from metabolic network as well, and create a new bio-orthogonal system for in vivo synthetic biology (Wang et al. 2017). Coenzyme engineering is also essentially important in biocatalysis and in the *in vitro* synthetic biology. Often, enzyme engineers seek to change the coenzyme specificities of dehydrogenases from NADP to NAD or biomimetic coenzymes for biocatalysis because (1) NAD and biomimetic analogues are less costly than NADP, (2) NAD and biomimetic analogues are more stable than NADP (Huang et al. 2016), (3) the small size biomimetic coenzymes have higher rates of diffusion (Campbell et al. 2012) and (4) the reduced biomimetic coenzymes may outperform the natural coenzymes, as was the case with the flavin dependent "ene" reductase (Knaus et al. 2016). Intensive studies of coenzyme engineering of NADP-dependent dehydrogenases have demonstrated its effectiveness in increasing the enzyme activity on the less costly coenzymes (Chen et al. 2016; Nowak et al. 2017; Scrutton et al. 1990). The efficient use of engineered dehydrogenase along with a low cost and stable coenzyme help minimize the coenzyme cost in the biocatalysis, which is vital for the *in vitro* production of low-value biocommodities, such as hydrogen (Zhang et al. 2010).

The use of *in vitro* synthetic biosystem (ivSB) to produce hydrogen from starch, is one of the most important *in vitro* synthetic biology projects. The natural dehydrogenases involved in this system prefer to use NADP. With the assistance of 17 thermophilic enzyme cascade reactions, this biosystem has shown a nearly 100% utilization efficiency of water splitting based

starch oxidation to hydrogen and a more than 90 mmole H_2/L/h of productivity rate at 50ºC (Kim et al. 2017). As compared to traditional whole-cell biosystem for hydrogen production, this system also contains numerous engineering advantages, such as higher product yield, faster reaction rate, easier product separation, tolerance of toxic compounds, broaden reaction conditions, good engineering flexibility and more. Several strategies, such as development of enzyme complexes, creation of an artificial electron transfer chain (ETC) and optimization of recombinant protein expression have been addressed to further increase the enzymatic performance and decrease enzyme cost in the ivSB based hydrogen production. The efficient use of dehydrogenases along with low cost and stable coenzyme has become the last obstacle to industrial biomanufacturing for hydrogen production.

6-Phosphogluconate dehydrogenase (6PGDH) is one of the rate-limiting enzymes in this biohydrogen production system. The 6PGDH catalyzes the oxidation of 6-phosphogluconate to ribulose 5-phosphate and simultaneously reduces $NADP^+$ to NADPH for hydrogen generation. Because 6PGDH usually shows strong coenzyme selectivity on $NADP^+$ and low activities on NAD^+ and biomimetic coenzymes, the biosystem with wild-type dehydrogenases has shown poor productivity rate when using unnatural coenzymes, although they are cheaper and more stable than $NADP^+$. For producing low-cost biohydrogen, the coenzyme engineering of the 6PGDH is urgently required for increasing their activities on NAD or biomimetic coenzymes.

One of the key issues of coenzyme engineering is to develop an efficient method for identification of the desired mutants from large mutant libraries. The 96-well microplate method is commonly used to screen mutants based on the absorbency of reduced coenzymes (Brinkmann-Chen et al. 2013) or redox dye linked colorimetric assay (Johannes et al. 2007; Mayer and Arnold 2002). However, the microplate-based screening is often regarded as a costly,

time consuming and labor intensive. It also suffers from background signals coming from mesophilic redox enzymes and reduced coenzymes in the cell lysate (Mayer and Arnold 2002). A native gel based screening method (Banta and Anderson 2002) and a Petri-dish based screening method (Flores and Ellington 2005) were developed to decrease the background signal from the cell lysate but they were limited by the modest throughput capacity. Thus, a simple and effective high-throughput screening (HTS) is urgently needed for coenzyme engineering of dehydrogenases. In this research, we developed a Petri-dish double layer-based screening method for coenzyme engineering of NADP-dependent 6PGDH from thermophilic host *Moorella thermoacetica* (*Moth*6PGDH). In this procedure, a heat treatment was used to lyse cells, deactivate mesophilic redox enzymes and oxidize reduced compounds, such as NAD(P)H, but retain active thermophilic *Moth*6PGDH. The positive dehydrogenase mutants had activity on the unnatural coenzyme NAD^+ and were identified by the PMS-TNBT colorimetric assay. Through two-rounds of directed evolution and screening, the coenzyme specificity of *Moth*6PGDH was changed from $NADP^+$ to NAD^+ and showed a 4,278-fold reversal of coenzyme selectivity in term of k_{cat}/K_M.

This screening method was also used to address the low thermostability of the highly active glucose 6-phosphate dehydrogenase (G6PDH) from *Zymomonas mobilis* (*Zm*G6PDH). The G6PDH is another rate-limiting enzyme in the ivSB hydrogen production system, which regenerates NADPH by oxidizing glucose 6-phosphate. For *in vitro* biocatalysis, G6PDH must posses both high activity and good thermostability due to the expense of the enzyme. Four generations of random mutagenesis and Petri-dish-based double-layer screening evolved the wild-type enzyme to a thermostable mutant Mut 4-1, which showed a more than 124-fold increase in half-life time ($t_{1/2}$) at 60°C, a 3.43°C increase in melting temperature (T_m), and a 5°C

increase in optimal temperature (T_{opt}), without compromising its activity. In addition, the thermostable mutant was conducted to generate hydrogen from maltodextrin via the *in vitro* enzymatic pathway, gaining a more than 8- fold improvement of productivity with 76% of theoretical yield.

The screening method was further optimized for coenzyme engineering of *Thermotaga maritima* 6PGDH (*Tm*6PGDH) on the smaller biomimetic coenzyme NMN^+. Coenzyme engineering for activity with biomimetics is more challenging than that with NAD^+, because the specific activity of the wild-type enzyme on biomimetic analogues can be three or four-orders of magnitude lower than those on $NAD(P)^+$. The background signal from the intracellular NAD(P) or other reduced biomolecules in cell lysate may overwhelm the signal of reduced biomimetics and result in the fail of screening. For the developed HTS method, we minimized the background signal from 45% to 14% of total chromogenic signal by cell washing and use of optimal redox dye and mediator. With this HTS, we applied six-round directed evolution to improve the catalytic efficiency of *Tm*6PGDH with NMN^+ by a factor of 50. The specific activity of the best mutant 6PGDH on NMN^+ was as high as 18 U/mg, comparable to that of the wild-type enzyme on its natural coenzyme NADP. Furthermore, we demonstrate the first NMN-based ETC comprised of engineered 6PGDH, FMN-containing diaphorase, and NiFe-hydrogenase for *in vitro* biohydrogen production, where the engineered enzyme led to a more than 6-fold increased hydrogen productivity rate compared to wild-type enzymes.

This dissertation emphasizes the development of a novel petri-dish based HTS and its use for coenzyme engineering of NAD(P)-dependent dehydrogenases. In chapter 2, the methodology of nicotinamide based coenzyme engineering and applications of engineered enzymes in improving product yield and decreasing product costs are reviewed. Chapter 3 describes the

development of the Petri-dish double layer based HTS for coenzyme engineering of thermophilic 6PGDH on NAD^+. In Chapter 4, this screening method is used to increase the thermostability of highly active *Zm*G6PDH, where the final mutant exhibited greatly improved thermostability without compromising its high specific activity. In Chapter 5, we further optimize the screening method developed for coenzyme engineering on NAD. The new Petri-dish based HTS exhibited its effectiveness in coenzyme engineering of Tm6PGDH for activity with the smaller biomimetic coenzyme NMN^+. Based on the engineered 6PGDH and biomimetic coenzyme, an NMN-dependent ETC was created for hydrogen production from 6PG. Chapter 6 summarizes this work and gives suggestions for future research directions.

References

Banta S, Anderson S. 2002. Verification of a novel NADH-binding motif: combinatorial mutagenesis of three amino acids in the cofactor-binding pocket of Corynebacterium 2, 5-diketo-D-gluconic acid reductase. J. Mol. Evol. 55(6):623-631.

Bastian S, Liu X, Meyerowitz JT, Snow CD, Chen MM, Arnold FH. 2011. Engineered ketol-acid reductoisomerase and alcohol dehydrogenase enable anaerobic 2-methylpropan-1-ol production at theoretical yield in *Escherichia coli*. Metab. Eng. 13(3):345-352.

Brinkmann-Chen S, Flock T, Cahn JK, Snow CD, Brustad EM, McIntosh JA, Meinhold P, Zhang L, Arnold FH. 2013. General approach to reversing ketol-acid reductoisomerase cofactor dependence from NADPH to NADH. Proc. Natl. Acad. Sci. U.S.A. 110(27):10946-10951.

Campbell E, Meredith M, Minteer SD, Banta S. 2012. Enzymatic biofuel cells utilizing a biomimetic cofactor. Chem. Commun. 48(13):1898-1900.

Chen H, Zhu Z, Huang R, Zhang Y-HP. 2016. Coenzyme engineering of a hyperthermophilic 6-phosphogluconate dehydrogenase from $NADP^+$ to NAD^+ with its application to biobatteries. Sci. Rep. 6:36311.

Chin JW, Cirino PC. 2011. Improved NADPH supply for xylitol production by engineered *Escherichia coli* with glycolytic mutations. Biotechnol. Prog. 27:333-341.

Cracan V, Titov DV, Shen H, Grabarek Z, Mootha VK. 2017. A genetically encoded tool for manipulation of $NADP^+$/NADPH in living cells. Nat. Chem. Biol. 13:1088-1095.

Flores H, Ellington AD. 2005. A modified consensus approach to mutagenesis inverts the cofactor specificity of *Bacillus stearothermophilus* lactate dehydrogenase. Protein. Eng. Des. Sel. 18(8):369-377.

Huang R, Chen H, Zhong C, Kim JE, Zhang Y-HP. 2016. High-throughput screening of coenzyme preference change of thermophilic 6-phosphogluconate dehydrogenase from $NADP^+$ to NAD^+. Sci. Rep. 6:32644.

Johannes TW, Woodyer RD, Zhao H. 2007. Efficient regeneration of NADPH using an engineered phosphite dehydrogenase. Biotechnol. Bioeng. 96(1):18-26.

Kim J-E, Kim E-J, Chen H, Wu C-H, Adams MW, Zhang Y-HP. 2017. Advanced water splitting for green hydrogen gas production through complete oxidation of starch by *in vitro* metabolic engineering. Metab. Eng.

Knaus T, Paul CE, Levy CW, de Vries S, Mutti FG, Hollmann F, Scrutton NS. 2016. Better than nature: nicotinamide biomimetics that outperform natural coenzymes. J. Am. Chem. Soc. 138(3):1033-1039.

Mayer KM, Arnold FH. 2002. A colorimetric assay to quantify dehydrogenase activity in crude cell lysates. J. Biomol. Screen. 7:135-140.

Nowak C, Pick A, Lommes P, Sieber V. 2017. Enzymatic reduction of nicotinamide biomimetic cofactors using anengineered glucose dehydrogenase: providing a regeneration system for artificial cofactors. ACS Catal. 7:5202-5208.

Rollin JA, del Campo JM, Myung S, Sun F, You C, Bakovic A, Castro R, Chandrayan SK, Wu C-H, Adams MWW and others. 2015. High-yield hydrogen production from biomass by *in vitro* metabolic engineering: Mixed sugars coutilization and kinetic modeling. Proc. Natl. Acad. Sci. U.S.A. 112:4964-4969.

Rollin JA, Tam TK, Zhang Y-HP. 2013. New biotechnology paradigm: cell-free biosystems for biomanufacturing. Green chem. 15(7):1708-1719.

Scrutton NS, Berry A, Perham RN. 1990. Redesign of the coenzyme specificity of a dehydrogenase by protein engineering. Nature 343(6253):38-43.

Wang L, Ji D, Liu Y, Wang Q, Wang X, Zhou YJ, Zhang Y, Liu W, Zhao ZK. 2017. Synthetic cofactor-Linked Metabolic Circuits for Selective Energy Transfer. ACS Catal.

Wasylenko TM, Stephanopoulos G. 2015. Metabolomic and (13)C-Metabolic Flux Analysis of a Xylose-Consuming *Saccharomyces cerevisiae* Strain Expressing Xylose Isomerase. Biotechnol. Bioeng. 112:470-483.

You C, Huang R, Wei X, Zhu Z, Zhang Y-HP. 2017. Protein engineering of oxidoreductases utilizing nicotinamide-based coenzymes, with applications in synthetic biology. Syst. Synth. Biol. 2:208-218.

Zhang Y-HP, Sun J, Zhong J-J. 2010. Biofuel production by *in vitro* synthetic enzymatic pathway biotransformation. Curr. Opin. Biotechnol. 21(5):663-669.

Chapter 2: Protein Engineering of Oxidoreductases on Nicotinamide-Based Coenzymes with the Applications to Synthetic Biology

Short title: Nicotinamide coenzyme engineering

Chun You[1*], Rui Huang[2], Zhiguang Zhu[1], Yi-Heng Percival Zhang[1,2*]

[1] Tianjin Institute of Industrial Biotechnology, Chinese Academy of Sciences, 32 West 7th Avenue, Tianjin Airport Economic Area, Tianjin 300308, People's Republic of China

[2] Biological Systems Engineering Department, Virginia Tech, 304 Seitz Hall, Blacksburg, Virginia 24061, USA

CY and HR contributed equally on writing this review.

*Corresponding authors：

Chun You

Email: you_c@tib.cas.cn

Yi-Heng Percival Zhang

Email: zhang_yh@tib.cas.cn

Abstract

Two natural nicotinamide-based coenzymes (NAD and NADP) are indispensably required by most oxidoreductases for catabolism and anabolism, respectively. Most NAD(P)-dependent oxidoreductases prefer one coenzyme as an electron acceptor or donor to the other due to their different metabolic roles. This coenzyme preference associated with coenzyme imbalance brings some challenges for high-efficiency of *in vivo* and *in vitro* synthetic biology pathways. Changing coenzyme preference of NAD(P)-dependent oxidoreductases is an important area of protein engineering, which is closely related to product-oriented synthetic biology projects. This review focuses on the methodology of nicotinamide-based coenzyme engineering with its application for improving product yields and decreasing production costs. Biomimetic nicotinamide-containing coenzymes have been proposed to replace natural coenzymes because they are more stable and less costly than natural coenzymes. Recent advances in switching of coenzyme preference from natural to biomimetic coenzymes are also covered in this review. Engineering coenzyme preference from natural to biomimetic coenzymes is becoming an importation direction for coenzyme engineering, especially for *in vitro* synthetic pathways and *in vivo* bioorthogonal redox pathways.

Keywords: Coenzyme engineering; Nicotinamide-based coenzymes; NAD; NADP; Protein engineering; Synthetic biology; Biomimetic coenzymes

1. Introduction

Protein engineering is the process of modifying amino acid sequence of proteins toward desired properties. The desired properties include improved substrate spectrum [1, 2], product selectivity [3, 4], enzyme activity [5], thermostability [6-8], solvent tolerance [8], etc. Protein engineering has been a powerful tool in biotechnology to generate a vast number of enhanced or novel enzymes for industrial applications and played a crucial role in advancing synthetic biology [9].

Synthetic biology is an emerging discipline that brings engineering principles to design and assemble biological components toward synthetic biological entities with an ultimate goal of cost-effective biomanufacturing [10]. The purpose of synthetic biology can be described as the design and construction of novel biological pathways, organisms or devices, or the redesign of existing natural biological systems to understand the complexity of biological systems and improve a wide variety of applications [11]. Its most important application may be the low-cost production of new drugs, chemicals, biomaterials, and bioenergy [12-18]. Synthetic biology could influence many other scientific and engineering fields as well as various aspects of daily life and society [17]. It can be divided into two areas: *in vivo* and *in vitro* [19]. *In vivo* synthetic biology mainly focuses on fundamental biological research facilitated by the use of synthetic DNA and genetic circuits on typical model microorganisms, such as *Escherichia coli*, *Bacillus subtilis* and *Saccharomyces cerevisiae*. It is a current predominant research area because living organisms can self-duplicate without major concerns of the biocatalyst preparation and possibly due

to a biotechnology paradigm based on thousands-of-year fermentation. In contrast, *in vitro* synthetic biology, sometimes called cell-free synthetic biology, is based on reconstituted enzyme mixture or cell lysates in one pot for the ultimate purpose of biomanufacturing [20-24]. Strictly speaking, *in vitro* synthetic biology is a little different from cell-free synthetic biology, where the former is based on reconstitution of (purified) enzymes, coenzymes and/or other abiotic components (for example, benzyl viologen for in vitro biohydrogen generation, and the latter is mainly based on cell lysates of one or multiple cell cultures. The *in vitro* synthetic biology platform has some distinctive advantages, like high product yield, fast reaction rate, highly engineering flexibility, high tolerance in toxic environment et al [19-21, 25]. The first industrial biomanufacturing example of cost-effective production of myo-inositol from starch has been demonstrated in China.

Oxidoreductases are the largest group of enzymes in the Enzyme Commission nomenclature. Coenzymes are usually required in these oxidoreductase-catalyzed reactions to transport electron, hydride, hydrogen, oxygen, or other atoms or small molecules in different enzymatic pathways [26, 27]. Typical coenzymes are nicotinamide adenine dinucleotide (NAD)/nicotinamide adenine dinucleotide phosphate (NADP), ubiquinone (CoQ), and flavin mononucleotide (FMN)/flavin adenine dinucleotide (FAD). Nicotinamide-based coenzymes for the transport and storage of electrons in the form of hydride groups are the most important because 80% of characterized oxidoreductases need NAD as a coenzyme and 10% of them need NADP as a coenzyme [27]. NAD and NADP are two kinds of ubiquitous

pyridine nucleotide coenzymes, which differ only by the additional 2'-phosphate group esterified to the adenosine monophosphate moiety of NADP (**Fig. 1a**). Because the phosphate group of NADP is sufficiently distant spatially and covalently from the chemically active nicotinamide moiety (red oval in **Fig. 1a**), nearly all oxidoreductases exhibit a strong preference for one to the other for implementing different metabolic roles [28].

Changing coenzyme preference of oxidoreductases is an important area of protein engineering. It has also been recognized as an important tool for *in vitro* and *in vivo* synthetic biology projects. For *in vitro* synthetic biology and cascade biocatalysis projects, coenzyme preference is usually switched from NADP to NAD, because the price of NADP is much higher than NAD (e.g., $200 per g for NADH (Sigma N8129), $6,000 per g for NADPH (Sigma N5130), $140 per g for NAD^+ (Sigma N7004) and $1000 per g for $NADP^+$ (Sigma N5755)). Also, NAD is more stable than NADP [2, 29, 30]. Furthermore, more NADH regeneration enzymes *in vitro* are available than NADPH regeneration enzymes [26, 31]. For *in vivo* synthetic biology projects, the switch of coenzyme preference can be conducted in both directions from NAD to NADP or from NADP to NAD for balancing coenzyme availability to increase metabolic pathway efficiency [32-36]. Coenzyme engineering from natural to biomimetic nicotinamide-based coenzymes (**Fig. 1b and c**) might further decrease the production cost for *in vitro* synthetic biology, because the cost and stability of biomimics are much better than natural coenzymes [37, 38]. Engineered enzymes with specificities on biomimetic nicotinamide coenzymes could

be used to develop bioorthogonal redox systems *in vivo* without interfering with native biochemical processes [39-41].

In this review, we focus on methods of coenzyme engineering on switching nicotinamide-based coenzyme preference of oxidoreductases and the application of the mutant enzymes with different coenzyme preference in product-oriented synthetic biology. Latest advances in general design of coenzyme engineering and high-throughput screening methods for directed evolution are highlighted. Coenzyme preference change from natural to biomimetic coenzymes could be extremely important, especially for *in vitro* synthetic biology, such as biohydrogen and bioelectricity generation from oligosaccharides [42-49].

2. Coenzyme engineering methods of nicotinamide-based coenzymes

Coenzyme engineering that changes enzymatic coenzyme preference has three major methods: rational design, semi-rational design and random mutagenesis (**Fig. 2**) [50, 51]. **Table 1** presents some representatives of product-oriented coenzyme engineering for *in vivo* and *in vitro* synthetic biology by using these engineering methods. Rational design is a knowledge-based strategy on the basis of prior structural and/or functional knowledge, using specific residues to replace specific residues of the targeted enzymes by site-directed mutagenesis and hoping to get the mutant with the desired properties. Semi-rational design is also knowledge-based strategy, creating a mutant library by site-saturated mutagenesis (where all 20 natural

amino acids or a fraction of 20 are tested) at the specific residues. Random mutagenesis is a knowledge-free strategy, creating a mutant library by error-prone PCR or gene shuffling for the whole-gene randomization. The last two strategies always need an extra step for the screening or selection of the mutated enzymes possessing the desired properties from the mutant library. Chica and Doucet proposed a strategy and drew a flow chart about how to select the enzyme engineering approaches based on the availability of experimental tools and prior knowledge of structure and function [51]. Because most NAD(P)-based oxidoreductases usually have a highly conserved coenzyme-binding motif -- Rossmann fold, which was the first identified conserved protein domain based on sequence alignment and crystal structures [52, 53], rational design and semi-rational design creating ‘smart’ libraries are more widely used in coenzyme engineering projects than random mutagenesis that renders a large size of mutant library.

2.1 Rational design

Rational design is the oldest protein engineering tool to switch coenzyme preference of oxidoreductases. It mutates specific amino acid residues with another certain residue through site-directed mutagenesis on the basis of structures of NAD(P)-enzyme complexes and catalytic mechanisms. Generally speaking, coenzyme engineering starts with the identification of residues near coenzyme-binding sites [54, 55], residues binding with the 2’ phosphate group [56] or adenosine-binding pocket [57], or residues essential for catalytic activity [2, 58-61]. Chen et al.

performed amino acid-sequence alignment of the coenzyme-binding motifs of NADP- and NAD-preferred 6-phosphogluconate dehydrogenases (6PGDH) from *Thermotoga maritima* (**Fig. 3a**) [2]. The loop region amino acids (in red box of **Fig. 3a**) are responsible for interaction between enzymes and 2'-phosphate of NADP. The alignment of the loop region indicates that three amino acids (positions 32, 33, and 34) in $NADP^+$-preferred 6PGDHs are highly conservative (**Fig. 3b**). NADP-preferred 6PGDH has Asn32, Arg33 and Thr34, while NAD-preferred 6PGDH wild-type enzymes and NAD-preferred mutant have very conservative sequences (i.e., acidic aspartate residues) at the N-terminal end of loop region. When the key amino acid residues responsible for binding the 2'-phosphate group of $NADP^+$ were changed by site-directed mutagenesis on this 6PGDH, the best mutant N32E/R33I/T34I exhibited a ratio of 96 of catalytic efficiency (k_{cat}/K_m) on NAD^+ and $NADP^+$, which is a ~64,000-fold reversal of the coenzyme selectivity from $NADP^+$ to NAD^+. In these residues, Arginine 33 plays a critical role in $NADP^+$ binding by contributing a positively charged planar residue that interacts primarily with 2'-phosphate of $NADP^+$. The most important point of coenzyme preference from NADP to NAD was a change of this key arginine to aspartate or glutamate [62-64]. Cui developed a novel computational strategy of altering the coenzyme preference that enhances the hydrogen-bond interaction between an enzyme and a coenzyme. This novel computational strategy only required the structure of the target enzyme without other homologous enzymes. By this rational design method, *Gluconobacter oxydans* Gox2181, which belongs to the short-chain dehydrogenases/reductases superfamily

(SDR superfamily), was engineered to show a much higher enzymatic activity by utilizing NADPH as its coenzyme through two-site mutation of Q20R&D43S [65].

Module swapping is another rational design method to switch coenzyme preference by replacing the original coenzyme binding pocket with new one from homology enzymes [66]. For example, Yaoi et al. changed the coenzyme preference of an isocitrate dehydrogenase by replacing the NADP-binding pocket with homogenous NAD-binding pocket [67]. Similarly, coenzyme preferences of a β-isopropylmalate dehydrogenase [68] and a short-chain dehydrogenase [69] have been reversed by using this strategy.

2.2 Semi-rational design

Semi-rational design is a powerful method to switch coenzyme preference by site-saturated mutagenesis on some critical amino acid residues deduced from bioinformatics analysis followed by screening of mutant libraries. Coenzyme engineering of an *E. coli* ketol-acid reductoisomerase (KARI) from NADP to NAD is a typical example of semi-rational design from Arnold's lab [36]. Five amino acids in Rossmann fold of this KARI were determined based on previous work [70], sequence alignment and structure of cofactor binding pocket. Five individual libraries on each amino acid were made by site-saturation mutagenesis and screened for variants exhibiting a higher ratio of NADH to NADPH activities. A library was constructed by combining all beneficial mutations as well as the wild-type residues. The best variant, which had four mutation sites, exhibited much higher activity on NADH to NADPH,

resulting in a 54,000-fold change in the ratio of catalytic efficiency (k_{cat}/K_m) on NADH to NADPH compared to wild type enzyme [36]. Later, the same group proposed a general semi-rational approach to switch the coenzyme preference of KARI from NADPH to NADH by integrating previous results of an engineered NADH-dependent mutant of *E. coli* KARI, available KARI crystal structures, and comprehensive KARI-sequence alignment [59]. The specific patterns of amino acid residue replacement in β2αB loop showed positive effect on reversing the coenzyme specificity of KARI. Steps include (1) identification of the loop, (2) determination of β2αB-loop length and mutation based on loop length by site-directed mutagenesis and site-saturated mutagenesis to achieve coenzyme switch, and (3) improvement of overall activity on NADH via random mutagenesis. Recently, this group developed a structure-guided, semi-rational strategy for reversing enzymatic nicotinamide-based coenzyme specificity to all oxidoreductases [28] with the increased number of protein crystal structures with high resolution and homogenous oxidoreductase sequences with different coenzyme preference. It comprised three steps: enzyme structural analysis, design and screening of focused mutant libraries for reversing cofactor preference, and, finally, recovery of catalytic efficiency. The recovery of catalytic efficiency is based on the predicted positions in the amino acid sequence with dramatically increased probabilities of harboring compensatory mutations, not like random mutagenesis on the whole gene in the KARI engineering [59]. This online tool has shown the efficacy of inverting coenzyme preference of four structurally diverse NADP-dependent enzymes: glyoxylate reductase, cinnamyl alcohol

dehydrogenase, xylose reductase, and iron-containing alcohol dehydrogenase. The analytical components of this approach have been fully automated and available in the form of an easy-to-use web tool: Cofactor Specificity Reversal-Structural Analysis and Library Design (CSR-SALAD).

2.3 Random mutagenesis

Random mutagenesis of the entire DNA sequence may be the last solution to change enzyme properties without relying on crystal or modeling structure of target protein [71, 72]. However, this method is rarely used in changing coenzyme preference between NADP and NAD because coenzyme-binding domains are highly conserved based on some specific residues near to coenzyme-binding sites. However, this method may be very important to screen mutants that can work on biomimetic coenzymes, whose structures largely differ from NADP and NAD (**Fig. 1**). Random mutagenesis sometimes is very useful because some compensatory mutations that may be remote from the cofactor-binding sites [28].

2.4 Directed evolution based on high-throughput screening (HTS)

High-throughput screening method is urgently required to identify positive mutants from the library constructed by site-saturated mutagenesis or random mutagenesis. The use of 96-well microplate screening based on the absorbency of NAD(P)H at 340 nm or coenzyme linked colorimetric assay is straightforward to measure the activities of dehydrogenases [30, 59, 73]. However, the microplate-based screening is labor-intensive, time-consuming and may require automated machines

[28, 74]. It is urgently needed to develop a simple and effective HTS method to determine coenzyme preference change of oxidoreductases. Recently, Zhang's group developed a Petri-dish double layer-based screening method to identify mutants of thermophilic 6-phosphogluconate dehydrogenase (6PGDH) from *Moorella thermoacetica* with reversed coenzyme preference from $NADP^+$ to NAD^+ [1]. Colonies of a 6PGDH mutant library were treated by heat to deactivate intracellular mesophilic dehydrogenases and reductive compounds (i.e., NADPH and NADH), and disrupt cell membrane. A second semi-solid layer was made by pouring the melted agarose solution containing a redox dye tetranitroblue tetrazolium (TNBT), phenazine methosulfate (PMS), NAD^+, and 6-phosphogluconate. In it, 6PGDH catalyzes the hydration of 6-phosphogluconate, coproducing NAD^+ to NADH. In the presence of PMS and NADH, the colorless redox dye TNBT was reduced to black TNBT-formazan (**Fig. 4A**). More active 6PGDH mutants on NAD^+ can be examined with eyes (**Fig. 4B**). Positive mutants were recovered by direct extraction of plasmid from dead-cell colonies followed by plasmid transformation into *E. coli* TOP10 [1]. By using this method, our lab has also switched the coenzyme preference of *T. maritima* glucose 6-phosphate dehydrogenase (G6PDH) from $NADP^+$ to NAD^+ (submitted for publication).

3. Applications of coenzyme engineering in *in vivo* synthetic biology

In vivo synthetic biology and metabolic engineering is widely investigated for

its potential production of biofuels, amino acids, alcohols, natural products, and antibiotics [75, 76]. Because NAD and NADP have their different roles in catabolism and anabolisms, respectively, their supply and consumption as well as their balance is essentially important for engineered organisms. However, some synthetic pathways do not match of coenzyme supply and consumption, possibly resulting in low product yields and slow volumetric productivity. For example, Liao's isobutanol synthesis pathway has a NADH-generation pathway for the production of isobutanol precursor followed by a NADPH-consumption step for the formation of isobutanol [77, 78]. As shown in **Fig. 5**, one coenzyme is more prevalent than the other coenzyme. The one enzyme in the pathway prefers high abundant coenzyme, while the other enzyme prefers low abundant coenzyme. This coenzyme imbalance leads to low-efficiency biosynthesis of desired product. To balance different coenzymes, several solutions could be taken. (1) The supply of oxygen to balance energy flux, possibly resulting in lowering product yield compared to theoretical yields. (2) The introduction of a transhydrogenase [79] catalyzes the reversible transfer of a hydride ion between of NADH and $NADP^+$. However, transhydrogenase may not always shift the hydride ion in the correct direction [80]. Also, the introduction of new components into cells might increase the burden of the cells to manufacture products or direct energy flux to undesired directions. (3) Replacement of native enzymes with enzymes having different coenzyme specificity [81, 82]. However, finding a sequence with specific desired properties could be difficult, particularly when a few members of a protein family only have been characterized [60]. (4) The best solution is changing the

coenzyme specificity of the pathway oxidoreductases by protein engineering, and then introduce the mutant enzyme into the cells for the replacement of the wild-type enzyme to solve the coenzyme match and imbalance. Unlike preferred coenzyme engineering from NADP to NAD *in vitro*, coenzyme preference of enzymes *in vivo* could be changed both directions from NADP to NAD and from NAD to NADP [83]. In this section, we introduce some examples about improving the productivity of microbial cell factories by changing enzyme's coenzyme preference.

3.1 From NAD to NADP

Amino acids represent one of the largest classes of fermentative products, whose production closely correlates with the availability of NADPH. For example, the synthesis of one mole of lysine requires four moles of NADPH in *Corynebacterium glutamicum*. Bommareddy et al. changed the coenzyme specificity of a native NAD-dependent glyceraldehyde 3-phosphate dehydrogenase (GAPDH) from *C. glutamicum* to NADP by rational protein design (D35G/L36T/T37K/P192S) to produce more NADPH from glycolysis. The mutant GAPDH-containing *C. glutamicum* strain showed approximately 60% improvement of lysine production than wild-type strain [84]. A recombinant *S. cerevisiae* strain containing xylose reductase (XR) and xylitol dehydrogenase (XDH) genes from *Pichia stipitis* can convert xylose to ethanol, along with the unfavorable excretion of xylitol due to intercellular redox imbalance caused by the different coenzyme specificity between NADPH-preferring XR and NAD^+-dependent XDH. Watanabe et al. succeeded in generating several *P.*

stipitis XDH mutants with a reversal of coenzyme specificity toward $NADP^+$ by multiple site-directed mutagenesis of coenzyme-binding domain. For example, a quadruple mutant (D207A/I208R/F209S/N211R) showed more than 4,500-fold higher values in k_{cat}/K_m with $NADP^+$ than the wild-type enzyme, reaching a comparable value with the k_{cat}/K_m with NAD^+ of the wild-type enzyme [85]. They constructed a recombinant yeast coexpressing NADPH-preferring PsXR and $NADP^+$-dependent PsXDH, and the resultant recombinant yeast increased ethanol production and decreases xylitol excretion [32, 86].

3.2 From NADP to NAD

Isobutanol can be produced from glucose by the recombinant *E. coli* through a modified biosynthesis of branched-chain amino acids (BCAAs) pathway [59, 60, 77, 78]. The pathway generates two pyruvates and two NADH via glycolysis while consumes two equivalents of NADPH per isobutanol synthesis, where NADPH is consumed by ketol-acid reductoisomerase (KARI) and alcohol dehydrogenase (ADH). The fermentation of this strain was operated aerobically or micro-aerobically to activate the pentose phosphate pathway (PPP) or the tricarboxylic acid (TCA) cycle to provide sufficient NADPH. However, anaerobic conditions are preferred for large-scale biofuel production due to lower operating costs (e.g., cooling, mixing and aeration) as well as higher product yields. Under anaerobic conditions, isobutanol production by engineered *E. coli* suffered from a limited supply of NADPH because of the shutdown of PPP or TCA cycle [34, 36]. Bastian et al. investigated the

construction of an NADH-dependent pathway by using NADH-preferring engineered *E. coli* KARI and ADH to produce high-yield isobutanol under anaerobic conditions. The introduction of this NADH-dependent pathway enabled anaerobic isobutanol production at a theoretical yield [36]. Similarly, the NADH-dependent pathway containing PsXDH and PsXR was also introduced into *S. cerevisiae* [87, 88]. PsXR was engineered to use NADH by the mutation of R276H. The expression of PsXR/R276H mutant and wild-type (WT) PsXDH in *S. cerevisiae* can lead to a 20% increase in ethanol production and a 52% decrease in xylitol excretion,as compared with the WT strain.

4. Applications of coenzyme engineering for *in vitro* synthetic biology

In vitro synthetic biology is an emerging biomanufacturing platform with such advantages as, high product yield, improved energy conversion efficiency, fast reaction rates, broad reaction conditions, etc. [89]. This platform has shown great potential on the production of bioenergy (e.g., hydrogen and electricity), pharmaceuticals (e.g., heparin), and biochemicals (i.e., α-ketoglutarate, myo-inositol, isobutanol, fructose 1,6-biphosphate, polyhydroxybutyrate, and (R)-phenylethanol) [42, 90-97]. The pathway design principle of the *in vitro* synthetic biology platform requires balances between coenzyme supply and consumption as well as their type. so that it benefits from high energy-retaining efficiency biotransformation, having product yields and less energy consumption such as aeration, mixing and cooling

energy, especially important for biomanufacturing biocommodities [12, 25]. NAD is preferable to NADP for *in vitro* synthetic biology because of its lower price [30, 66], higher stability [98], and more NAD-preferred oxidoreductases [26, 31]. In this section, we highlight several examples of *in vitro* synthetic (enzymatic) biosystems (ivSEB) involving coenzyme engineering from NADP to NAD. Cascade biocatalysis by engineered oxidoreductases with NADH or biomimetic cofactors along with coenzyme regeneration are not covered here, which can be referred elsewhere [38, 99, 100].

Biohydrogen is believed to be the best future transportation fuel. Hydrogen can be produced by ivSEBs from advanced water splitting energized by starch, sucrose and cellodextrins with a theoretical yield of 12 mol H_2 from per mol hexose and water [42, 45, 46], breaking Thauer limit of four moles of H_2 per mol glucose unit [101, 102]. In these ivSEBs, glucose 6-phosphate (G6P) is generated from ATP-free enzymatic phosphorylation of glucan (i.e., starch) and regenerated from non-oxidative pentose phosphate pathway and partial gluconeogenesis pathway. Two cascade dehydrogenases, G6PDH and 6PGDH oxidize G6P to ribulose 5-phosphate (Ru5P) and simultaneously reduce two $NADP^+$ to two NADPH, which are converted into hydrogen with the help of hydrogenase or even a biomimetic electron-transport chain containing an abiotic electron mediator [42]. Economic analysis suggests that the replacement of $NADP^+$ with NAD^+ shows great impact on cost decrease of *in vitro* hydrogen production by changing coenzyme preference of G6PDH and 6PGDH from $NADP^+$ to NAD^+. Chen et al. changed the coenzyme preference of hyperthermophilic

T. maritima 6PGDH from $NADP^+$ to NAD^+ by rational design [2]. The best mutant shows ~64,000-fold reversal of the coenzyme preference from $NADP^+$ to NAD^+, resulting 25% higher current density of 6PGDH-diaphorase electricity production system [2]. Also, we further engineered *T. maritima* G6PDH to change its coenzyme preference. The best mutant shows a more than 262-fold reversal of the coenzyme preference from $NADP^+$ to NAD^+ (submitted for publication). By coupling the G6PDH and 6PGDH mutants into hydrogen production pathway, we achieved the highest *in vitro* hydrogen production rate of 530 mmole H_2/L/h at 80°C from starch (submitted for publication). Polyhydroxybutyrate (PHB) is a type of biodegradable polyester. It can be produced by microbes in response to physiological stress [103] or engineered *E. coli* harboring *Streptomyces aureofaciens* PHB biosynthesis genes [104]. Recently, Opgenorth *et.al* designed an *in vitro* pentose-bifido-glycolysis (PBG) cycle to breakdown glucose for the PHB synthesis. Through the PBG cycle, one mole of glucose can be converted to two moles of acetyl-CoA with four mole of NAD(P)H and two moles of CO_2. To prevent the accumulation of NADPH due to coenzyme imbalance, G6PDH and 6PGDH involved in the PBG cycle were engineered to change the coenzyme preference from $NADP^+$ to NAD^+. Engineered dehydrogenases were used to regulate the efficiency of pathway by incorporation with NADH oxidase, $NADP^+$-dependent wide-type G6PDH and 6PGDH, exhibiting a more than two-fold improvement of product yield [91]. Sieber and coworkers designed an ATP-free ivSEB to produce pyruvate from glucose with two NADH molecules per glucose molecule; pyruvate can then be converted to ethanol and isobutanol, consuming the 2

moles of NADH per two moles of ethanol and one mole of isobutanol molecule, respectively [105]. The NADH-generating enzymes are glucose dehydrogenase (GDH) and glyceraldehyde dehydrogenase (AIDH). However, AIDH has a very low activity on NAD^+ compared to $NADP^+$. In order to minimize reaction complexity, the designed pathway was further consolidated to use the coenzyme NADH as the only electron carrier, AlDH was engineered by directed evolution to have a 8-fold higher activity for NAD^+ [106].

5. Biomimetic coenzyme engineering

To further decease coenzyme costs *in vitro*, the best solution is the replacement of natural coenzymes with low-cost biomimetic ones [37, 66]. Biomimetic coenzymes, such as nicotinamide mononucleotide (NMN), nicotinamide mononucleoside (NR) (**Fig. 1b**) and 1-benzyl nicotinamide (BNA) (**Fig. 1c**), are not only less costly but also have better stability [38, 66]. NMN and NR are precursors of NAD(P) and is much smaller in size than NAD(P) (**Fig. 1b**) and BNA is a typical biomimetic nicotinamide coenzyme. Few wild-type redox enzymes have been reported to have promiscuous activities on NMN, including liver alcohol dehydrogenase [107] and glutamic dehydrogenase [108]. Scott and his coworkers have engineered *Pyrococcus furiosus* alcohol dehydrogenase working on NMN but its activity remains very low [109]. Fish *et al.* found that the pyrophosphate and adenosine groups in NAD(P) are not essential for the hydride transfer for some flavin-

containing oxidoreducatases and proposed the use of BNA chloride to replace NAD(P) [110]. Clark and Fish collaborated to show that an engineered flavin-containing P450 mutant with two amino acid changes can utilize BNA [111]. Also, another group showed that engineered P450 can utilize Zinc dust as an electron source rather than natural coenzymes [112, 113]. In 2011, Zhao and coworkers presented a bio-orthogonal system that catalyzed the oxidative decarboxylation of L-malate with a dedicated biomimetic coenzyme, nicotinamide flucytosine dinucleotide (NFCD, **Fig. 1b**). The redox enzymes were engineered using site-saturation mutagenesis of the key amino acid sites [39], and the balance of this biomimetic coenzyme was achieved through a design enzymatic pathway containing two engineered enzymes, which can both use NFCD as coenzymes. This research opened the window to engineer bio-orthogonal redox systems for a wide variety of applications in *in vivo* synthetic biology.

Although a number of papers pertaining to engineering of NAD/NADP preference of oxidoreductases [89, 114, 115] (**Table 1**) and some general rules have been proposed for coenzyme engineering [28, 59, 65], coenzyme engineering on biomimetic coenzymes remains in its early stage due to their significant difference in structures and sizes (**Fig. 1**) [109]. This direction is becoming one of the top R&D priorities of *in vitro* synthetic biology.

6. Conclusions

Due to different coenzyme types, the imbalance of supply and consumption, coenzyme cost and stability, coenzyme engineering is one of the most important areas of protein engineering with its great application to *in vivo* and *in vitro* synthetic biology projects. With the increasing number of protein crystal structures with high-resolution and homogenous oxidoreductase sequences and the development of novel high-throughput screening methods, semi-rational design of switching coenzyme preference between NAD and NADP is becoming mature. Coenzyme engineering on biomimics is becoming an urgent task because such biomimics are more stable and less costly than natural ones [37, 66]. It is more and more acceptable that the *in vitro* synthetic biology platform could become a cornerstone of advanced biomanufacturing 4.0 for cost-competitive biomanufacturing low-value biocommodities and new food [116].

Acknowledgements

This study was mainly supported by the Key Research Program of the Chinese Academy of Sciences (Grant No. ZDRW-ZS-2016-3) and 1000-youth program of China to CY. Funds were partially provided by DOE EERE award (DE-EE0006968) to YPZ.

References

[1] Huang R, Chen H, Zhong C, Kim JE, Zhang Y-HP. High-throughput screening of coenzyme preference change of thermophilic 6-phosphogluconate dehydrogenase from $NADP^+$ to NAD^+. Sci Rep 2016; 6:32644.

[2] Chen H, Zhu Z, Huang R, Zhang Y-HP. Coenzyme engineering of a hyperthermophilic 6-phosphogluconate dehydrogenase from $NADP^+$ to NAD^+ with its application to biobatteries. Sci Rep 2016; 6:36311.

[3] McIntosh JA, Coelho PS, Farwell CC, Wang ZJ, Lewis JC, Brown TR, Arnold FH. Enantioselective intramolecular C-H amination catalyzed by engineered cytochrome P450 enzymes in vitro and in vivo. Angew Chem Int Ed Engl 2013; 52:9309-12.

[4] Agudo R, Roiban GD, Reetz MT. Achieving regio- and enantioselectivity of P450-catalyzed oxidative CH activation of small functionalized molecules by structure-guided directed evolution. Chembiochem 2012; 13:1465-73.

[5] van Leeuwen JG, Wijma HJ, Floor RJ, van der Laan JM, Janssen DB. Directed evolution strategies for enantiocomplementary haloalkane dehalogenases: from chemical waste to enantiopure building blocks. Chembiochem 2012; 13:137-48.

[6] You C, Huang Q, Xue H, Xu Y, Lu H. Potential hydrophobic interaction between two cysteines in interior hydrophobic region improves thermostability of a family 11 xylanase from Neocallimastix patriciarum. Biotechnol Bioeng 2010; 105:861-70.

[7] Blum JK, Ricketts MD, Bommarius AS. Improved thermostability of AEH by combining B-FIT analysis and structure-guided consensus method. J Biotechnol 2012; 160:214-21.

[8] Reetz MT, Soni P, Fernandez L, Gumulya Y, Carballeira JD. Increasing the stability of an enzyme toward hostile organic solvents by directed evolution based on iterative saturation mutagenesis using the B-FIT method. Chem Commun (Camb) 2010; 46:8657-8.

[9] Foo JL, Ching CB, Chang MW, Leong SS. The imminent role of protein engineering in synthetic biology. Biotechnol Adv 2012; 30:541-9.

[10] Wellhausen R, Oye KA. Intellectual property and the commons in synthetic Biology: strategies to facilitate an emerging technology. In: *2007 Atlanta Conference on Science, Technology and Innovation Policy: 2007*. 1-2.

[11] Osbourn AE, O'Maille PE, Rosser SJ, Lindsey K. Synthetic biology. New Phytol 2012; 196:671-7.

[12] Zhang Y-HP, Myung S, You C, Zhu Z, Rollin JA. Toward low-cost biomanufacturing through in vitro synthetic biology: bottom-up design. J Mater Chem 2011; 21:18877-86.

[13] Chang MC, Keasling JD. Production of isoprenoid pharmaceuticals by engineered microbes. Nat Chem Biol 2006; 2:674-81.

[14] Stephanopoulos G. Synthetic biology and metabolic engineering. ACS Synth Biol 2012; 1:514-25.

[15] Cheng AA, Lu TK. Synthetic biology: an emerging engineering discipline. Annu Rev Biomed Eng 2012; 14:155-78.

[16] Haseloff J, Ajioka J. Synthetic biology: history, challenges and prospects. J R Soc Interface 2009; 6 Suppl 4:S389-91.

[17] Andrianantoandro E, Basu S, Karig DK, Weiss R. Synthetic biology: new engineering rules for an emerging discipline. Mol Syst Biol 2006; 2.

[18] Heinemann M, Panke S. Synthetic biology--putting engineering into biology. Bioinformatics 2006; 22:2790-9.

[19] Forster AC, Church GM. Synthetic biology projects in vitro. Genome Res 2007; 17:1-6.

[20] Dudley QM, Karim AS, Jewett MC. Cell-free metabolic engineering: Biomanufacturing beyond the cell. Biotechnol J 2015; 10:69-82.

[21] Hodgman CE, Jewett MC. Cell-free synthetic biology: Thinking outside the cell. Metab Eng 2012; 14:261-9.

[22] Rupp S. Next-generation bioproduction systems: Cell-free conversion concepts for industrial biotechnology. Eng Life Sci 2013; 13:19-25.

[23] Morgado G, Gerngross D, Roberts TM, Panke S. Synthetic biology for cell-free biosynthesis: fundamentals of designing novel In vitro multi-enzyme reaction networks. In: Adv Biochem Eng Biotechnol. Berlin, Heidelberg: Springer; 2016, p. 1-30.

[24] Fessner WD. Systems Biocatalysis: Development and engineering of cell-free "artificial metabolisms" for preparative multi-enzymatic synthesis. N Biotechnol 2015; 32:658-64.

[25] You C, Zhang Y-HP. Biomanufacturing by in vitro biosystems containing complex enzyme mixtures. Process Biochem 2017; 52:106-14.

[26] Wichmann R, Vasic-Racki D. Cofactor regeneration at the lab scale. In: Adv Biochem Engin/Biotechnol. Berlin, Heidelberg: Springer; 2005, p. 225-60.

[27] Wu H, Tian C, Song X, Liu C, Yang D, Jiang Z. Methods for the regeneration of nicotinamide coenzymes. Green Chem 2013; 15:1773.

[28] Cahn JKB, Werlang CA, Baumschlager A, Brinkmann-Chen S, Mayo SL, Arnold FH. A general tool for engineering the NAD/NADP cofactor preference of oxidoreductases. ACS Synth Biol 2017; 6:326-33.

[29] Banta S, Swanson BA, Wu S, Jarnagin A, Anderson S. Alteration of the specificity of the cofactor-binding pocket of Corynebacterium 2,5-diketo-D-gluconic acid reductase A. Protein Eng 2002; 15:131-40.

[30] Woodyer R, van der Donk WA, Zhao H. Relaxing the nicotinamide cofactor specificity of phosphite dehydrogenase by rational design. Biochemistry 2003; 42:11604-14.

[31] Weckbecker A, Groger H, Hummel W. Regeneration of nicotinamide coenzymes: principles and applications for the synthesis of chiral compounds. In: Adv Biochem Eng Biotechnol. Berlin, Heidelberg: Springer; 2010, p. 195-242.

[32] Matsushika A, Watanabe S, Kodaki T, Makino K, Inoue H, Murakami K, Takimura O, Sawayama S. Expression of protein engineered $NADP^+$-dependent xylitol dehydrogenase increases ethanol production from xylose in recombinant *Saccharomyces cerevisiae*. Appl Microbiol Biotechnol 2008; 81:243-55.

[33] Bengtsson O, Hahn-Hägerdal B, Gorwa-Grauslund MF. Xylose reductase from *Pichia stipitis* with altered coenzyme preference improves ethanolic xylose fermentation by recombinant *Saccharomyces cerevisiae*. Biotechnol Biofuels 2009; 2:9.

[34] Hasegawa S, Uematsu K, Natsuma Y, Suda M, Hiraga K, Jojima T, Inui M, Yukawa H. Improvement of the redox balance increases L-valine production by *Corynebacterium glutamicum* under oxygen deprivation conditions. Appl Environ Microbiol 2012; 78:865-75.

[35] Tamakawa H, Ikushima S, Yoshida S. Ethanol production from xylose by a recombinant *Candida utilis* strain expressing protein-engineered xylose reductase and xylitol

dehydrogenase. Biosci Biotechnol Biochem 2011; 75:1994-2000.

[36] Bastian S, Liu X, Meyerowitz JT, Snow CD, Chen MM, Arnold FH. Engineered ketol-acid reductoisomerase and alcohol dehydrogenase enable anaerobic 2-methylpropan-1-ol production at theoretical yield in *Escherichia coli*. Metab Eng 2011; 13:345-52.

[37] Paul CE, Arends IWCE, Hollmann F. Is simpler better? Synthetic nicotinamide cofactor analogues for redox chemistry. ACS Catalysis 2014; 4:788-97.

[38] Paul CE, Hollmann F. A survey of synthetic nicotinamide cofactors in enzymatic processes. Appl Microbiol Biotechnol 2016; 100:4773-8.

[39] Ji D, Wang L, Hou S, Liu W, Wang J, Wang Q, Zhao ZK. Creation of bioorthogonal redox systems depending on nicotinamide flucytosine dinucleotide. J Am Chem Soc 2011; 133:20857-62.

[40] Ji D, Wang L, Liu W, Hou S, Zhao KZ. Synthesis of NAD analogs to develop bioorthogonal redox system. Sci China Chem 2013; 56:296-300.

[41] Wang L, Ji D, Liu Y, Wang Q, Wang X, Zhou YJ, Zhang Y, Liu W, Zhao ZK. Synthetic cofactor-linked metabolic circuits for selective energy transfer. ACS Catalysis 2017; 7:1977-83.

[42] Kim EJ, Wu CH, Adams MW, Zhang Y-HP. Exceptionally high rates of biological hydrogen production by biomimetic in vitro synthetic enzymatic pathways. Chemistry 2016; 22:16047-51.

[43] Rollin JA, Martin del Campo J, Myung S, Sun F, You C, Bakovic A, Castro R, Chandrayan SK, Wu C-H, Adams MWW *et al*. High-yield hydrogen production from biomass by in vitro metabolic engineering: Mixed sugars coutilization and kinetic modeling. Proc Natl Acad Sci USA 2015; 112:4964-9.

[44] Myung S, Rollin J, You C, Sun F, Chandrayan S, Adams MW, Zhang Y-HP. In vitro metabolic engineering of hydrogen production at theoretical yield from sucrose. Metab Eng 2014; 24:70-7.

[45] Ye X, Wang Y, Hopkins RC, Adams MWW, Evans BR, Mielenz JR, Zhang Y-HP. Spontaneous high-yield production of hydrogen from cellulosic materials and water catalyzed by enzyme cocktails. ChemSusChem 2009; 2:149-52.

[46] Zhang Y-HP, Evans BR, Mielenz JR, Hopkins RC, Adams MWW. High-yield hydrogen production from starch and water by a synthetic enzymatic pathway. PLoS One 2007; 2:e456.

[47] Zhu Z, Zhang Y-HP. Use of nonimmobilized enzymes and mediators achieved high power densities in closed biobatteries. Energy Science & Engineering 2015; 3:490-7.

[48] Zhu Z, Zhang Y-HP. In vitro metabolic engineering of bioelectricity generation by the complete oxidation of glucose. Metab Eng 2017; 39:110-6.

[49] Zhu Z, Wang Y, Minteer SD, Zhang Y-HP. Maltodextrin-powered enzymatic fuel cell through a non-natural enzymatic pathway. J Power Sources 2011; 196:7505-9.

[50] Li Y. Beyond protein engineering: its applications in synthetic biology. Enzyme Eng 2012; 1:1000e103.

[51] Chica RA, Doucet N, Pelletier JN. Semi-rational approaches to engineering enzyme activity: combining the benefits of directed evolution and rational design. Curr Opin Biotechnol 2005; 16:378-84.

[52] Lesk AM. NAD-binding domains of dehydrogenases. Current opinion in structural biology 1995; 5:775-83.

[53] Rao ST, Rossmann MG. Comparison of super-secondary structures in proteins. J Mol Biol 1973; 76:241-56.

[54] Wulf H, Mallin H, Bornscheuer UT. Protein engineering of a thermostable polyol dehydrogenase. Enzyme Microb Technol 2012; 51:217-24.

[55] Bubner P, Klimacek M, Nidetzky B. Structure-guided engineering of the coenzyme specificity of Pseudomonas fluorescens mannitol 2-dehydrogenase to enable efficient utilization of NAD(H) and NADP(H). FEBS Lett 2008; 582:233-7.

[56] Rosell A, Valencia E, Ochoa WF, Fita I, Pares X, Farres J. Complete reversal of coenzyme specificity by concerted mutation of three consecutive residues in alcohol dehydrogenase. J Biol Chem 2003; 278:40573-80.

[57] Morikawa S, Nakai T, Yasohara Y, Nanba H, Kizaki N, Hasegawa J. Highly active mutants of carbonyl reductase S1 with inverted coenzyme specificity and production of optically active alcohols. Biosci Biotechnol Biochem 2014; 69:544-52.

[58] Rosado LA, Caceres RA, de Azevedo WF, Basso LA, Santos DS. Role of Serine140 in the mode of action of *Mycobacterium tuberculosis* β-ketoacyl-ACP Reductase (MabA). BMC Res Notes 2012; 5:526.

[59] Brinkmann-Chen S, Flock T, Cahn JKB, Snow CD, Brustad EM, McIntosh JA, Meinhold P, Zhang L, Arnold FH. General approach to reversing ketol-acid reductoisomerase cofactor dependence from NADPH to NADH. Proc Nat Acad Sci USA 2013; 110:10946-51.

[60] Brinkmann-Chen S, Cahn JK, Arnold FH. Uncovering rare NADH-preferring ketol-acid reductoisomerases. Metab Eng 2014; 26:17-22.

[61] Geertz-Hansen HM, Blom N, Feist AM, Brunak S, Petersen TN. Cofactory: Sequence-based prediction of cofactor specificity of Rossmann folds. Proteins: Struct, Funct, Bioinf 2014; 82:1819-28.

[62] Levy HR, Vought VE, Yin X, Adams MJ. Identification of an arginine residue in the dual coenzyme-specific glucose-6-phosphate dehydrogenase from *Leuconostoc mesenteroides* that plays a key role in binding NADP+ but not NAD+. Arch Biochem Biophys 1996; 326:145-51.

[63] Li L, Cook PF. The 2′ -phosphate of NADP Is responsible for proper orientation of the nicotinamide ring in the oxidative decarboxylation reaction catalyzed by sheep liver 6-phosphogluconate dehydrogenase. J Biol Chem 2006; 281:36803-10.

[64] Tetaud E, Hanau S, Wells JM, Le Page RWF, Adams MJ, Arkison S, Barrett MP. 6-Phosphogluconate dehydrogenase from *Lactococcus lactis*: a role for arginine residues in binding substrate and coenzyme. Biochem J 1999; 338:55-60.

[65] Cui D, Zhang L, Jiang S, Yao Z, Gao B, Lin J, Yuan YA, Wei D. A computational strategy for altering an enzyme in its cofactor preference to NAD(H) and/or NADP(H). Febs J 2015; 282:2339-51.

[66] Rollin JA, Tam TK, Zhang Y-HP. New biotechnology paradigm: cell-free biosystems for biomanufacturing. Green Chem 2013; 15:1708-19.

[67] Yaoi T, Miyazaki K, Oshima T, Komukai Y, Go M. Conversion of the coenzyme specificity of isocitrate dehydrogenase by module replacement. J Biochem 1996; 119:1014-8.

[68] Miller SP, Lunzer M, Dean AM. Direct demonstration of an adaptive constraint. Science 2006; 314:458-61.

[69] Takase R, Mikami B, Kawai S, Murata K, Hashimoto W. Structure-based conversion of the coenzyme requirement of a short-chain dehydrogenase/reductase involved in bacterial alginate metabolism. J Biol Chem 2014; 289:33198-214.

[70] Rane MJ, Calvo KC. Reversal of the nucleotide specificity of ketol acid reductoisomerase by site-directed mutagenesis identifies the NADPH binding site1. Arch Biochem Biophys 1997; 338:83-9.

[71] Kim JE, Huang R, Chen H, You C, Zhang Y-HP. Facile construction of random gene mutagenesis library for directed evolution without the use of restriction enzyme in *Escherichia coli*. Biotechnol J 2016; 11:1142-50.

[72] Chusacultanachai S, Yuthavong Y. Random mutagenesis strategies for construction of large and diverse clone libraries of mutated DNA fragments. Methods Mol Biol 2004; 270:319-34.

[73] Mayer KM, Arnold FH. A colorimetric assay to quantify dehydrogenase activity in crude cell lysates. J Biomol Screen 2002; 7:135-40.

[74] Liu W, Hong J, Bevan DR, Zhang Y-HP. Fast identification of thermostable beta-glucosidase mutants on cellobiose by a novel combinatorial selection/screening approach. Biotechnol Bioeng 2009; 103:1087-94.

[75] Demain AL. Pickles, pectin, and penicillin. Annu Rev Microbiol 2004; 58:1-42.

[76] Zhang X, Jantama K, Moore JC, Shanmugam KT, Ingram LO. Production of L -alanine by metabolically engineered Escherichia coli. Appl Microbiol Biotechnol 2007; 77:355-66.

[77] Atsumi S, Wu TY, Eckl EM, Hawkins SD, Buelter T, Liao JC. Engineering the isobutanol biosynthetic pathway in Escherichia coli by comparison of three aldehyde reductase/alcohol dehydrogenase genes. Appl Microbiol Biot 2010; 85:651-7.

[78] Atsumi S, Hanai T, Liao JC. Non-fermentative pathways for synthesis of branched-chain higher alcohols as biofuels. Nature 2008; 451:86-9.

[79] Gameiro PA, Laviolette LA, Kelleher JK, Iliopoulos O, Stephanopoulos G. Cofactor balance by nicotinamide nucleotide transhydrogenase (NNT) coordinates reductive carboxylation and glucose catabolism in the tricarboxylic acid (TCA) cycle. J Biol Chem 2013; 288:12967-77.

[80] Nissen TL, Anderlund M, Nielsen J, Villadsen J, Kielland-Brandt MC. Expression of a cytoplasmic transhydrogenase in Saccharomyces cerevisiae results in formation of 2-oxoglutarate due to depletion of the NADPH pool. Yeast 2001; 18:19-32.

[81] Martinez I, Zhu J, Lin H, Bennett GN, San KY. Replacing *Escherichia coli* NAD-dependent glyceraldehyde 3-phosphate dehydrogenase (GAPDH) with a NADP-dependent enzyme from *Clostridium acetobutylicum* facilitates NADPH dependent pathways. Metab Eng 2008; 10:352-9.

[82] Takeno S, Murata R, Kobayashi R, Mitsuhashi S, Ikeda M. Engineering of *Corynebacterium glutamicum* with an NADPH-generating glycolytic pathway for L-lysine production. Appl Environ Microbiol 2010; 76:7154-60.

[83] Ehsani M, Fernández MR, Biosca JA, Dequin S. Reversal of coenzyme specificity of 2,3-butanediol dehydrogenase from *Saccharomyces cerevisae* and *in vivo* functional analysis. Biotechnol Bioeng 2009; 104:381-9.

[84] Bommareddy RR, Chen Z, Rappert S, Zeng AP. A de novo NADPH generation pathway for improving lysine production of *Corynebacterium glutamicum* by rational design of the coenzyme specificity of glyceraldehyde 3-phosphate dehydrogenase. Metab Eng 2014; 25:30-

7.

[85] Watanabe S, Kodaki T, Makino K. Complete reversal of coenzyme specificity of xylitol dehydrogenase and increase of thermostability by the introduction of structural zinc. J BiolChem 2005; 280:10340-9.

[86] Matsushika A, Watanabe S, Kodaki T, Makino K, Sawayama S. Bioethanol production from xylose by recombinant *Saccharomyces cerevisiae* expressing xylose reductase, $NADP^+$-dependent xylitol dehydrogenase, and xylulokinase. J Biosci Bioeng 2008; 105:296-9.

[87] Petschacher B, Nidetzky B. Altering the coenzyme preference of xylose reductase to favor utilization of NADH enhances ethanol yield from xylose in a metabolically engineered strain of *Saccharomyces cerevisiae*. Microb Cell Fact 2008; 7:9.

[88] Watanabe S, Abu Saleh A, Pack SP, Annaluru N, Kodaki T, Makino K. Ethanol production from xylose by recombinant *Saccharomyces cerevisiae* expressing protein-engineered NADH-preferring xylose reductase from *Pichia stipitis*. Microbiology 2007; 153:3044-54.

[89] Zhang Y-HP. Simpler Is better: high-Yield and potential low-cost biofuels production through cell-free synthetic pathway biotransformation (SyPaB). ACS Catalysis 2011; 1:998-1009.

[90] Xu Y, Masuko S, Takieddin M, Xu H, Liu R, Jing J, Mousa SA, Linhardt RJ, Liu J. Chemoenzymatic synthesis of homogeneous ultralow molecular weight heparins. Science 2011; 334:498-501.

[91] Opgenorth PH, Korman TP, Bowie JU. A synthetic biochemistry module for production of bio-based chemicals from glucose. Nat Chem Biol 2016; 12:393-5.

[92] You C, Shi T, Li Y, Han P, Zhou X, Zhang Y-HP. An in vitro synthetic biology platform for the industrial biomanufacturing of myo-inositol from starch. Biotechnol Bioeng 2017; doi: 10.1002/bit.26314.

[93] Moustafa HMA, Kim EJ, Zhu Z, Wu CH, Zaghloul TI, Adams MWW, Zhang YHP. Water splitting for high‐yield hydrogen production energized by biomass xylooligosaccharides catalyzed by an enzyme cocktail. Chemcatchem 2016; 8:2898-902.

[94] Zhu Z, Sun F, Zhang X, Zhang Y-HP. Deep oxidation of glucose in enzymatic fuel cells through a synthetic enzymatic pathway containing a cascade of two thermostable dehydrogenases. Biosens Bioelectron 2012; 36:110-5.

[95] Zhu Z, Kin Tam T, Sun F, You C, Zhang Y-HP. A high-energy-density sugar biobattery based on a synthetic enzymatic pathway. Nat Commun 2014; 5:3026.

[96] Beer B, Pick A, Sieber V. In vitro metabolic engineering for the production of α-ketoglutarate. Metab Eng 2017; 40:5-13.

[97] Johannes TW, Woodyer RD, Zhao H. Efficient regeneration of NADPH using an engineered phosphite dehydrogenase. Biotechnol Bioeng 2007; 96:18-26.

[98] Wu JT, Wu LH, Knight JA. Stability of NADPH: effect of various factors on the kinetics of degradation. Clin Chem 1986; 32:314-9.

[99] Löw SA, Löw IM, Weissenborn MJ, Hauer B. Enhanced ene-reductase activity through alteration of artificial nicotinamide cofactor substituents. ChemCatChem 2016; 8:911-5.

[100] Knaus T, Paul CE, Levy CW, de Vries S, Mutti FG, Hollmann F, Scrutton NS. Better than nature: nicotinamide biomimetics that outperform natural coenzymes. J Am Chem Soc 2016; 138:1033-9.

[101] Thauer K, Jungermann K, Decker K. Energy conservation in chemotrophic anaerobic bacteria. Bacteriol Rev 1977; 41:100-80.

[102] Maeda T, Sanchez-Torres V, Wood TK. Hydrogen production by recombinant *Escherichia coli* strains. Microb Biotechnol 2012; 5:214-25.

[103] Ackermann J-u, Müller S, Lösche A, Bley T. *Methylobacterium rhodesianum* cells tend to double the DNA content under growth limitations and accumulate PHB. J Biotechnol 1995; 39:9-20.

[104] Mahishi LH, Tripathi G, Rawal SK. Poly(3-hydroxybutyrate) (PHB) synthesis by recombinant Escherichia coli harbouring *Streptomyces aureofaciens* PHB biosynthesis genes: effect of various carbon and nitrogen sources. Microbiol Res 2003; 158:19-27.

[105] Guterl JK, Garbe D, Carsten J, Steffler F, Sommer B, Reisse S, Philipp A, Haack M, Ruhmann B, Koltermann A *et al*. Cell-free metabolic engineering: production of chemicals by minimized reaction cascades. ChemSusChem 2012; 5:2165-72.

[106] Steffler F, Guterl J-K, Sieber V. Improvement of thermostable aldehyde dehydrogenase by directed evolution for application in synthetic cascade biomanufacturing. Enz Microb Technol 2013; 53:307-14.

[107] Plapp BV, Sogin DC, Dworschack RT, Bohlken DP, Woenckhaus C, Jeck R. Kinetics and native and modified liver alcohol dehydrogenase with coenzyme analogs: isomerization of enzyme-nicotinamide adenine dinucleotide complex. Biochemistry 1986; 25:5396-402.

[108] Fisher HF, McGregor LL. The ability of reduced nicotinamide mononucleotide to function as a hydrogen donor in the glutamic dehydrogenase reaction. Biochem Biophys Res Commun 1969; 34:627-32.

[109] Campbell E, Meredith M, Minteer SD, Banta S. Enzymatic biofuel cells utilizing a biomimetic cofactor. Chem Commun 2012; 48:1898-900.

[110] Lo HC, Leiva C, Buriez O, Kerr JB, Olmstead MM, Fish RH. Bioorganometallic chemistry. 13. regioselective reduction of NAD^+ models, 1-benzylnicotinamde triflate and beta-nicotinamide ribose-5'-methyl phosphate, with in situ generated $[Cp^*Rh(Bpy)H]^+$: structure --activity relationships, kinetics, and mechanistic aspects in the formation of the 1,4-NADH derivatives. Inorg Chem 2001; 40:6705-16.

[111] Ryan JD, Fish RH, Clark DS. Engineering cytochrome P450 enzymes for improved activity towards biomimetic 1,4-NADH cofactors. Chembiochem 2008; 9:2579-82.

[112] Nazor J, Schwaneberg U. Laboratory evolution of P450 BM-3 for mediated electron transfer. ChemBioChem 2006; 7:638-44.

[113] Nazor J, Dannenmann S, Adjei RO, Fordjour YB, Ghampson IT, Blanusa M, Roccatano D, Schwaneberg U. Laboratory evolution of P450 BM3 for mediated electron transfer yielding an activity-improved and reductase-independent variant. Protein Eng Des Sel 2008; 21:29-35.

[114] Zhang Y-HP, Huang W-D. Constructing the electricity-carbohydrate-hydrogen cycle for a sustainability revolution. Trends Biotechnol 2012; 30:301-6.

[115] Zhang Y-HP. Production of biocommodities and bioelectricity by cell-free synthetic enzymatic pathway biotransformations: challenges and opportunities. Biotechnol Bioeng 2010; 105:663-77.

[116] Zhang Y-HP, Sun J, Ma Y. Biomanufacturing: history and perspective. J Ind Microbiol Biotechnol 2017; 44:773-84.

[117] Bommareddy RR, Chen Z, Rappert S, Zeng AP. A de novo NADPH generation pathway for improving lysine production of *Corynebacterium glutamicum* by rational design of the

coenzyme specificity of glyceraldehyde 3-phosphate dehydrogenase. Metab Eng 2014; 25:30-7.

[118] Petschacher B, Staunig N, Müller M, Schürmann M, Mink D, De Wildeman S, Gruber K, Glieder A. Cofactor specificity engineering of *Streptococcus mutans* NADH oxidase 2 for NAD(P)+ regeneration in biocatalytic oxidations. Comput Struct Biotechnol J 2014; 9:1-11.

[119] Dambe TR, Kühn AM, Brossette T, Giffhorn F, Scheidig AJ. Crystal structure of NADP (H)-dependent 1,5-anhydro-d-fructose reductase from *Sinorhizobium morelense* at 2.2 Å resolution: Construction of a NADH-accepting mutant and its application in rare sugar synthesis. Biochemistry 2006; 45:10030-42.

[120] Gand M, Thöle C, Müller H, Brundiek H, Bashiri G, Höhne M. A NADH-accepting imine reductase variant: Immobilization and cofactor regeneration by oxidative deamination. J Biotechnol 2016; 230:11-8.

[121] Petschacher B, Nidetzky B. Altering the coenzyme preference of xylose reductase to favor utilization of NADH enhances ethanol yield from xylose in a metabolically engineered strain of *Saccharomyces cerevisiae*. Microb Cell Fact 2008; 7:9.

[122] Chen H, Zhu Z, Huang R, Zhang Y-HP. Coenzyme engineering of a hyperthermophilic 6-phosphogluconate dehydrogenase from $NADP^+$ to NAD^+ with its application to biobatteries. Sci Rep 2016; 6:36311.

[123] Opgenorth PH, Korman TP, Bowie JU. A synthetic biochemistry module for production of bio-based chemicals from glucose. Nat Chem Biol 2016; 12:393-5.

Figure legends

Figure 1. Structures of nicotinamide-based coenzymes and biomimetic nicotinamide coenzymes. a) two natural coenzymes, NAD^+ and $NADP^+$, the chemical groups in the open red ovals are where the redox reaction occurs, these chemical groups are the same in all the coenzymes, b) biomimetic coenzymes derived from natural coenzymes, nicotinamide flucytosine dinucleotide ($NFCD^+$), nicotinamide mononucleotide (NMN^+), nicotinamide mononucleoside (NR^+), the chemical group in shaded area indicates the structure difference between $NFCD^+$ and NAD^+, c) synthetic biomimetic coenzyme, 1-benzyl nicotinamide (BNA^+).

Figure 2. Scheme of coenzyme engineering methods, including rational design, semi-rational design and directed evolution.

Figure 3. a) Amino acid sequence alignment of the coenzyme-binding motif of various 6PGDH enzymes. The residues composing the loop region and responsible for coenzyme recognition are boxed. Red stars represent *M. thermoacetica* wild-type $NADP^+$-preferred 6PGDH and NAD^+-preferred 6PGDH mutant. Blue star indicates *T. maritima* 6PGDH studied in this research. b) Sub-alignments of key amino acid residues playing an important role in 2'-phosphate interaction. Colors in sequence logo refer to hydrophobic (black), positive charge (blue), negative charge (red) and polar (green) residues (This figure is a courtesy from (Chen et al. 2016a)).

Figure 4. a) Scheme of double layer based screening. The 6PGDH catalyze the oxidation of 6-phosphogluconate to ribulose 5-phosphate and CO_2, and reduction of

NAD^+ to NADH. In the presence of PMS, the NADH transfers its hydride and reduces the colorless redox dye TNBT to black color TNBT formazan. b). the process of double layer based screening method. The mutant library was treated by heat and overlaid by second agarose layer with reagents. The colonies featuring as darker color with halo were identified as positive mutants.

Figure 5. Engineering the coenzyme preference of oxidoreductases in a metabolic pathway by protein engineering *in vitro* followed by the replacement of the wild-type enzyme with the mutant enzyme to solve the problem of coenzyme un-match.

Table 1. List of product-oriented coenzyme engineering on natural nicotinamide coenzymes NAD(P).

Enzyme	Source	Specificity	Mutations	Product	Increasing effect	Reference
Glyceraldehyde 3-phosphate dehydrogenase	*Corynebacterium glutamicum*	NADH→NADPH	D35G/L36R/P192S	Lysine	~60% higher yield	[117]
NADH oxidase 2	*Streptococcus mutans*	NADH→NADPH	V193R/V194H	2-heptanone	ND	[118]
1,5-anhydro-D-fructose reductase	*Sinorhizobium Morelense*	NADPH→NADH	A13G	1,5-anhydro-D-mannitol	ND	[119]
Imine reductase	*Streptomyces sp. GF3587*	NADPH→NADH	K40A	2-methylpyrolidine	~64% higher conversion	[120]
Ketol-acid reductoisomerase	*Escherichia coli*	NADPH→NADH	A71S/R76D/S78D/Q110V	2-methylpropan-1-ol (isobutanol)	3-fold higher titer	[36]
Xylose reductase	*Pichia stipitis*	NADPH→NADH	R276H	Ethanol	~20% higher yield	[88]
Xylose reductase	*Candida tenuis*	NADPH→NADH	K274R/N276D	Ethanol	~42% higher yield	[121]
6-phosphogluconate dehydrogenase	*Thermotoga maritima*	$NADP^+$→NAD^+	N32E/R33I/T34I	Electricity	~25% higher maximum power density and current density	[122]
6-phosphogluconate dehydrogenase	*Geobacillus stearothermophilus*	$NADP^+$→NAD^+	N33D/R34Y/K38L	Polyhydroxybutyrate	ND	[123]
Glucose 6-phosphate dehydrogenase	*Geobacillus stearothermophilus*	$NADP^+$→NAD^+	A47D	Polyhydroxybutyrate	ND	[123]
Glucose 6-phosphate dehydrogenase	*Thermotoga maritima*	$NADP^+$→NAD^+	S33E/R65M/T66S	Hydrogen	ND	Unpublished

Figure 1. Structures of nicotinamide-based coenzymes and biomimetic nicotinamide coenzymes

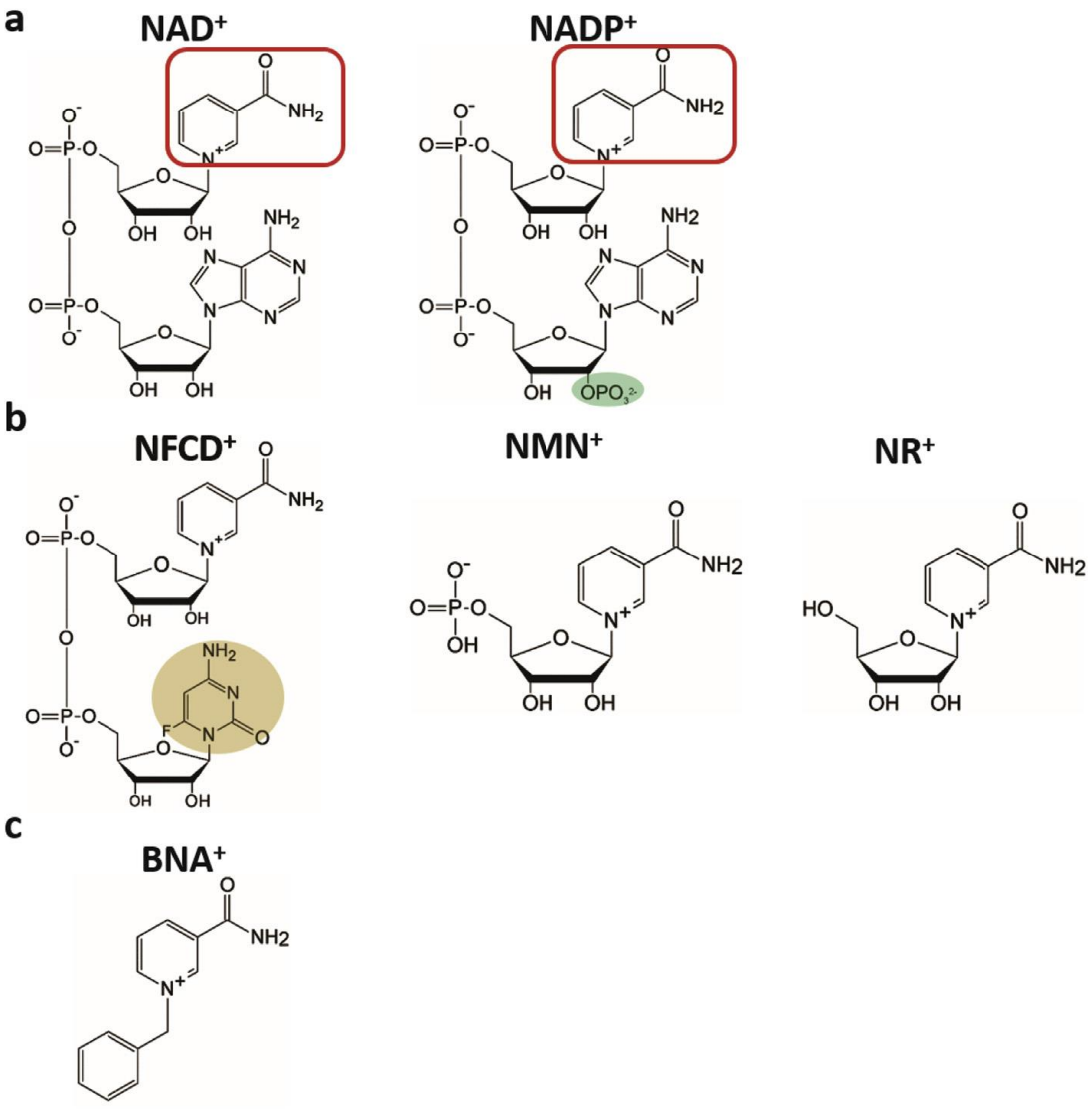

Figure 2. Scheme of coenzyme engineering methods, including rational design, semi-rational design and directed evolution

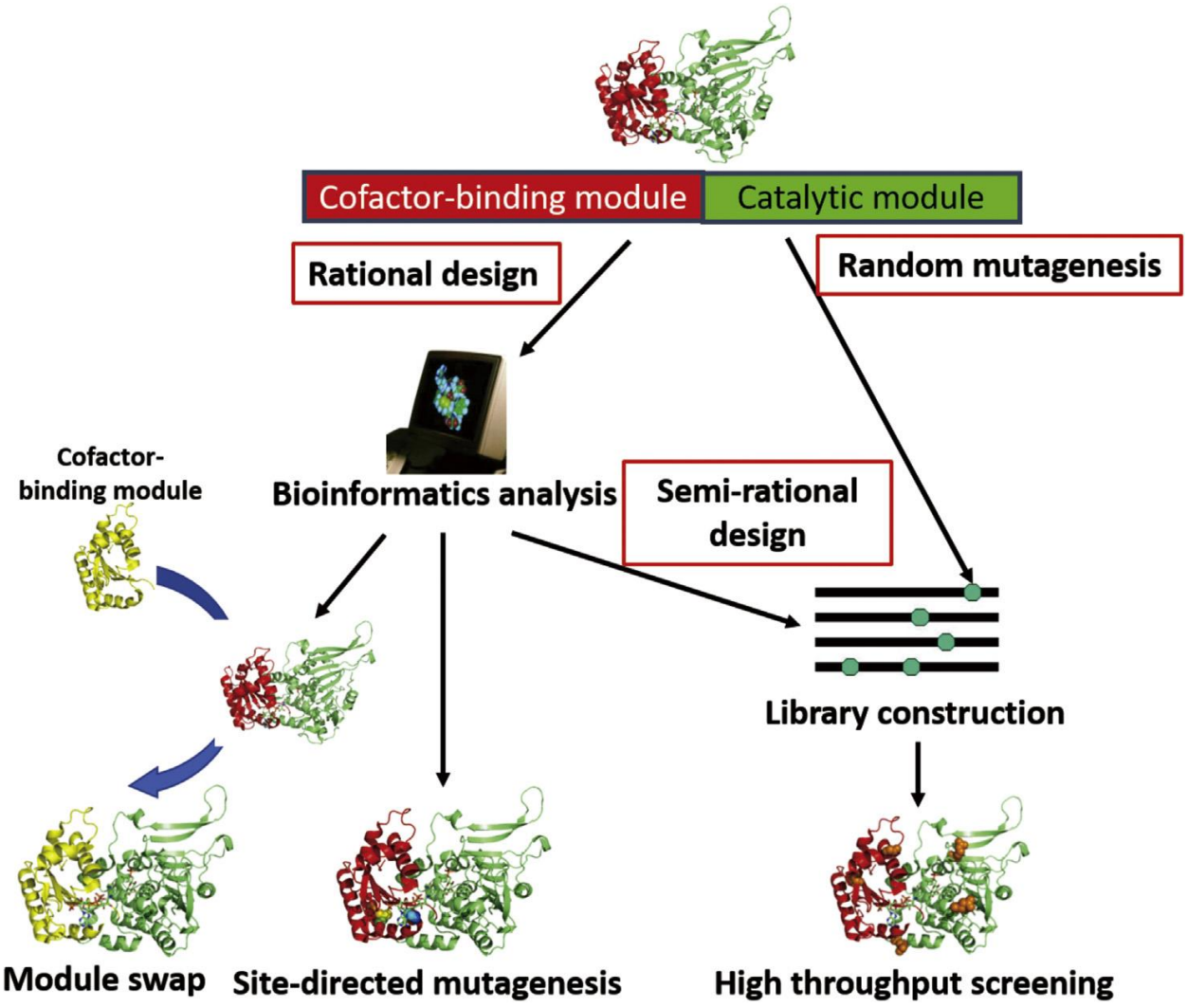

Figure 3. Amino acid sequence alignment of the coenzyme-binding motif of various 6PGDH enzymes

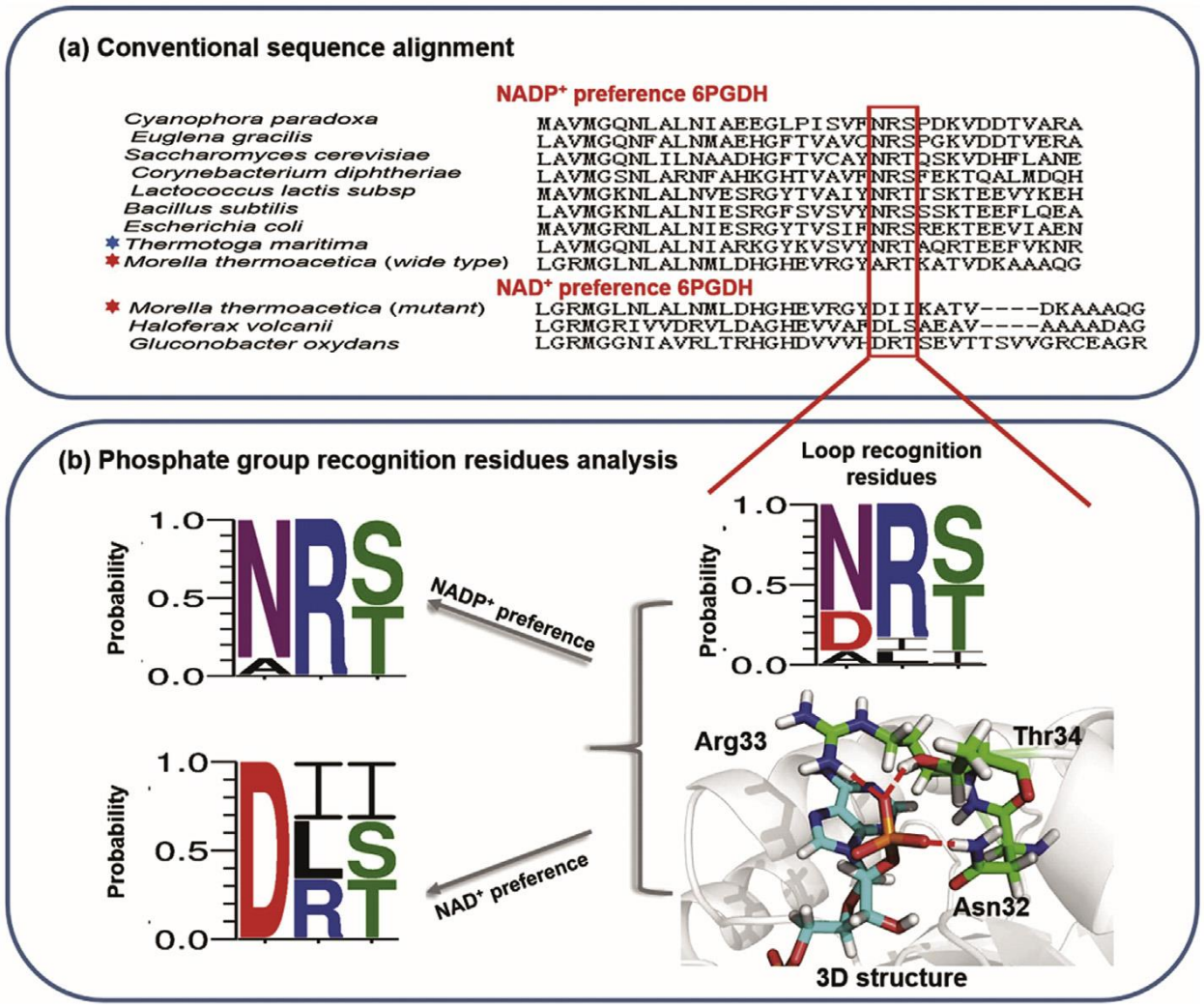

Figure 4. Scheme of double layer based screening. The 6PGDH catalyze the oxidation of 6-phosphogluconate to ribulose 5-phosphate and CO_2, and reduction of NAD^+ to NADH

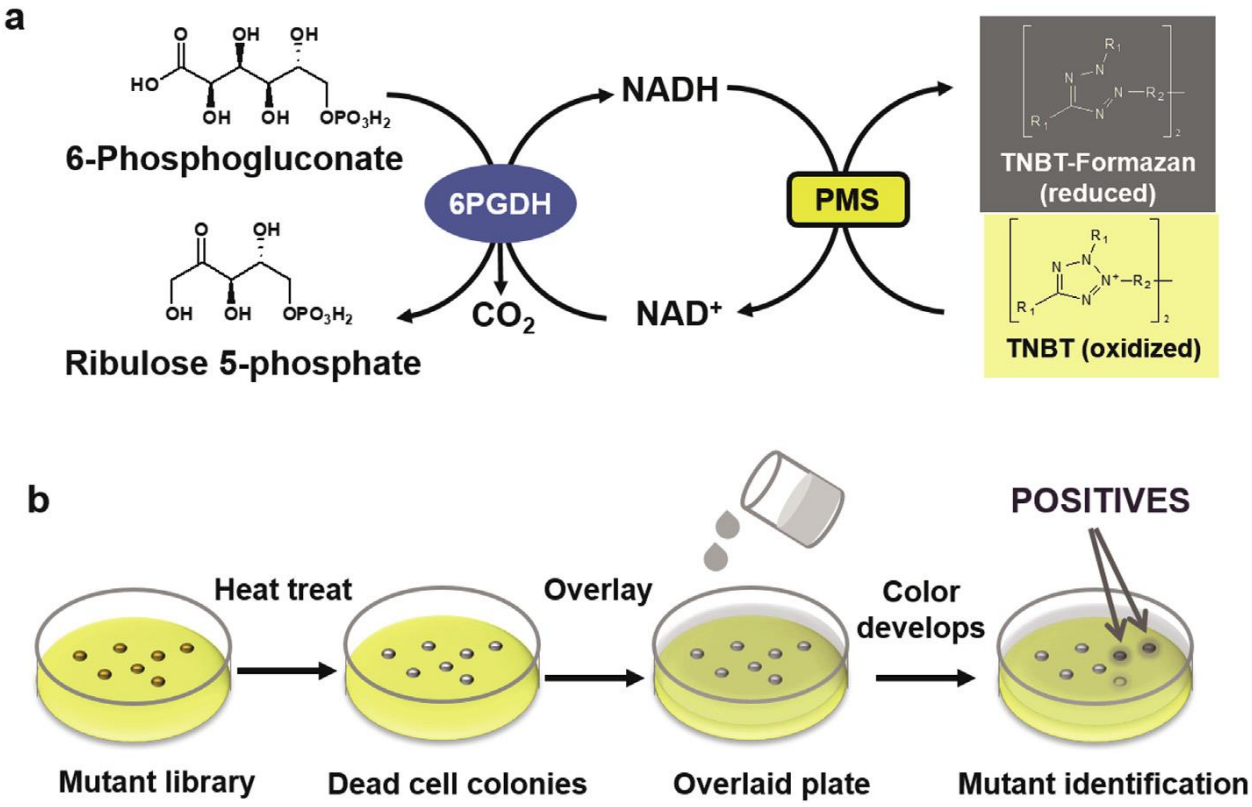

Figure 5. Engineering the coenzyme preference of oxidoreductases in a metabolic pathway by protein engineering in vitro followed by the replacement of the wild-type enzyme with the mutant enzyme to solve the problem of coenzyme un-match

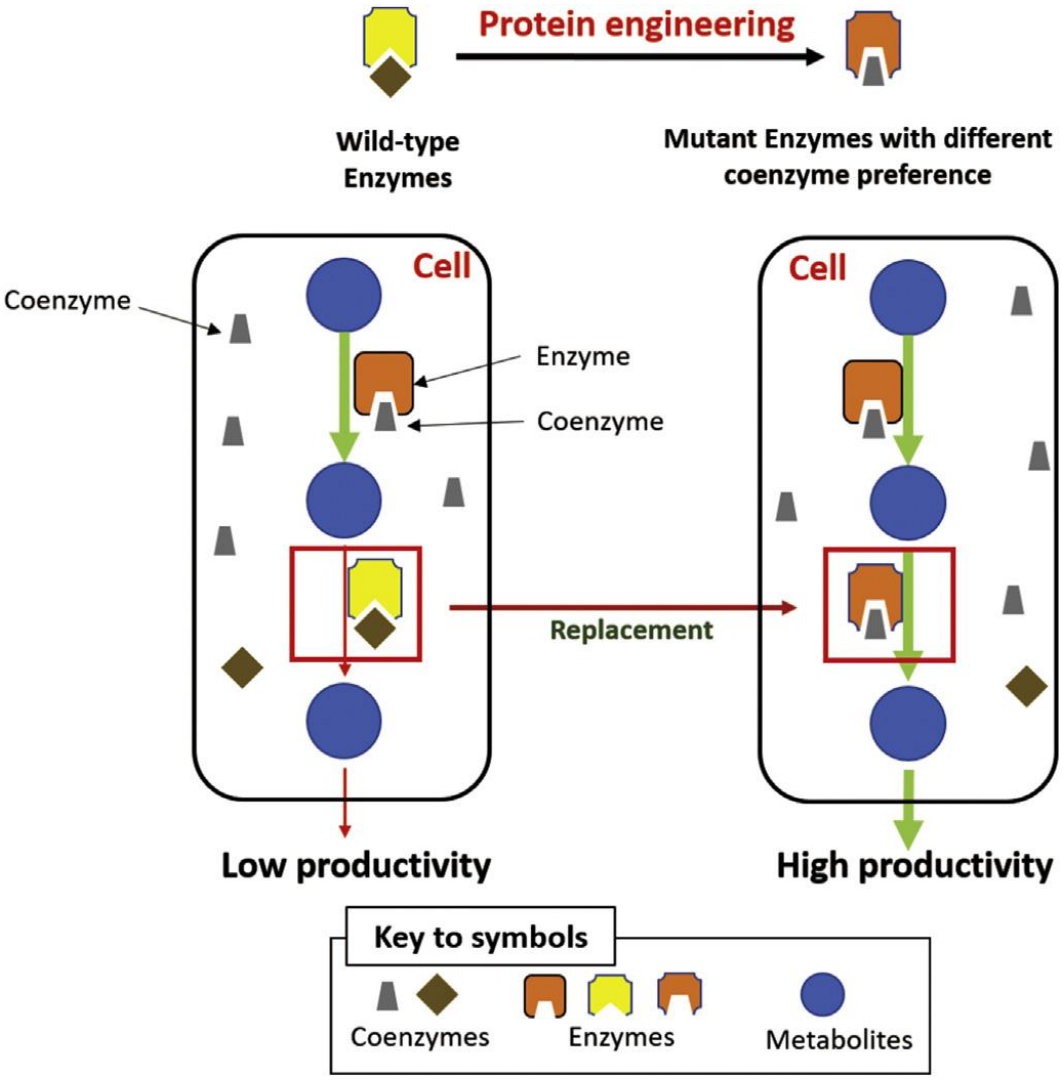

Chapter 3: High-Throughput Screening of Coenzyme Preference Change of Thermophilic 6-Phosphogluconate Dehydrogenase from $NADP^+$ to NAD^+

Rui Huang,[1] Hui Chen,[1] Chao Zhong,[1] Jae Eung Kim,[1] Yi-Heng Percival Zhang[1,2]*‡

[1] Biological Systems Engineering Department, Virginia Tech, 304 Seitz Hall, Blacksburg, Virginia 24061, USA

[2] Tianjin Institute of Industrial Biotechnology, Chinese Academy of Sciences, 32 West 7th Avenue, Tianjin Airport Economic Area, Tianjin 300308, China

* Corresponding Author: Y.-H. Percival Zhang (ypzhang@vt.edu), Tel: 540-231-7414, Fax: 540-231-3199

Abstract

Coenzyme engineering that changes NAD(P) selectivity of redox enzymes is an important tool in metabolic engineering, synthetic biology, and biocatalysis. Here we developed a high throughput screening method to identify mutants of 6-phosphogluconate dehydrogenase (6PGDH) from a thermophilic bacterium *Moorella thermoacetica* with reversed coenzyme selectivity from $NADP^+$ to NAD^+. Colonies of a 6PGDH mutant library growing on the agar plates were treated by heat to minimize the background noise (i.e., deactivate intracellular dehydrogenases and degrade inherent NAD(P)H) and disrupt cell membrane. The melted agarose solution containing a redox dye tetranitroblue tetrazolium (TNBT), phenazine methosulfate (PMS), NAD^+, and 6-phosphogluconate was poured on colonies, forming a second semi-solid layer. More active 6PGDH mutants were examined via an enzyme-linked TNBT-PMS colorimetric assay. Positive mutants were recovered by direct extraction of plasmid from dead cell colonies followed by plasmid transformation into *E. coli* TOP10. By utilizing this double-layer screening method, six positive mutants were obtained from two-round saturation mutagenesis. The best mutant 6PGDH A30D/R31I/T32I exhibited a 4,278-fold reversal of coenzyme selectivity from $NADP^+$ to NAD^+. This screening method could be widely used to detect a large number of redox enzymes, which can generate NAD(P)H reacted with the redox dye TNBT.

Keywords: 6-phosphogluconate dehydrogenase, coenzyme engineering, cofactor engineering, directed evolution, high-throughput screening

Introduction

Nicotinamide adenine dinucleotide (NAD, which includes NAD^+ and NADH) and nicotinamide adenine dinucleotide phosphate (NADP, which includes $NADP^+$ and NADPH) play distinctive roles in catabolism and anabolism, respectively. NAD and NADP differ in an additional phosphate group esterified at the 2'-hydroxyl group of adenosine monophosphate moiety of NADP (**Fig. 1**). Numerous redox enzymes use NAD(P) as a coenzyme, which is usually held within the Rossmann fold. Coenzyme engineering that changes coenzyme selectivity (i.e., NAD vs. NADP) of dehydrogenases and reductases is one of the important tools for metabolic engineering and synthetic biology. For example, to produce high-yield biofuels (e.g., butanol, fatty acid esters) under anaerobic conditions, it is essential to balance NADH generation and NAD(P)H consumption (Bastian et al. 2011; Brinkmann-Chen et al. 2013; Huang and Zhang 2011). In addition to using transhydrogenase to transfer hydride ion equivalents (H^-) from NADH to NADPH (Gameiro et al. 2013; Hou et al. 2009), coenzyme engineering matching coenzyme selectivity of dehydrogenases and reductases is essential to achieve nearly theoretical product yields (Bommareddy et al. 2014; Ehsani et al. 2009; King and Feist 2014). Coenzyme engineering is also essentially important in biocatalysis. Most times, changing the coenzyme selectivity of dehydrogenases from NADP to NAD is preferable due to (1) NAD is less costly than NADP (Rollin et al. 2013; Woodyer et al. 2003) and (2) NADH is more stable than NADPH (Banta and Anderson 2002; Wong and Whitesides 1981; Wu et al. 1986). Also, there are more NADH regeneration enzymes than NADPH regeneration enzymes (van der Donk and Zhao 2003). Intensive studies have been conducted for changing coenzyme selectivity of dehydrogenases from NADP to NAD (Brinkmann-Chen et al. 2013; Lerchner et al. 2013; Scrutton et al. 1990) and from NAD to NADP (Hoelsch et al. 2013; Johannes et al. 2007; Zheng

et al. 2013) as well as broadening coenzyme selectivity (Woodyer et al. 2003). Recent coenzyme engineering studies have expanded the coenzyme selectivity of some redox enzymes to biomimetic coenzymes (Ji et al. 2011; Paul et al. 2014; Rollin et al. 2013; Zhang et al. 2016).

Directed evolution is one of the powerful protein engineering tools that can change enzymes' substrate selectivity. The most challenging task of directed evolution is the efficient identification of desired mutants from a large mutant library (Liu et al. 2009). As for coenzyme engineering, the use of 96-well microplate screening based on the absorbency of NAD(P)H at 340 nm is a straightforward choice (Brinkmann-Chen et al. 2013). Also, the signal of NAD(P)H can be detected by colorimetric redox indicators. For example, the Arnold's group utilized a redox dye nitroblue tetrazolium (NBT) plus catalyst phenazine methosulfate (PMS) to determine enhanced thermal stability of 6-phosphogluconate dehydrogenase (6PGDH) with the natural coenzyme ($NADP^+$) in the cell lysate of *E. coli* (Mayer and Arnold 2002). Later, Zhao and his coworkers applied this method to find out dehydrogenase mutants with relaxed coenzyme selectivity (Woodyer et al. 2003). However, the microplate-based screening is labor-intensive and time-consuming, involving colony picking, liquid cell culture, cell lysis, centrifugation, and enzyme activity assay. Due to high background noise of the intracellular reducing compounds and other redox enzymes in the cell lysate, Banta et al. utilized native gels to separate mutants of 2,5-diketo-D-gluconic acid reductase from the cell lysate, followed by the measurement of UV absorbency changes (Banta and Anderson 2002). However, this method required more steps and had lower capability of screening. Holbrook and his coworkers (El Hawrani et al. 1996) developed a method to duplicate colonies from Petri dishes to nitrocellulose paper followed by cell lysis by using lysozyme, detergent, and heat treatment. The targeted dehydrogenase activity was measured by the NBT-PMS assay (El Hawrani et al. 1996). Later, Ellington's group applied

this method to identify lactate dehydrogenase mutants with their coenzyme preference change from NAD^+ to $NADP^+$ (Flores and Ellington 2005). Nevertheless, this screening method still requires a lot of steps and the throughput is modest due to smearing effect of colony duplication on nitrocellulose paper (El Hawrani et al. 1996). Therefore, it is urgently needed to develop a simple and effective high-throughput screening method to determine coenzyme selectivity change of dehydrogenases.

6-phosphogluconate dehydrogenase (6PGDH, EC 1.1.1.44), the third enzyme in the pentose phosphate pathway, converts the 6-phophogluconate and $NADP^+$ to ribulose 5-phosphate, NADPH, and CO_2. 6PGDH from a thermophilic bacterium *Moorella thermoacetica* was utilized to generate NADPH for the high-yield hydrogen production (Rollin et al. 2015) and generate NADH for electricity generation in biobattery (Zhu et al. 2014), but the catalytic efficiency (k_{cat}/K_m) for $NADP^+$ was far higher than that for NAD^+. Increasing this enzyme's coenzyme selectivity for NAD^+ could be important to decrease $NADP^+$ use and increase lift-time of biobattery and other applications, such as low-cost biohydrogenation powered by sugars (Wang et al. 2011).

In this study, we developed a simple Petri-dish-based double-layer screening for the identification of 6PGDH mutants with enhanced catalytic efficiencies for NAD^+, where the second agarose layer contained a redox dye tetranitroblue tetrazolium (TNBT), a catalyst PMS, 6-phophogluconate, and NAD^+ and positive mutants were observed by darker color of heat treated colonies. Via this method, several 6GPDH mutants were identified with coenzyme selectivity reversed from $NADP^+$ to NAD^+.

Results

Dual promoter plasmid for screening and protein expression

For directed evolution, it is important to create the library with a large number of mutants and express enough recombinant proteins for characterization. In this study, the dual *T7-tac* promoter was constructed to control the expression of 6PGDH in both high transformation efficiency host *E. coli* TOP10 and high protein expression host *E.coli* BL21(DE3) (**Fig. 2a**). Plasmids and strains were listed in Table 1. Plasmid pET28a-P_{tac}-*6pgdh* consists of a strong inducible promoter *T7*, a modest inducible promoter *tac*, a lac operator, a ribosome binding site (RBS) and downstream *6pgdh* gene. In *E. coli* TOP10, the modest expression of 6PGDH was accomplished by the *tac* promoter, while the *T7* promoter was inactive due to a lack of T7 RNA polymerase. In *E. coli* BL21(DE3), high expression levels of 6PGDH was obtained under the control of both *T7* and *tac* promoter. As SDS-PAGE analysis showed, although the 6PGDH expression was modest in *E. coli* TOP10, the 6PGDH expression level in *E. coli* BL21(DE3) was high and displayed 4.3-fold greater than that in *E. coli* TOP10 (**Fig. 2b**).

Optimization of screening conditions

The mechanism of colorimetric assay in double-layer screening was shown in **Fig. 3**. The reduced NADH generated by 6PGDH reacts with TNBT in the presence of PMS, yielding a black TNBT-formazan. Heat-treatment was applied to reduce the background noise from host mesophilic enzymes and metabolites (e.g., NADPH and NADH) (Berridge et al. 2005; Fahimi and Karnovsky 1966; Ishizuka et al. 1992) and disrupt cell membranes for NAD^+ diffusion (Ninh et al. 2015; Zhou et al. 2011). For choosing the optimal heat-treatment temperature, two control colonies of *E. coli* TOP10, positive colonies with pET28a-P_{tac}-*6pgdh* and negative colonies with

pET28a-P_{tac}, were treated at 23, 60, 70 and 80ºC for 1 h and color changes were observed after overlaying the second layer. As the result showed in **Fig. 4a**, the positive colonies and the negative colonies treated at 23ºC (no heat-treatment) developed the same black color. When the heat-treatment temperature was greater than 70ºC, the colonies of the negative control did not develop the black color, indicating the reduced background noises. From the colonies of positive control expressing 6PGDH, the colonies exhibited the darker color with haloes regardless of heat-treatment temperatures. Based on the result, the optimal heat-treatment temperature was 70ºC.

The screening conditions were also influenced by NAD^+ concentration and reaction time. As shown in **Fig. 4b**, the *E. coli* colonies expressing 6PGDH developed darker color and larger haloes with increasing NAD^+ concentration and time interval. The colonies with the second layer containing 0 mM NAD^+ started developing the dark color after 2 h, while *E. coli* TOP10 colonies (pET28a-P_{tac}) did not develop the color under the same condition (data not shown), implying that the heat-treatment was not enough to degrade *E. coli* $NAD(P)^+$ completely (Hofmann et al. 2010; Honda et al. 2016). To minimize the impact of *E. coli* inherent $NAD(P)^+$, the screening time was recommended to be less than 2 h.

Screening 6PGDH mutants for increasing NAD^+ activity

After optimization of heat-treatment temperature and color development time, the double-layer screening method was used to determine 6PGDH mutants' coenzyme selectivity change. **Fig. 5** and **Fig. S1** shows the image of a typical double-layer screening plate containing positive mutants compared to wild-type and negative mutants. It was found that the color densities of colonies were related to mutant activities for NAD^+ (data not shown).

To make a reasonable size mutant library with 5-fold coverage, the 6PGDH mutant library was conducted through two-round saturation mutagenesis. In the first round, the site-directed mutagenesis of R31 was conducted and approximately 200 colonies were screened. Two positive mutants, R31T and R31I, were identified and characterized (**Table 2**). Starting from the best mutant R31I, the two-site-saturated mutagenesis library A30/T32 was constructed. After screening of 5,000 mutants, another four positive mutants, R31I/T32G, A30C/R31I/T32K, A30E/R31I/T32D and A30D/R31I/T32I were identified.

Characterization of 6PGDH mutants

The activity and kinetic constants for $NAD(P)^+$ of wild-type 6PGDH and mutants were summarized in Table 2. Through the first round screening, the R31I had a double K_m value (26.5 μM) for $NADP^+$ and a one fourth K_m value (354 μM) for NAD^+ compared to those of wild-type. Similarly, the R31T exhibited a 3.5-fold reversal due to higher K_m value for $NADP^+$ and lower K_m value for NAD^+. Starting from R31I, the second round mutant R31I/T32G had higher K_m of 104.4 μM for $NADP^+$ than that of R31I but no significant change in K_m for NAD^+. The A30C/R31I/T32K obtained lower k_{cat} of 6.23 s^{-1} but much higher K_m of 698 μM for $NADP^+$. Meanwhile, its k_{cat} for NAD^+ decreased to 6.0 s^{-1} and the K_m for NAD^+ decreased to 404 μM. The A30E/R31I/T32D had a very low k_{cat} value of 3.1 s^{-1} but a high K_m value of 660 μM for $NADP^+$, resulting in catalytic efficiency for $NADP^+$ as low as 4.7 mM^{-1} s^{-1}. However, the k_{cat} and K_m for NAD^+ decreased to 10.8 s^{-1} and 127 μM, respectively, resulting in an increase in catalytic efficiency for NAD^+ to 85.1 mM^{-1} s^{-1}.

The best mutant was A30D/R31I/T32I in terms of k_{cat}/K_m for NAD^+. Comparing with wild-type, the k_{cat} value for $NADP^+$ decreased to 1.81 s^{-1} but the K_m value increased to 228 μM. On the other hand, the k_{cat} value for NAD^+ reduced to 5.75 s^{-1} and the K_m value decreased to

11.87 μM, which was comparable to the K_m value of wild-type for $NADP^+$ (13.9 μM). The catalytic efficiency of A30D/R31I/T32I for $NADP^+$ was decreased by 80-fold, while the catalytic efficiency for NAD^+ was increased by 54-fold, from 9 to 484.2 mM^{-1} s^{-1}, resulting in a 4,278-fold reversal of coenzyme selectivity from $NADP^+$ to NAD^+.

Discussion

Here we developed an easy high-throughput screening method based on double-layer Petri dishes for determining the coenzyme selectivity of 6PGDH for NAD^+. In this screening, the reduced NADH generated from 6-phosphogluconate catalyzed by 6PGDH mutants could react with TNBT, generating the black TNBT formazan. Although double-layer screening is a very classical enzyme- or microorganism-screening technique without costly instruments, it was surprising that there were few efforts in coenzyme engineering possibly due to multiple reasons. Compared to colony duplication developed by the Holbrook's group (El Hawrani et al. 1996), our method avoided colony duplication and possible smear effects during colony duplication, resulting in less labor and higher throughput screening capacity (e.g., 800 colonies per dish). Furthermore, we applied heat-treatment to kill the *E. coli* cells, disrupt cell membrane (Ninh et al. 2015; Ninh et al. 2013; Ren et al. 2007), degrade metabolites including NAD(P)H, and deactivate other *E. coli* enzymes that can work with NAD^+, but retain intracellular thermostable 6PGDH for a quick screening. This heat-treatment was efficient to decrease background interference and facilitate substrate mass transfer (**Fig. 4**) but it also killed the *E. coli* cells, resulting in a problem for recovering *E. coli* cells. To avoid living cell colony replication before heat-treatment as performed previously (Liu et al. 2009; Ye et al. 2012), we developed an alternative technique to recover the plasmid from dead *E. coli* colonies – picking black dead-cell colonies for micro-plasmid purification followed by the transformation of *E. coli* TOP10. We had a high-throughput screening capacity without any colony replication associated with smear effects and possible cross contamination.

The thermophilic redox enzymes are promising to be applied in biocatalysis because of the excellent thermal and operational stabilities. With the improved thermal stabilities of NAD^+

by *in vitro* salvage synthesis pathway (Honda et al. 2016) and the increased number of thermophilic redox enzymes from thermophiles (Wang and Zhang 2009) or engineered mesophilic counterparts (Mayer and Arnold 2002), the thermophilic redox enzymes have gained a great deal of interest as biocatalyst for the application in large scale (Turner et al. 2007). As a key issue involved in commercialization of biocatalytic processes, the coenzyme engineering of these enzymes will be continued and greatly needed in the future. The high-throughput screening method, which minimizes the background noise of *E.coli* and detects the specific activity of thermophilic redox enzymes, can be widely used in this important area. Besides that, this method can be possibly used on screening of mesophilic enzymes due to (1) thermal stabilities of mesophilic enzymes can be higher than the corresponding subtle mesophiles (Kwon et al. 2008). (2) Overexpressed enzymes are further thermal stabilized by intracellular factors such as high protein concentrations, salts, substrates and other general stabilizers (Vieille and Zeikus 2001). (3) Inherent counterpart of target redox enzyme can be knocked out to minimize the background noise (Mayer and Arnold 2002). Also, the heat-treatment temperature and observation time window in screening can be adjusted (e.g., treated at 60^{o}C and observed for 15 min) to reduce the negative effect on target enzymes and obtain the optimal signal-to-noise ratio.

It was essentially important to find out a suitable redox dye for detecting NADH. Our preliminary experiment had tested a few redox dyes, including methyl viologen (Do et al. 2009), benzyl viologen (Mihara et al. 2002), neutral red (Park and Zeikus 2000), methylene blue (Wilner et al. 2009) and TNBT (Fahimi and Karnovsky 1966; Ishizuka et al. 1992; Kugler 1979). It was found that TNBT was the best because black formazan was very stable in the exposure of air and it had the strongest color change comparing with controls (data not shown). For example, oxidized methylene blue (blue color) is a pH-dependent redox dye that can react with NADH.

But its reduced form (colorless) can react with oxygen in air, resulting in slow regeneration of blue color. As a result, this dye was not suitable for screening dehydrogenases whose specific activities were low on non-natural coenzymes.

The *E. coli* TOP10 is a good strain for mutant library construction because of the high transformation efficiencies (e.g., 10^{8-9} cfu/μg plasmid DNA). However, its ability of recombinant protein expression is much lower than that of *E. coli* BL21(DE3) utilizing the pET expression system, which suffers from low transformation efficiencies (e.g., 10^{6} cfu/μg plasmid DNA) and possible undesired DNA recombination. A typical directed evolution protocol often involves screening in *E. coli* TOP10 followed by subcloning of mutant's DNA sequences into pET plasmid and recombinant protein expression in *E. coli* BL21(DE3) (Shin et al. 2014; Weiß et al. 2014). To delete the subcloning step between screening and protein expression, we developed a dual promoter *T7-tac* (**Fig. 2a**). In *E. coli* TOP10 host growing on the LB medium, the *tac* promoter was responsible for modest expression of the target protein. In *E. coli* BL21(DE3) host plus IPTG, higher protein expression levels were achieved (**Fig. 2b**).

Six positive mutants were identified through two round mutant libraries. The arginine at position 31 of wild-type 6PGDH was critical to recognize 2'-phosphate of $NADP^+$ and formed double hydrogen bonds with 2'-phosphate by the side chain, which was supported by previous studies (Sundaramoorthy et al. 2007; Tetaud et al. 1999). Similarly, T32 made another hydrogen bond with 2'-phosphate through the side chain. Besides that, A30 was also responsible for the formation of the NADP-binding pocket because of close proximity to 2'-phosphate in the structure model (**Fig. 6a**). After one-site mutation to isoleucine, the mutant R31I lost the ability of binding the 2'-phosphate of $NADP^+$, resulting in a double increase in K_m for $NADP^+$ and a four-time decrease in NAD^+ (**Table 2**). Similarly, after mutating to threonine, the R31T had a

three-fold K_m increase for $NADP^+$ but a two-fold K_m decrease for NAD^+.

The A30D/R31I/T32I was the best mutant in terms of k_{cat}/K_m for NAD^+. In addition to R31I, the extra mutation of alanine to aspartate at position 30 formed new hydrogen bonds with both 2' and 3'-hydroxyl group of adenosine monophosphate moiety of NAD^+ (**Fig. 6b**) and helped increasing the binding affinity for NAD^+, further 30-fold decline in K_m for NAD^+ compared to R31I. The replacement to the other acidic amino acid glutamate at the same position was also found at A30E/R31I/T32D with 3-fold lower K_m for NAD^+ as compared to R31I. Recently, the mutant included replacement to aspartate at same position was reported for 6PGDH from *G. stearothermophilus* with slightly decreased K_m (Opgenorth et al. 2016). The mutation threonine to isoleucine at position 32 broke the residual hydrogen bonds with 2'-phosphate of $NADP^+$ and possibly decreased enzyme binding with $NADP^+$, another 55-fold decrease in catalytic efficiency for $NADP^+$. A decrease in binding affinity for $NADP^+$ due to a mutation to a hydrophobic amino acid at the same threonine position was also reported for sheep liver 6PGDH mutant T34A (Li and Cook 2006). Overall, a combination of the deletion of hydrogen bonds with 2' phosphate of $NADP^+$ at positions 31 and 32 and then addition of more hydrogen bonds with hydroxyl group of NAD^+ at position 30 resulted in a more than 4,000-fold reversal of coenzyme selectivity from $NADP^+$ to NAD^+.

In conclusion, a high-throughput screening method was established for determining the NAD^+ selectivity of 6PGDH mutants. This double-layer method based on the colorimetric TNBT-PMS assay dramatically decreased dehydrogenase screening labor. The best 6PGDH mutant A30D/R31I/T32I showed a 4,278-fold reversal of coenzyme preference from $NADP^+$ to NAD^+.

Materials and Methods

Chemicals, plasmids and strains

All chemicals were reagent grade or higher, purchased from Sigma-Aldrich (St. Louis, MO) or Fisher Scientific (Pittsburgh, PA), unless otherwise noted. The *M. thermoacetica* genomic DNA was purchased from the American Type Culture Collection (Manassas, VA). All enzymes for molecular biology experiments were purchased from New England Biolabs (NEB, Ipswich, MA). Strains, plasmids, and oligonucleotides used in this study are listed in **Table 1**.

Construction of pET28a-P$_{tac}$-*6pgdh*

Plasmid pET28a-P$_{tac}$-*6pgdh* was constructed as follows. The inserted *6pgdh* gene was amplified from *M. thermoacetica* genomic DNA by using a pair of primers 6PG_F/6PG_R and the linearized vector backbone was amplified from pET28a by using a pair of primers 28_back_F/28_back_R. The insertion and vector backbone were assembled into multimeric plasmids by prolonged overlap extension-PCR (You et al. 2012). The PCR product was directly transformed into *E. coli* TOP10, yielding pET28a-*6pgdh*. To make the dual promoter plasmid pET28a-P$_{tac}$-*6pgdh*, the linear backbone of plasmid pET28a-P$_{tac}$-*6pgdh* was amplified based on pET28a-*6pgdh* by using a pair of 5' phosphorylated primers T7_Tac_F/T7_Tac_R containing each half of the promoter P$_{tac}$ and was self-ligated by NEB Quick Ligation™ Kit. After transformation into *E. coli* TOP10, plasmid pET28a-P$_{tac}$-*6pgdh* was obtained.

Construction of mutant libraries by saturation mutagenesis

The two-round DNA mutant libraries were constructed by the NEB Phusion site-directed mutagenesis kit. In the first round, the single-site saturation mutagenesis library R31 was

amplified based on pET28a-P_{tac}-*6pgdh* by using a pair of degenerate primers 31_NNK_F/31_NNK_R. The two-site saturation mutagenesis library A30/T32 was amplified from plasmid of pET28a-P_{tac}-*6pgdh* (R31I) by using a pair of degenerate primers 30_32_NNK_F/30_32_NNK_R. PCR reaction solution (50 μL) containing 1 ng of plasmid template was conducted as follows: 98ºC denaturation for 1 min; 20 cycles of 98ºC denaturation for 30 s, 60ºC annealing for 30 s and 72ºC extension for 3 min; and 72ºC extension for 5 min. The PCR product was digested by *Dpn*I followed by purification of gel electrophoresis and Zymoclean™ Gel DNA Recovery Kit (Zymo Research, Irvine, CA). The purified plasmid library was transformed into *E. coli* TOP10 for screening.

Optimization of heat treated temperature and time window

In order to test optimal heat treated temperature and time window for screening, the TOP10 carrying blank plasmid pET28a-P_{tac} and TOP10 with pET28a-P_{tac}-*6pgdh* were cultivated on the 1.5% agar LB medium with 50 μM kanamycin at 37ºC overnight and at room temperature for another day. For optimizing heat treated temperature, colonies of TOP10 (pET28a-P_{tac}) and TOP10 (pET28a-P_{tac}-*6pgdh*) was treated at 23, 60, 70 and 80ºC for 1 h, respectively. After cooling down, 8 mL of 0.5% melted agarose solution (60ºC) containing final concentration of 50 mM Tris-HCl (pH 7.5), 50 μM TNBT, 10 μM PMS, 2 mM 6-phosphogluconate, and 1 mM NAD^+ was poured on the heat-treated colonies. After incubation at room temperature for 1 h, the 6PGDH activity of colonies was observed by the darkness of black color on white background. For detecting the suitable time window for screening, the colonies of TOP10 (pET28a-P_{tac}-*6pgdh*) were treated at 70ºC for 1 h. After cooling down, the heat treated cell was overlaid by the same melted agarose reagent solution except changing the final concentration of NAD^+ to 0, 0.1,

0.3 and 1 mM, respectively. The color change of different groups was then observed at room temperature for 0, 0.5, 1 and 2 h. Each treatment contained three independent replicates.

High-throughput screening of mutant libraries for increasing NAD^+ activity

The double-layer screening of 6PGDH mutants for NAD^+ was performed as follows. After transformation of the mutant plasmid library, the *E. coli* TOP10 cells were spread on the 1.5% agar LB medium containing 50 μM kanamycin with an expected colony number of 500-800 per Petri dish. The dishes were incubated overnight at 37ºC and at room temperature for another day to ensure enough recombinant 6PGDH expression due to the leaky activity of *tac* promoter in the LB medium (Xu et al. 2012). The colonies on plates were treated at 70ºC for 1 h to kill cells, deactivate *E. coli* mesophilic enzymes, and degrade metabolites and reduced coenzymes. Eight mL of 0.5% melted agarose solution (60ºC) containing final concentration of 50 mM Tris-HCl (pH 7.5), 50 μM TNBT, 10 μM PMS, 2 mM 6-phosphogluconate, and 1 mM (for library R31) or 0.1 mM (for library A30/T32) NAD^+ was poured on the heat-treated colonies. After incubation at room temperature for 1 h, positive colonies were identified based on the formation of black colors. The agarose gel containing the single colony was isolated and mixed with 200 μL of the P1 buffer of Zymo ZR Plasmid Miniprep™ kit to resuspend the cell. The plasmid extracted by the plasmid purification kit was transformed into *E. coli* TOP10 for plasmid purification and DNA sequencing.

Overexpression and purification of wild-type 6PGDH and mutants

Plasmid pET28a-P_{tac}-*6pgdh* of wild-type or mutants was transformed to *E. coli* TOP10 for screening and BL21(DE3) for overexpression and protein purification. The transformed cells

were grown in the LB medium with 50 μM kanamycin at 37ºC until A_{600} reached ~0.6-0.8 and then 0.1 mM IPTG was added to induce protein expression at 37ºC for 6 h. Cell pellets were harvested by centrifugation and then were re-suspended in a 20 mM sodium phosphate and 0.3 M NaCl buffer (pH 7.5) containing 10 mM imidazole. After sonication and centrifugation, the His-tagged protein in the supernatant was loaded onto the column packed with HisPur Ni-NTA Resin (Fisher Scientific, Pittsburgh, PA) and eluted with 20 mM sodium phosphate buffer (pH 7.5) containing 300 mM NaCl buffer and 250 mM imidazole. Mass concentration of protein was determined by the Bradford assay using bovine serum albumin (BSA) as the standard and the 6PGDH expression level in different strain and purified 6PGDH were checked by SDS-PAGE and analyzed by using densitometry analysis (ImageJ).

6PGDH activity assays

The activities of 6PGDH and mutants were measured in 100 mM HEPES buffer (pH 7.5) with final concentration of 2 mM 6-phosphogluconate, 2 mM $NAD(P)^+$, 5 mM $MgCl_2$ and 0.5 mM $MnCl_2$ at 50°C for 5 min, as described elsewhere (Zhu et al. 2014). The formation of NAD(P)H was measured at 340 nm by a UV/visible spectrophotometer (Beckman Coulter, Fullerton, CA). The enzyme unit was defined as one μmole of NAD(P)H produced per min. For determining enzyme kinetic parameters on coenzymes, the enzyme activity was measured in same buffer as described above except changing the concentration of $NAD(P)^+$ from 5 to 5000 μM. The result was regressed by GraphPad Prism 5 (Graphpad Software Inc, La Jolla, CA) and apparent K_m and k_{cat} for $NAD(P)^+$ of 6PGDH was given based on Michaelis-Menten nonlinear regression. All the reactions contained three independent replicates and fitted with linear range.

Structural analysis

The three-dimensional structure modeling of wild-type 6PGDH and mutants were built by SWISS-MODEL based on the human 6PGDH (PDB: 2JKV) with 39.4% sequence identity. The structures of $NADP^+$ and NAD^+ were built by using Chemdraw (PerkinElmer, Waltham, MA). Starting from the initial protein and coenzyme structures, the conformation space accessible by $NADP^+$ and NAD^+ binding to the corresponding coenzyme binding area was analyzed by using the Autodock program (Scripps Research Institute, La Jolla, CA).

Acknowledgment

This project cannot be carried out without the support of the Biological System Engineering Department, Virginia Polytechnic Institute and State University, Virginia, USA. This study is based upon work supported by the Department of Energy, Office of Energy Efficiency and Renewable Energy, Fuel Cell Technologies Office under Award Number DE-EE0006968. Funding to YPZ for this work was partially supported by the Virginia Agricultural Experiment Station and the Hatch Program of the National Institute of Food and Agriculture, U.S. Department of Agriculture. Also, RH thanked Professor James Bowie for project discussion and thanked Professors Ryan Senger and Xueyang Feng for accessing some of their lab instruments.

Author Contributions Statement

P.Z. and R.H. wrote the main manuscript text, table and figures. R.H. conducted major experiments. H.C. conducted experiments of structure modeling of 6PGDH in Figure 6. C.Z. and J.K. were involved project discussion. All authors reviewed the manuscript.

Competing Financial Interests statement

The authors declare no competing financial interests.

Corresponding author

Correspondence to Yi-Heng Percival Zhang.

References

Banta S, Anderson S. 2002. Verification of a novel NADH-binding motif: combinatorial mutagenesis of three amino acids in the cofactor-binding pocket of *Corynebacterium* 2,5-diketo-D-gluconic acid reductase. J. Mol. Evol. 55(6):623-631.

Banta S, Swanson BA, Wu S, Jarnagin A, Anderson S. 2002. Alteration of the specificity of the cofactor-binding pocket of *Corynebacterium* 2,5-diketo-D-gluconic acid reductase A. Protein. Eng. 15(2):131-140.

Bastian S, Liu X, Meyerowitz JT, Snow CD, Chen MM, Arnold FH. 2011. Engineered ketol-acid reductoisomerase and alcohol dehydrogenase enable anaerobic 2-methylpropan-1-ol production at theoretical yield in *Escherichia coli*. Metab. Eng. 13(3):345-352.

Berridge MV, Herst PM, Tan AS. 2005. Tetrazolium dyes as tools in cell biology: new insights into their cellular reduction. Biotechnol. Annu. Rev 11:127-152.

Bommareddy RR, Chen Z, Rappert S, Zeng AP. 2014. A de novo NADPH generation pathway for improving lysine production of *Corynebacterium glutamicum* by rational design of the coenzyme specificity of glyceraldehyde 3-phosphate dehydrogenase. Metab. Eng 25:30-37.

Brinkmann-Chen S, Flock T, Cahn JK, Snow CD, Brustad EM, McIntosh JA, Meinhold P, Zhang L, Arnold FH. 2013. General approach to reversing ketol-acid reductoisomerase cofactor dependence from NADPH to NADH. Proc. Natl. Acad. Sci. U. S. A. 110(27):10946-10951.

Do PM, Angerhofer A, Hrdy I, Bardonova L, Ingram LO, Shanmugam KT. 2009. Engineering *Escherichia coli* for fermentative dihydrogen production: potential role of NADH-ferredoxin oxidoreductase from the hydrogenosome of anaerobic protozoa. Appl. Biochem. Biotechnol. 153(1-3):21-33.

Ehsani M, Fernandez MR, Biosca JA, Dequin S. 2009. Reversal of coenzyme specificity of 2,3-butanediol dehydrogenase from *Saccharomyces cerevisae* and in vivo functional analysis. Biotechnol. Bioeng. 104(2):381-389.

El Hawrani AS, Sessions RB, Moreton KM, Holbrook JJ. 1996. Guided evolution of enzymes with new substrate specificities. J. Mol. Biol. 264(1):97-110.

Fahimi HD, Karnovsky MJ. 1966. Cytochemical localization of two glycolytic dehydrogenases in white skeletal muscle. J. Cell Biol 29(1):113-28.

Flores H, Ellington AD. 2005. A modified consensus approach to mutagenesis inverts the cofactor specificity of *Bacillus stearothermophilus* lactate dehydrogenase. Protein. Eng. Des. Sel. 18(8):369-377.

Gameiro PA, Laviolette LA, Kelleher JK, Iliopoulos O, Stephanopoulos G. 2013. Cofactor balance by nicotinamide nucleotide transhydrogenase (NNT) coordinates reductive carboxylation and glucose catabolism in the tricarboxylic acid (TCA) cycle. J. Biol. Chem. 288(18):12967-12977.

Hoelsch K, Suhrer I, Heusel M, Weuster-Botz D. 2013. Engineering of formate dehydrogenase: synergistic effect of mutations affecting cofactor specificity and chemical stability. Appl. Microbiol. Biotechnol. 97(6):2473-2481.

Hofmann D, Wirtz A, Santiago-Schübel B, Disko U, Pohl M. 2010. Structure elucidation of the thermal degradation products of the nucleotide cofactors NADH and NADPH by nano-ESI-FTICR-MS and HPLC-MS. Anal. Bioanal. Chem 398(7-8):2803-2811.

Honda K, Hara N, Cheng M, Nakamura A, Mandai K, Okano K, Ohtake H. 2016. In vitro metabolic engineering for the salvage synthesis of NAD+. Metab. Eng 35:114-120.

Hou J, Lages NF, Oldiges M, Vemuri GN. 2009. Metabolic impact of redox cofactor perturbations in *Saccharomyces cerevisiae*. Metab. Eng. 11(4-5):253-261.

Huang W-D, Zhang Y-HP. 2011. Analysis of biofuels production from sugar based on three criteria: Thermodynamics, bioenergetics, and product separation. Energy. Environ. Sci. 4(3):784-792.

Ishizuka H, Tokuoka K, Sasaki T, Taniguchi H. 1992. Purification and some properties of an erythrose reductase from an Aureobasidium sp. mutant. Biosci. Biotechnol. Biochem. 56(6):941-945.

Ji D, Wang L, Hou S, Liu W, Wang J, Wang Q, Zhao ZK. 2011. Creation of bioorthogonal redox systems depending on nicotinamide flucytosine dinucleotide. J. Am. Chem. Soc. 133(51):20857-20862.

Johannes TW, Woodyer RD, Zhao H. 2007. Efficient regeneration of NADPH using an engineered phosphite dehydrogenase. Biotechnol. Bioeng 96(1):18-26.

King ZA, Feist AM. 2014. Optimal cofactor swapping can increase the theoretical yield for chemical production in *Escherichia coli* and *Saccharomyces cerevisiae*. Metab. Eng. 24:117-128.

Kugler P. 1979. A gel-sandwich technique for the qualitative and quantitative determination of dehydrogenases in the enzyme histochemistry. I. Development of the new methods on the example of LDH (E.C. 1.1.1.27). Histochemistry. 60(3):265-293.

Lerchner A, Jarasch A, Meining W, Schiefner A, Skerra A. 2013. Crystallographic analysis and structure-guided engineering of NADPH-dependent Ralstonia sp. alcohol dehydrogenase toward NADH cosubstrate specificity. Biotechnol. Bioeng. 110(11):2803-2814.

Li L, Cook PF. 2006. The 2'-phosphate of NADP is responsible for proper orientation of the nicotinamide ring in the oxidative decarboxylation reaction catalyzed by sheep liver 6-phosphogluconate dehydrogenase. J. Biol. Chem. 281(48):36803-36810.

Liu W, Hong J, Bevan DR, Zhang YH. 2009. Fast identification of thermostable beta-glucosidase mutants on cellobiose by a novel combinatorial selection/screening approach. Biotechnol Bioeng.

Mayer KM, Arnold FH. 2002. A colorimetric assay to quantify dehydrogenase activity in crude cell lysates. J. Biomol. Screen. 7(2):135-140.

Mihara H, Kato S-i, Lacourciere GM, Stadtman TC, Kennedy RA, Kurihara T, Tokumoto U, Takahashi Y, Esaki N. 2002. The *iscS* gene is essential for the biosynthesis of 2-selenouridine in tRNA and the selenocysteine-containing formate dehydrogenase H. Proc. Natl. Acad. Sci. U.S.A. 99(10):6679-6683.

Ninh PH, Honda K, Sakai T, Okano K, Ohtake H. 2015. Assembly and multiple gene expression of thermophilic enzymes in Escherichia coli for in vitro metabolic engineering. Biotechnol. Bioeng 112(1):189-196.

Ninh PH, Honda K, Yokohigashi Y, Okano K, Omasa T, Ohtake H. 2013. Development of a continuous bioconversion system using a thermophilic whole-cell biocatalyst. Appl. Environ. Microbiol. 79(6):1996-2001.

Opgenorth PH, Korman TP, Bowie JU. 2016. A synthetic biochemistry module for production of bio-based chemicals from glucose. Nat. Chem. Biol.

Park DH, Zeikus JG. 2000. Electricity generation in microbial fuel cells using neutral red as an electronophore. Appl. Environ. Microbiol. 66(4):1292-1297.

Paul CE, Arends IW, Hollmann F. 2014. Is simpler better? Synthetic nicotinamide cofactor analogues for redox chemistry. ACS Catalysis 4(3):788-797.

Ren X, Yu D, Yu L, Gao G, Han S, Feng Y. 2007. A new study of cell disruption to release recombinant thermostable enzyme from *Escherichia coli* by thermolysis. J. Biotechnol 129(4):668-673.

Rollin JA, Martin del Campo J, Myung S, Sun F, You C, Bakovic A, Castro R, Chandrayan SK, Wu C-H, Adams MWW and others. 2015. High-yield hydrogen production from biomass by in vitro metabolic engineering: Mixed sugars coutilization and kinetic modeling. Proc. Natl. Acad. Sci. U. S. A. 112(16):4964-4969.

Rollin JA, Tam TK, Zhang Y-HP. 2013. New biotechnology paradigm: cell-free biosystems for biomanufacturing. Green. Chem. 15(7):1708-1719.

Scrutton NS, Berry A, Perham RN. 1990. Redesign of the coenzyme specificity of a dehydrogenase by protein engineering. Nature. 343(6253):38-43.

Shin H, Cho Y, Choe D-h, Jeong Y, Cho S, Kim SC, Cho B-K. 2014. Exploring the functional residues in a flavin-binding fluorescent protein using deep mutational scanning. PloS one. 9(6):e97817.

Sundaramoorthy R, Iulek J, Barrett MP, Bidet O, Ruda GF, Gilbert IH, Hunter WN. 2007. Crystal structures of a bacterial 6-phosphogluconate dehydrogenase reveal aspects of specificity, mechanism and mode of inhibition by analogues of high-energy reaction intermediates. Febs j 274(1):275-286.

Tetaud E, Hanau S, Wells JM, Le Page RW, Adams MJ, Arkison S, Barrett MP. 1999. 6-Phosphogluconate dehydrogenase from *Lactococcus lactis*: a role for arginine residues in binding substrate and coenzyme. Biochem. J. 338 (Pt 1):55-60.

van der Donk WA, Zhao H. 2003. Recent developments in pyridine nucleotide regeneration. Curr. Opin. Biotechnol. 14(4):421-426.

Wang Y, Huang W, Sathitsuksanoh N, Zhu Z, Zhang YH. 2011. Biohydrogenation from biomass sugar mediated by in vitro synthetic enzymatic pathways. Chem. Biol. 18(3):372-380.

Weiß MS, Pavlidis IV, Vickers C, Höhne M, Bornscheuer UT. 2014. Glycine oxidase based high-throughput solid-phase assay for substrate profiling and directed evolution of *(R)*-and *(S)*-selective amine transaminases. Anal. Chem. 86(23):11847-11853.

Wilner OI, Weizmann Y, Gill R, Lioubashevski O, Freeman R, Willner I. 2009. Enzyme cascades activated on topologically programmed DNA scaffolds. Nat. Nano. 4(4):249-254.

Wong C-H, Whitesides GM. 1981. Enzyme-catalyzed organic synthesis: NAD (P) H cofactor regeneration by using glucose-6-phosphate and the glucose-5-phosphate dehydrogenase from *Leuconostoc mesenteroides*. J. Am. Chem. Soc. 103(16):4890-4899.

Woodyer R, van der Donk WA, Zhao H. 2003. Relaxing the nicotinamide cofactor specificity of phosphite dehydrogenase by rational design. Biochemistry 42(40):11604-11614.

Wu JT, Wu LH, Knight JA. 1986. Stability of NADPH: effect of various factors on the kinetics of degradation. Clin. Chem. 32(2):314-319.

Xu J, Banerjee A, Pan SH, Li ZJ. 2012. Galactose can be an inducer for production of therapeutic proteins by auto-induction using *E. coli* BL21 strains. Protein Expr. Purif 83(1):30-36.

Ye X, Zhang C, Zhang YH. 2012. Engineering a large protein by combined rational and random approaches: stabilizing the Clostridium thermocellum cellobiose phosphorylase. Mol. Biosyst 8(6):1815-1823.

You C, Zhang XZ, Zhang Y-HP. 2012. Simple cloning via direct transformation of PCR product (DNA Multimer) to *Escherichia coli* and *Bacillus subtilis*. Appl. Environ. Microbiol. 78(5):1593-1595.

Zhang L, Yuan J, Xu Y, Zhang Y-HP, Qian X. 2016. New artificial fluoro-cofactor of hydride transfer with novel fluorescence assay for redox biocatalysis. *Chem. Comm*.

Zheng H, Bertwistle D, Sanders DA, Palmer DR. 2013. Converting NAD-specific inositol dehydrogenase to an efficient NADP-selective catalyst, with a surprising twist. Biochemistry. 52(34):5876-5883.

Zhou Y, Wang L, Yang F, Lin X, Zhang S, Zhao ZK. 2011. Determining the Extremes of the Cellular NAD(H) Level by Using an *Escherichia coli* NAD(+)-Auxotrophic Mutant. Appl. Environ. Microbiol 77(17):6133-6140.

Zhu Z, Kin Tam T, Sun F, You C, Zhang Y-HP. 2014. A high-energy-density sugar biobattery based on a synthetic enzymatic pathway. Nat. Commun. 5:3026.

Figure Legends

Figure 1. Chemical structures of $NADP^+$ and NAD^+. Structures of $NADP^+$ and NAD^+ were shown and the additional phosphate group on NADP+ was highlighted in gray.

Figure 2. Validation of the dual *T7-tac* promoter for 6PGDH screening in *E. coli* TOP10 and protein expression in *E. coli* BL21(DE3). (a) plasmid design of pET28a-P*tac-6pgdh*. The DNA sequence of P*tac*, *lac* operator and RBS were shown as underlined, italic and lower case, respectively. (b) SDS-PAGE analysis of 6PGDH expression from *E. coli* TOP10 and BL21(DE3). M, protein marker; Control, pET28a-Ptac; WT, pET28a-P*tac-6pgdh*; P, purified *Moth*6PGDH. The 6PGDH was indicated with an arrow.

Figure 3. Scheme of the colorimetric assay for 6PGDH activity for NAD^+. 6PGDH oxidizes 6-phosphogluconate (6PG) into ribulose-5-phosphate and CO_2, and reduces NAD^+ to NADH. With the catalyst phenazine methosulphate (PMS), redox dye tetranitroblue tetrazolium (TNBT) is converted to black TNBT-formazan by the reduction of NADH.

Figure 4. Optimization of heat treated temperature and color development time. (a) Optimization of heat-treated temperature for screening. Colonies of *E. coli* TOP10 (pET28a-P*tac*) was set as a negative control and *E. coli* TOP10 (pET28a-P*tac-6pgdh*) was set as a positive control (6PGDH). Colonies were treated at 23, 60, 70 and 80oC for 1 h, respectively and observed after overlaying second layer. (b) Optimization of color development time. Heat-treated colonies of E. coli TOP10 (pET28a-P*tac-6pgdh*) was overlaid by second layer containing 0, 0.1, 0.3 and 1 mM NAD^+, and the color change profiles of colonies were photographed at 0, 0.5, 1 and 2 h.

Figure 5. Photo image of the double layer screening of the library containing two-site mutagenesis of A30/T32. The second layer contained 0.1 mM NAD^+. The color development time was 1 h. The positive mutants featuring darker colony color with halo were identified red arrows.

Figure 6. Surface view of wild-type 6PGDH with $NADP^+$ (a) and mutant A30D/R31I/T32I with NAD^+ (b). The amino acid residues A30, R31 and T32 of wild type 6PGDH and corresponding mutated residues of mutant A30D/R31I/T32I were depicted as sticks and replacements were marked as red. Atoms were colored based on types: N, blue; O, red; P, orange; C, green and H, white. Hydrogen bonding between residues and cofactor were shown as yellow line.

Table 1. The strains, plasmids, and oligonucleotides used in this study

Description	Contents	Reference/sources
Strain		
E. coli Bl21^{star}(DE3)	B F$^{–}$ *ompT gal dcm lon hsdS$_B$*($r_B^- m_B^-$) *rne131* (DE3)	Invitrogen
E. coli TOP10	F– *mcr*A cr*mrr-hsd*RMS-*mcr*BC) Φ80*lac*Zac80 Δ*lac*X74 *rec*A1 *ara*D139 Δ(*ara leu*) 7697 *gal*U *gal*K *rps*L (StrR) *end*A1 *nup*G	Invitrogen
Plasmid		
pET28a		Invitrogen
pET28a-*6pgdh*	Precusor of pET28a-P$_{tac}$-*6pgdh*	in this study
pET28a-P$_{tac}$-*6pgdh*	dual promoter (P$_{T7}$ and P$_{tac}$) and moth6pgdh	In this study
primers*		
28_back_F	5’-CGACCAAGACCGACTAAGCCGATATGCATATGTATATCTCCTTCTTAAAG-3’	pET28a
28_back_R	5’-GGCCACGACGTGGCCCGGAAACACCACCACCACCACCACTGAGAT-3’	
6PG_F	5’-CTTTAAGAAGGAGATATACATATGCATATCGGCTTAGTCGGTCTTGGTCG-3’	*Moorella thermoacetica*
6PG_R	5’-ATCTCAGTGGTGGTGGTGGTGTTTCCGGGCCACGTCGTGGCC-3’	
T7_Tac_F	5’-Phos-GGCTCGTATAATGTGTGGAATTGTGAGCGGATAACAATTC-3’	pET28a-*6pgdh*
T7_Tac_R	5’-Phos-GATGATTAATTGTCAACCTATAGTGAGTCGTATTAATTTCG-3’	
31_NNK_F	5’-GAAGTGCGAGGATACGCC**NNK**ACTAAGGCTACCGTGG-3’	pET28a-P$_{tac}$-*6pgdh*
31_NNK_R	5’-CCACGGTAGCCTTAGT**MNN**GGCGTATCCTCGCACTTC-3’	
30_32_NNK_F	5’-CATGGTCATGAAGTGCGAGGATAC**NNK**ATT**NNK**AAGGCTACCGTGGACAAAGC-3’	pET28a-P$_{tac}$-*6pgdh* R31I
30_32_NNK_R	5’-GCTTTGTCCACGGTAGCCTT**MNN**AAT**MNN**GTATCCTCGCACTTCATGACCATG-3’	

*Boldface nucleotide sequences indicate randomized positions.

Table 2. Kinetics parameters of 6PGDH and mutants

Mutations	K_m [μ M]		k_{cat} [s^{-1}]		k_{cat}/K_m [$mM^{-1} * s^{-1}$]		**Ratio k_{cat}/K_m**
	$NADP^+$	NAD^+	$NADP^+$	NAD^+	$NADP^+$	NAD^+	$NAD^+/NADP^+$
WT	13. 9±1.1	1397±111	8.73±0.02	12.6±0.4	628.8	9.0	0.014
R31T	35.5±1.7	605±47	10.83±0.13	9.12±0.23	305.6	15	0.049
R31I	26.5±1.3	354±12	11.53±0.15	15.01±0.17	435.0	42.4	0.097
R31I/T32G	104.4±5.4	362±23	11.9±0.16	12.94±0.27	114.0	35.8	0.31
A30C/R31I/T32K	698±49	404±33	6.23±0.18	6.0±0.2	8.9	14.8	1.66
A30E/R31I/T32D	660±64	127±7	3.1±0.1	10.8±0.2	4.7	85.1	18.1
A30D/R31I/T32I	228±16	11.87±0.55	1.81±0.05	5.75±0.05	7.9	484.2	61.1

Each value represents the average of three independent measurements.

Figure 1. Chemical structures of $NADP^+$ and NAD^+

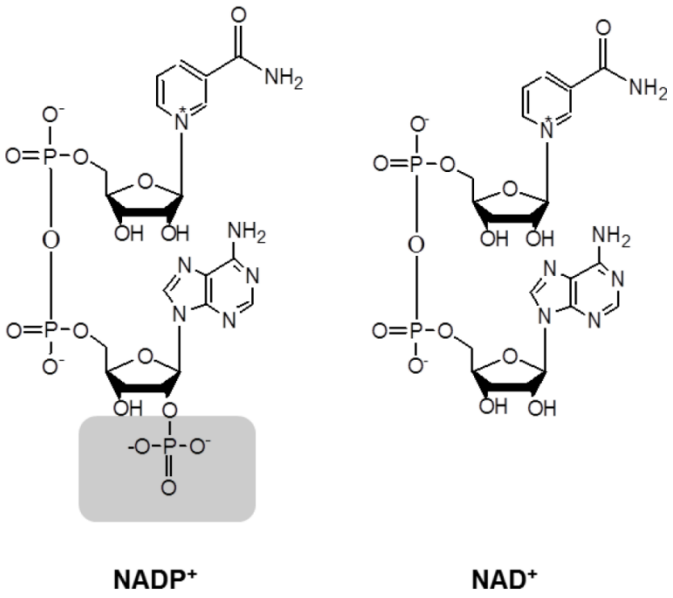

Figure 2. Validation of the dual *T7-tac* promoter for 6PGDH screening in *E. coli* TOP10 and protein expression in *E. coli* BL21(DE3)

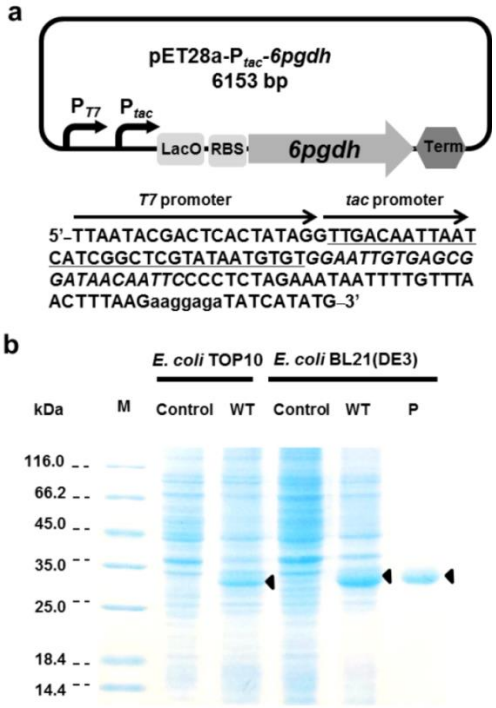

Figure 3. Scheme of the colorimetric assay for 6PGDH activity for NAD^+

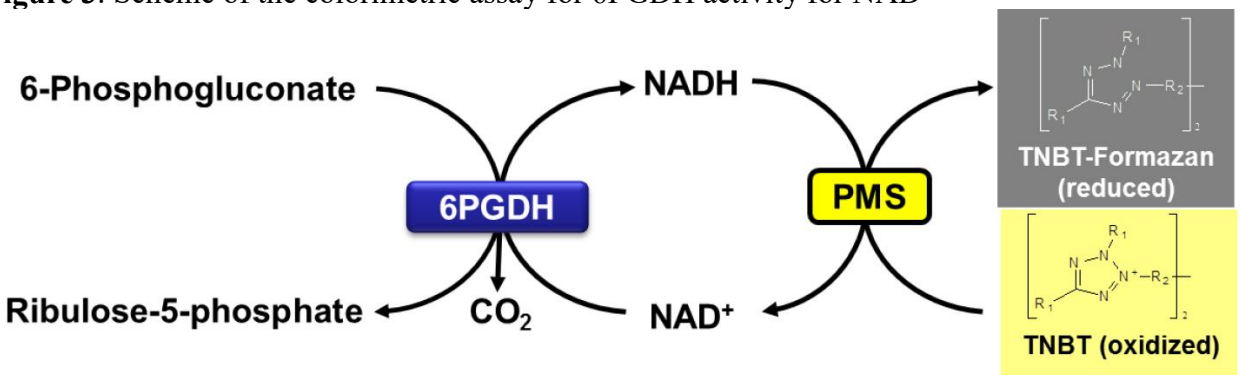

Figure 4. Optimization of heat treated temperature and color development time

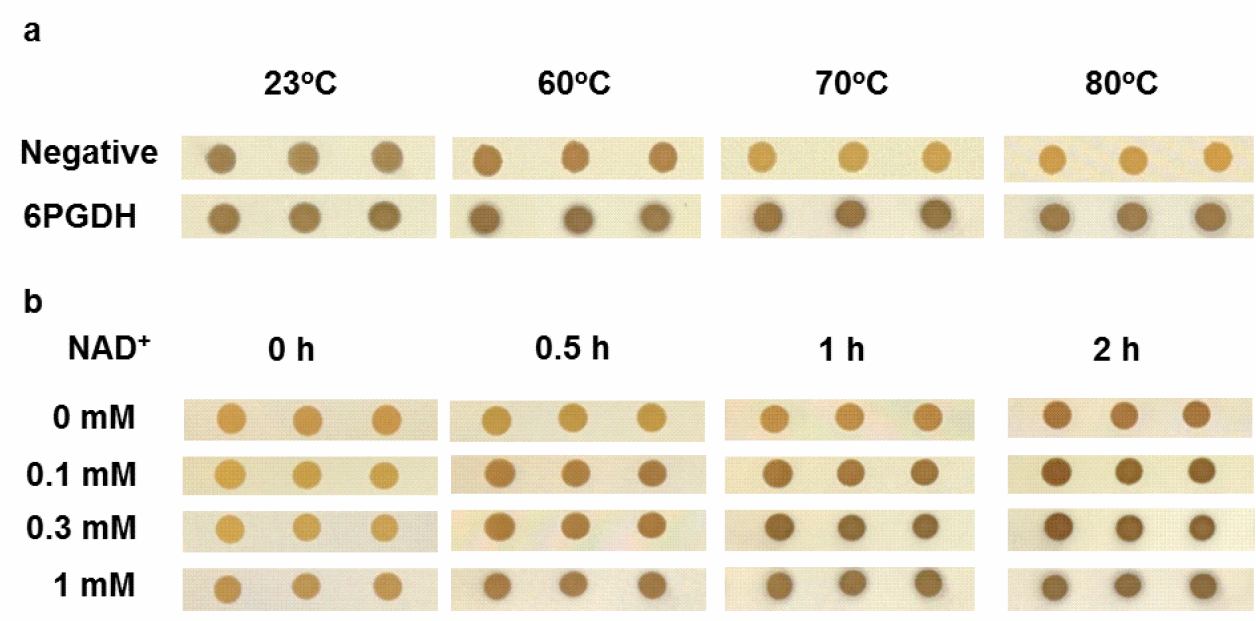

Figure 5. Photo image of the double layer screening of the library containing two-site mutagenesis of A30/T32

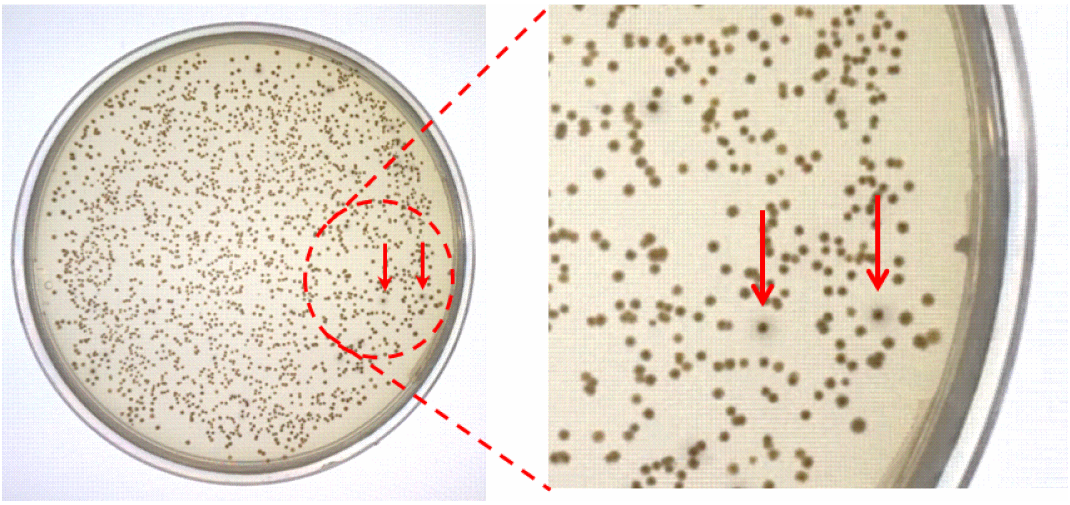

Figure 6. Surface view of wild-type 6PGDH with $NADP^+$ and mutant A30D/R31I/T32I with NAD^+

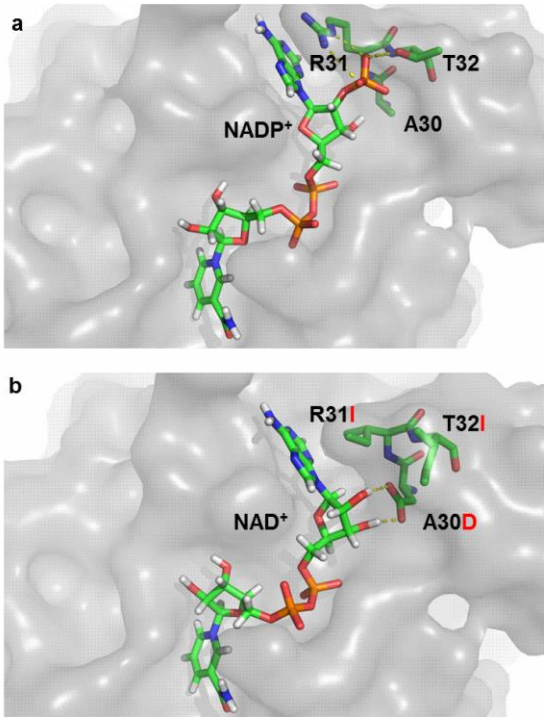

Chapter 4. Engineering a thermostable highly active glucose 6-phosphate dehydrogenase and its application to biohydrogen production *in vitro*

Rui Huang[1], Hui Chen[1], Wei Zhou[2], Chunling Ma[2], Yi Heng Percival Zhang[1,2*]

[1] Biological Systems Engineering Department, Virginia Tech, 304 Seitz Hall, Blacksburg, Virginia 24061, USA

[2] Tianjin Institute of Industrial Biotechnology, Chinese Academy of Sciences, 32 West 7th Avenue, Tianjin Airport Economic Area, Tianjin 300308, China

* Corresponding Author: Y.-H. Percival Zhang (ypzhang@vt.edu), Tel: 540-231-7414, Fax: 540-231-3199

Abstract

Glucose 6-phosphate dehydrogenase (G6PDH) is one of the most important dehydrogenases responsible for generating reduced NADPH for anabolism and is also the rate-limiting enzyme in the Entner-Doudoroff pathway. For *in vitro* biocatalysis, G6PDH must possess both high activity and good thermostability due to requirements of efficient use and low expense of biocatalyst. Here we used directed evolution to improve thermostability of the highly active G6PDH from *Zymomonas mobilis*. Four generations of random mutagenesis and Petri-dish-based double-layer screening evolved the thermolabile wild-type enzyme to the thermostable mutant Mut 4-1, which showed a more than 124-fold increase in half-life time ($t_{1/2}$) at 60ºC, a 3.4ºC increase in melting temperature (T_m), and a 5ºC increase in optimal temperature (T_{opt}), without compromising the specific activity. In addition, the thermostable mutant was conducted to generate hydrogen from maltodextrin via *in vitro* synthetic biosystems (ivSB), gaining a more than 8- fold improvement of productivity rate with 76% of theoretical yield at 60ºC. Thus, the engineered G6PDH has been shown to effectively regenerate NADPH at high temperatures and will be applicable for NAD(P)H regeneration in numerous *in vitro* biocatalysis applications.

Key words: Glucose 6-phosphate dehydrogenase, thermostability, high activity, biohydrogen, directed evolution

Introduction

Glucose 6-phosphate dehydrogenase (G6PDH, EC 1.1.1.49) catalyzes the oxidation of glucose 6-phosphate (G6P) to 6-phosphogluconolactone (6PGL) with the concomitant reduction of $NADP^+$ to NADPH. It is the first enzyme of the pentose phosphate pathway and one of the key enzymes in central metabolism (Iyer et al. 2002). It is also the rate-limiting enzyme of the Entner-Doudoroff (ED) pathway in *Zymomonas mobilis*, one of the fastest sugar utilizing microorganisms (Conway 1992; He et al. 2014). Because G6PDH is one of the most important enzymes for cellular NADPH regeneration, its overexpression has been used to produce sufficient NADPH in metabolic engineering and synthetic biology applications *in vivo* (Sekar et al. 2017; Zhao et al. 2015).

G6PDHs are distributed widely in many species from bacteria to humans. The G6PDH from *Z. mobilis* (*Zm*G6PDH), one of the most active characterized G6PDHs, has specific activities of 316 and 852 U/mg at 30 and 60°C (**Table 1**), respectively. However, this enzyme is not thermostable and loses its activity rapidly at elevated temperatures with a half-life time ($t_{1/2}$) of about seven minutes at 60°C (**Table 1**), which is inacceptable for biocatalysis processes (i.e., hydrogen) operating at high temperature (Kim et al. 2016). A few G6PDHs from hyperthermophilic microorganisms have been characterized and show increased thermostability. However, they have much lower specific activities compared to those of their mesophilic counterparts (**Table 1**), resulting in the poor space-time yield. Essentially, it is important to develop BioBrick enzymes (i.e., G6PDH) with both high specific activities (i.e., faster reaction) and great thermostability (i.e., prolonged lifetimes) so they can be used in effective and economically feasible ways for *in vitro* biocatalysis

applications, such as production of hydrogen (Rollin et al. 2015), bioelectricity (Zhu et al. 2014; Zhu and Zhang 2017), and NAD(P)H regeneration (Wang et al. 2011).

Directed evolution is a powerful engineering tool to improve enzyme properties without knowledge of protein structure and catalytic mechanism. It has been used to improve thermostability of numerous enzymes (Baik et al. 2003; Johannes et al. 2005; McLachlan et al. 2008; Zheng et al. 2017). For example, Arnold and coworkers evolved *Bacillus subtilis* esterase to thermostable mutants without compromising its specific activity at low temperatures by screening mutants retaining high activity and increased thermostability (Giver et al. 1998). Zhao and coworkers applied the same strategy to increase the thermostability of *Pseudomonas stutzeri* phosphite dehydrogenase greatly (>7,000 fold greater half-life time at 45^{o}C) with slightly higher catalytic efficiency (Johannes et al. 2005). A highly active G6PDH from a mesophilic bacterium *Leuconostoc mesenteroides* was engineered to increase thermostability through directed evolution (Kusumoto et al. 2010). However, in this approach, the best mutant retained 60% activity at 50^{o}C for 1 h. This half-life time must be improved further for use of G6PDH in numerous *in vitro* biocatalysis applications (Kim et al. 2016; Rollin et al. 2015; Wang et al. 2011; Zhu et al. 2014).

The most challenging task of directed evolution is the effective identification of desired mutants from large libraries. This is often quoted as, ‘‘you get what you screen for’’ (You and Arnold 1996). The 96-well microplate-based screening is a straightforward method to measure residual enzyme activities after heat treatment (Mayer and Arnold 2002). However, this method is labor-intensive and requires costly automated instruments. Several Petri-dish-based screening methods have been developed to avoid colony picking and the

microplate-based screening. For example, beta-glucosidase mutants have been selected based on cell growth on cellobiose followed by facilitated screening using the growth of a second indicator strain (Liu et al. 2009). Mutants of thermophilic $NADP^+$-preferred 6-phosphogluconate dehydrogenase (6PGDH) have been screened using a Petri-dish-based double-layer method for their enhanced activities on NAD^+ (Huang et al. 2016). Activities of positive mutants were able to be measured using heat treatment followed by tetranitroblue tetrazolium (TNBT)/ phenazine methosulfate (PMS) colorimetric assay. However, this screening method requires thermophilic dehydrogenases as the engineering template because the heat treatment can deactivate mesophilic redox enzymes and reduced compounds inside the cell.

In this work, we started with *Zm*G6PDH, one the most active G6PDHs, and applied directed evolution to enhance its thermostability. We expanded the previous Petri-dish-based double-layer screening method that was limited to thermophilic enzymes to this mesophilic dehydrogenase. Via multiple rounds of random mutagenesis and screening, the best mutant was obtained with both high specific activity and improved thermostability. Furthermore, this mutant was used to demonstrate enhanced performance in hydrogen generation from maltodextrin via ivSB at high temperature.

Material and Methods

Chemicals and Media

All chemicals were reagent grade, purchased from Fisher Scientific (Pittsburgh, PA, USA) or Sigma-Aldrich (St. Louis, MO, USA), unless otherwise noted. The genomic DNA of *Z. mobilis* ATCC31821 was gifted from Dr. Min Zhang of the National Renewable Energy Laboratory (Golden, CO, USA). The primers were synthesized from Integrated DNA Technologies (Coralville, IA, USA). All enzymes for molecular biology experiments were purchased from New England Biolabs (NEB, Ipswich, MA, USA). Strains, plasmids, and primers are listed in **Table 2**.

Preparation of plasmid pET28a-P*tac-g6pdh*

Plasmid pET28a-P*tac-g6pdh* containing 1,455-bp wild-type *Z. mobilis g6pdh* gene (GenBank accession number: AHJ70511.1) under control of dual promoter P*T7*-P*tac* was constructed for screening and overexpression of *Zm*G6PDH. The inserted *g6pdh* gene was amplified from *Z. mobilis* genomic DNA with a pair of primers G6P_F/G6P_R and the linearized vector backbone was amplified from pET28a-P*tac-6pgdh* with a pair of primers Vect_F/Vect_R by using the NEB Phusion® high-fidelity DNA polymerase. The two PCR fragments were assembled by prolonged overlap extension PCR (POE-PCR) (You et al. 2012). The POE-PCR product was transformed into *E.coli* TOP10, yielding the plasmid pET28a-P*tac-g6pdh*.

Random mutagenesis and library creation

A random mutant library encoding *g6pdh* gene was generated by error-prone PCR with a pair of primers G6P_F/G6P_R. The reaction solution with a total volume of 50 μL contained 5 ng/μL plasmid pET28a-P*tac*-g6pdh, 0.2 mM dATP, 0.2 mM dGTP, 1 mM dCTP, 1 mM dTTP, 5 mM $MgCl_2$, 0.004 mM $MnCl_2$, 0.05 U/μL the NEB regular Taq polymerase and 0.4 μM primer pairs (G6P_F/G6P_R). The PCR reaction was conducted as follows: 1 cycle of 94ºC for 2 min; 16 cycles of 94ºC for 30 s, 60ºC for 30 s, 68ºC for 1.5 min; and an extension cycle of 68ºC for 5 min. The linearized vector backbone was amplified from pET28a-P*tac*-6pgdh as described above. The two PCR products after digestion by *Dpn*I were purified and assembled into multimerized plasmid using POE-PCR. The multimerized plasmid was digested to monomer linearized plasmid by *Xho*I followed by DNA purification and ligation (You and Zhang 2012). The 5 μg of ligation product was transformed into *E.coli* TOP10 competent cell, yielding around 20,000 mutants for screening. The mutation rate was estimated by sequencing the *Zmg6pdh* gene from ten randomly picked mutants for each library. To validate the accuracy of DNA sequencing, both sense and antisense strands were sequenced.

Screening of thermostable mutants of *Zm*G6PDH

For identification of thermostable mutants of *Zm*G6PDH, a Petri-dish based double-layer screening method was carried-out based on the heat treatment and TNBT/PMS colorimetric assay as described previously (Huang et al. 2016), with minor modifications as follows. Transformed cells containing a mutant plasmid library were spread on 1.5% agar

solid LB medium with 50 μg/mL kanamycin to obtain an expected colony number of 500–800 per Petri-dish. The Petri-dish was incubated at 37°C for 48 hours to ensure enough recombinant *Zm*G6PDH expression by leakage of the *tac* promoter (Simon et al. 1994). For the first round of screening, Petri-dish colonies were heated to 70°C for 1 hour to lyse cells, degrade reduced coenzymes, and deactivate *E. coli* mesophilic redox enzymes, such as *E. coli* G6PDH as well as most negative mutants of *Zm*G6PDH. Eight mL of the color development solution (60°C) comprised of 0.5% agarose, 50 mM Tris-HCl (pH 7.5), 50 μM TNBT, 10 μM PMS, 2 mM G6P, and 1 mM $NADP^+$ was poured onto the heat-treated colonies. After incubation at room temperature for 2 hours, the thermostable mutants of *Zm*G6PDH were identified based on their darker color, and were isolated from Petri-dish by using sterile toothsticks followed by suspension in 200 μL of P1 buffer of Zymo ZR Plasmid Miniprep™ kit. Plasmids of positive mutants were extracted based on the protocol of Zymo ZR Plasmid Miniprep™ kit (Zymo Research Corp, Irvine, CA, USA) and transformed into *E. coli* TOP10 for DNA sequencing and *E. coli* BL21(DE3) for protein overexpression, respectively. For the second, third and fourth rounds of screening, colonies on Petri-dishes were heated to 70°C for 1.5, 2 and 2.5 hours, respectively. Positive mutants identified in the first, second, third and fourth generations were purified, diluted (1 μg/mL) and incubated in 100 mM HEPES buffer (pH 7.5) with 5 mM $MgCl_2$ and 0.5 mM $MnCl_2$ at 60°C for 0.5, 2, 9 and 12 hours, respectively. The initial and residual activities of mutants were measured based on the absorbency of NADPH at 340 nm. The mutant that showed highest ratio of residual activity to initial activity and no greatly loss of initial activity compared to that of the parent enzyme were selected and characterized for the next round of random mutagenesis and screening.

Protein overexpression and purification

The *E. coli* BL21(DE3) strains harboring plasmid encoding the *Zm*G6PDH or mutants were grown in LB medium with 50 μM kanamycin at 37ºC. The IPTG-inducible overexpression and Ni-NTA purification of targeted enzyme was conducted as described previously (Huang et al. 2016). Mass concentrations of purified proteins were determined by Bradford assay with bovine serum albumin as the standard.

Activity assay of *Zm*G6PDH and mutants

Activities of wild-type *Zm*G6PDH and mutants were measured in 100 mM HEPES buffer (pH 7.5) containing 2 mM G6P, 1 mM $NADP^+$, 5 mM $MgCl_2$ and 0.5 mM $MnCl_2$ for 3 minutes. The formation of NADPH was measured at 340 nm using a UV/visible spectrophotometer (Beckman Coulter, Fullerton, CA), where the millimolar extinction coefficients (ε) of NADPH is 6.22 mM^{-1} cm^{-1}. The enzyme unit was defined as one μmole of NADPH produced per minute. For determining the enzymatic optimal temperature, activities of G6PDHs were measured with 0.01 μg/mL enzyme in the same buffer from 23 to 70ºC. For determining steady-state kinetics of *Zm*G6PDH and mutants, enzyme activities were measured in the same buffer with 5-1000 μM $NADP^+$ and 30-1000 μM G6P at 30ºC. All the reactions were conducted in triplicate. All points were fit simultaneously to the ordered Bi-Bi rate equation (**Equation 1**), where the reaction mechanism was previously verified (Kanji et al. 1976). The kinetic constants were estimated by nonlinear least squares regression (SigmaPlot 12.5, San Jose, CA, USA). Reported errors are standard deviations.

$$V = \frac{\mathrm{E} * k_{cat} * [\mathrm{NADP}] * [\mathrm{G6P}]}{K_{ia}^{NADP} * K_M^{G6P} + K_M^{G6P} * [\mathrm{NADP}] + K_M^{NADP} * [\mathrm{G6P}] + [\mathrm{NADP}] * [\mathrm{G6P}]} \quad [1]$$

Half-life time of thermal deactivation

The purified protein (1 μg/mL) was incubated in 100 mM HEPES buffer (pH 7.5) containing 5 mM $MgCl_2$ and 0.5 mM $MnCl_2$ at 60ºC. Small aliquots were taken at specific time points and chilled on ice for 5 minutes. Residual activities of enzymes were measured at 30ºC as described above. Half-life times ($t_{1/2}$) of thermal deactivation were calculated using linear regression equation of semi-log plot of relative residual activities versus incubation time. All reactions were conducted in triplicate. Reported errors are standard deviations.

Estimation of total turnover number of *Zm*G6PDH

The total turnover number (TTN) of wild-type enzyme and final mutant Mut 4-1 were estimated based on their half-life times and specific activities at 60ºC and calculated by using the **equation 2** (Rogers and Bommarius 2010), where the molecular weight of *Zm*G6PDH was computed as 5.5 x 10^4 g/mol by using the online calculation tool https://web.expasy.org/compute_pi/.

$$TTN = \frac{Specific\ activity\left(\frac{U}{mg}\right) * enzyme\ molecular\ weight\left(\frac{g}{moi}\right) * half{-}life\ time\ (h) * 6}{ln2 * 100} \quad [2]$$

Differential scanning calorimetry analysis

Differential scanning calorimetry (DSC) was performed to determine the melting temperature (T_m) of G6PDHs by using VP-cap DS calorimeter (MicroCal, Inc. Northampton, MA, USA) with a scanning rate of 1ºC/min from 40ºC to 80ºC and 1 mg/mL of protein

concentration. Before measurements, enzymes were dialyzed against 10 mM phosphate-buffered saline (PBS) buffer (pH 7.5) for 14 hours with one change of buffer followed by the degassed process by stirring gently *in vacuo*. Experimental traces were corrected for the calorimeter baseline gained by scanning 10 mM PBS buffer in both cells. The T_m was determined based on the maximum of the transition peak. All reactions were conducted in triplicate.

Hydrogen production via *in vitro* synthetic biosystem

The wild-type *Zm*G6PDH and the best mutant Mut 4-1 were tested to produce hydrogen from maltodextrin via *in vitro* synthetic biosystem (ivSB), where the enzyme cocktail contained ZmG6PDH or Mut 4-1, *Thermotoga maritima* α-glucan phosphorylase (αGP, GenBank accession number: AKE30817.1), *Thermococcus kodakarensis* phosphoglucomutase (PGM, GenBank accession number: BAD85297.1), *Geobacillus stearothermophilus* diaphorase (DI, GenBank accession number: JQ040550.1), and *Pyrococcus furiosus* Ni-Fe hydrogenase I (SHI, GenBank accession number: AAL81018.1, alpha subunit; AAL81015.1, beta subunit; AAL81016.1, gamma subunit; AAL81017.1, delta subunit). αGP, PGM and DI were overexpressed in *E. coli* BL21(DE3) and purified as described elsewhere (Kim et al. 2016; You et al. 2017; Zhu et al. 2014). Soluble [NiFe]-hydrogenase I (SHI) was kindly provided by Michael W. W. Adams (Chandrayan et al. 2015). Activities of individual enzymes were measured as described elsewhere (Kim et al. 2016; You et al. 2017). Specific activities of αGP, PGM, DI and SHI are 10, 200, 4 and 6.8 U/mg at 60°C, respectively. Enzymatic H_2 reactions were conducted in a bioreactor at 60°C. The

reagent solution was comprised of 100 mM HEPES buffer (pH 7.5) containing 125 mM maltodextrin (dextrose equivalent (DE) 4.0~7.0), 125 mM sodium phosphate, 2 mM benzyl viologen, 1 mM $NADP^+$, 5 mM $MgCl_2$, 0.5 mM $MnCl_2$, 0.5 mg/mL of αGP (i.e., 5 U/mL), 0.025 mg/mL of PGM (i.e., 5 U/mL), 0.001 mg /mL wild-type *Zm*G6PDH or Mut 4-1(i.e., 0.8 U/mL), 0.2 mg/mL of DI (i.e., 0.8 U/mL), and 0.3 mg/mL of SHI (i.e., 2 U/mL). Continuous H_2 measurement was conducted in a continuous flow system as described elsewhere (Kim et al. 2016). The collected data were analyzed by Origin 8.0 (Northampton, MA, USA). All runs were conducted in triplicate.

Structural analysis of *Zm*G6PDH and mutants

The three-dimensional homology model of WT *Zm*G6PDH and Mut 4-1 were made by SWISS-MODEL based on the crystal structure of *Trypanosoma cruzi* G6PDH (PDB: 5AQ1, 37% sequence identifiy). The structures of $NADP^+$ and G6P were generated by using Chemdraw (PerkinElmer, Waltham, MA, USA). The conformation space of the corresponding coenzyme binding area was analyzed using the Autodock program (Scripps Research Institute, La Jolla, CA, USA). The putative catalytic active sites were predicted based on modeling comparsion with active sites of *Trypanosoma cruzi* G6PDH (Mercaldi et al. 2016). The results were presented and analyzed using PyMOL (Schrödinger, Inc, Portland, OR, USA).

Results

Petri-dish-based double-layer screening method

An efficient high-throughput screening method is critical to identify positive mutant enzymes in a directed evolution experiment. Here, we applied our previously-published Petri-dish-based double-layer screening method, which was originally limited to thermophillic 6PGDH, to a mesophilic *Zm*G6PDH in this work. The inducible dual promoter, P*T7*-P*tac*, was applied to control the expression level of *Zm*G6DPH and remove the subcloning step between screening of large mutant libaries in *E. coli* TOP10 and recombinant protein overexpression in *E. coli* BL21(DE3). In the *E. coli* TOP10, the modest expression of *Zm*G6PDH was accomplished by the *tac* promoter, while the T7 promoter remained inactive because of a lack of T7 RNA polymerase. In the *E. coli* BL21(DE3), high expression levels of *Zm*G6PDH were obtained under the control of both *T7* and *tac* promoters.

The scheme of Petri-dish-based double-layer screening method is shown as follows. Mutant colonies growing on the solid agar plates were heat-treated to break the cell membrane and deactivate reduced coenzymes, mesophilic redox enzymes, and most negative mutants of *Zm*G6PDH. The heat-treated colonies were overlaid by a second agarose layer containing $NADP^+$, G6P, phenazine methosulohate (PMS) and a redox dye tetranitroblue tetrazolium (TNBT). Only active thermostable mutants could reduce $NADP^+$ to NADPH by the oxidizaion of G6P to 6PGL. NADPH then reduced the colorless TNBT to black TNBT-formazan in the presence of PMS to complete the screening method (**Fig. 1a**). As the result, the color densities of colonies were closely correlated with residual activities of mutants after

heat treatment. Positive mutants with deeper black colors were identified easily for plasmid extraction and transformation (**Fig. 1b**).

Directed evolution of thermostable *Zm*G6PDH mutants

Error-prone PCR was used to generate the random mutant libraries of *Zm*G6PDH with an estimated average of three mutations per gene. Approximate 20,000 mutants were screened in each round of mutant library. Approximately 5-10 thermostable mutants exhibiting deeper black colors were identified each round. The key properties (e.g., residual activity at 60ºC and specific activity) of mutants were characterized. The best mutant with highest ratio of residual activity to initial activity without a significant decrease in specific activity was chosen as the parental gene for the next round of random mutagenesis. We repeated the mutagenesis, screening, and characterization four times, until no further improvement was achieved. During each round of screening, the heat treatment condition was increased more severely, for example, extended time length of heat treatment at 70ºC. Corresponding mutation sites, specific activities at ambient and high temperature, half-life times and melting temperature changes of mutants are summarized in the **Table 3**.

Characterization of ZmG6PDH mutants

All selected mutants, along with wild-type *Zm*G6PDH, were purified and characterized. Half-life times of wild-type *Zm*G6PDH and mutants at 60ºC were estimated by semi-log plot of relative residual activity vs. incubation time, showing first-order thermal deactivation kinetics (**Fig. 2)**. The wild-type *Zm*G6PDH had a half-life time of 0.125 h (7.47

min) at 60ºC (**Table 3**). The first round of random mutagenesis and screening selected the mutant Mut 1-1 with a half-life time of 1.69 h. Mutagenic PCR of Mut 1-1 created a second generation library, from which mutant Mut 2-1 was selected (half-life time of 9.35 hours). One additional mutation site was added in the third round of directed evolution, generating Mut 3-1 (half-life time of 11.82 hours). The process of random mutagenesis and screening was repeated, resulting in a more thermostable mutant Mut 4-1. At 60ºC, the half-life time of Mut 4-1 was 15.52 hours, which is more than 124-fold higher than that of wild-type *Zm*G6PDH.

The melting temperature (T_m) changes between wild-type *Zm*G6PDH and mutants were measured from 40 to 80ºC by DSC analysis. Similar with prolonged half-life times, positive mutants exhibited upward shifts of T_m (**Fig. 3a**). The most thermostable mutant Mut 4-1 showed the highest T_m (70.7ºC). It is 3.4ºC higher than that of wild-type enzyme (**Table 3**).

The activity-temperature profile for the wild-type enzyme and the most thermostable Mut 4-1 is shown in **Fig. 3b**. The activities increased with temperature until enzyme denature. The temperature optimum, T_{opt}, of the Mut 4-1 was 65ºC, 5ºC higher than that of wild-type *Zm*G6PDH. At the elevated optimal temperature (65ºC), the specific activity of Mut 4-1 was 932 U/mg, slightly higher than that of wild-type at its optimal temperature (852 U/mg at 60ºC). Although it was often observed a trade-off between high specific activity and good thermostablity, evolved thermostable mutants analyzed here did not exhibit a great loss of specific activity (<15% loss of activity) with respect to that of wild-type enzyme at ambient temperature (30ºC) or high temperature (60ºC) (**Table 3**). The kinetic constants of

wild-type *Zm*G6PDH and thermostable mutants at 30ºC are listed in **Table 4**. All mutants exhibited minor change of k_{cat} and K_M on $NADP^+$ and G6P compared to those of wild-type enzyme. The most thermostable mutant Mut 4-1 showed a comparable k_{cat} (288 s^{-1}) with unchanged K_M on $NADP^+$ and G6P, yielding the almost identical catalytic properties compared to those of wild-type enzyme.

Hydrogen production from maltodextrin via ivsB at elevated temperature

The G6PDH and thermostable mutants were consolidated with four thermophilic enzymes: (1) α-glucan phosphorylase from *Thermotoga maritima* (αGP); (2) phosphoglucomutase from *Thermococcus kodakarensis* (PGM); (3) diaphorase from *Geobacillus stearothermophilus* (DI) and (4) Ni-Fe hydrogenase I from *Pyrococcus furiosus* (SHI) to construct an ivSB and generate hydrogen from maltodextrin at 60ºC. **Fig. 4a** shows the mechanism of the enzymatic pathway, which includes five sequential cascade reactions: (1) Phosphorylation of maltodextrin to glucose 1-phosphate (G1P) catalyzed by αGP; (2) Isomerization of G1P to G6P catalyzed by PGM; (3) Regeneration of NADPH from $NADP^+$ with concomitant oxidation of G6P to 6PGL catalyzed by G6PDH; (4) Reduction of BV^+ from BV^{2+} and oxidation of NADPH catalyzed by DI; (5) Generation of hydrogen and oxidation of BV^+ catalyzed by SHI.

When the thermostable mutant Mut 4-1 was included for hydrogen production, a high productivity rate and yield were observed (**Fig. 4b**). The maximum of volumetric hydrogen productivity was 24.7 mmol/L/h after 2 hours of reaction, and hydrogen integrated yield was 95.6 μmole after 12 hours of reaction, indicating 76 % of theoretical yield was reached. In

contrast, the hydrogen production using wild-type exhibited a weaker production of hydrogen, showing only 3 mmol/L/h of volumetric productivity rate at 3 h and 9.8% of theoretical yield after 12 h of reaction. Compared to wild-type *Zm*G6PDH, Mut 4-1 led to an 8.3-fold and a 7.7-fold enhancement in productivity and yield, respectively.

Discussion

Obtaining enzymes featuring both good thermostability and high specific activity is a long sought goal for industrial biocatalysis and the *in vitro* synthetic biosystems. Enzymes with high activity enable to shorten reaction times, lower energy expenditure as well as minimize enzyme mass loading (Li et al. 2017). Enzyme with good thermostability means prolonged lifetime during production, storage and catalysis, and higher tolerance towards toxic chemicals (Wu and Arnold 2013). Provided with enzymes remain active, the elevated reaction temperature can display a series of advantages for catalysis, such as better degradation of bulky substrates (i.e., cellulose), faster mass transfer of intermediates, easier product separation (i.e., hydrogen) as well as decreased microbial contamination (Kim et al. 2016; Wu and Arnold 2013). However, natural enzymes characterized with both properties are very rare because a trade-off between activity and thermostability, as they seem to have evolved in different directions. Improving themorstability of highly active mesophilic enzymes (Giver et al. 1998) and inducing high activity of thermophilic enzymes (Li et al. 2017) are two conventional evolutionary paths to obtain engineered enzymes with both properties, showing success in protein engineering of numerous enzymes (de Abreu et al.

2013; Roth et al. 2017; Xu et al. 2015). Here, we started with *Zm*G6PDH, one of most active G6PDHs, and then increased its thermostability via directed evolution. The best mutant Mut 4-1 has a specific activity of 932 U/mg at 65ºC with a 124-fold improvement in half-life time at 60ºC, a 3.4ºC increase in melting temperature, a 5ºC increase in optimal temperature, compared to those of wild-type *Zm*G6PDH.

The *Zm*G6PDH mutant Mut 4-1 is characterized by both high specific activity and improved thermostability and has great potential for numerous biocatalysis applications. The Mut 4-1 is the most active characterized thermostable G6PDH and shows a specific activity of 932 U/mg at 65ºC, which is 4 to 49-fold higher than those of other characterized thermostable counterparts (**Table 1**). Its high specific activity ensures the efficient regeneration of NADPH and led to an increase in the space-time yield of biocatalysis processes, such as the ivSB based hydrogen production and enzymatic fuel cell (Rollin et al. 2015; Zhu and Zhang 2017). The engineered *Zm*G6DPH has been evolved with a half-life time of 15.52 hours at 60ºC, a more than 124-fold improvement compared to wild-type enzyme. Without a decrease in activity, the enhanced thermostability enables increase the total turn-over number (TTN) of *Zm*G6PDH by over two orders of magnitude (from 5 x 10^5 to 6 x 10^7) and greatly decrease the contribution of G6PDH to the overall production costs, which is critical for producing low-cost commodities (i.e., hydrogen, electricity) through the ivSB (Zhang et al. 2010; Zhu et al. 2014). Also, the *Zm*G6PDH has a high specific activity (355 U/mg at 30ºC) and a high affinity (K_M = 0.11 mM) on NAD^+ (Scopes 1997), a cheaper and more stable alternative of $NADP^+$. This character suggests a potential application of thermostable mutant for high-temperature NADH regeneration without fine-tuning the

coenzyme selectivity. Furthermore, working as the first and rate-limiting step of the ED pathway, overexpression of thermostable mutant of *Zm*G6DPH might facilitate the glucose uptake rate in the thermotolerant *Z. mobilis* variant strain and increase its production of bioethanol and other biochemicals at high temperature (Charoensuk et al. 2017; Yang et al. 2016).

To further investigate a possible mechanism for enhanced thermostability, three-dimensional homology models of wild-type *Zm*G6PDH and Mut 4-1 were created. Six amino acid substitutions (A117S/G225S/F277I/Q324H/M381I/A476V0 from the nine mutation points of the mutant were predicted to confer enhanced thermostability. None of these mutations occurred near the putative catalytic active site residues (E212 and H236) (Mercaldi et al. 2016) or binding pocket of G6P and coenzymes (>5.5 Å) (**Fig. 5**), which is consistent with minor changes of kinetic data between wild-type enzyme and mutants. The thermostabilizing mutations are all distributed over the surface of *Zm*G6PDH except M381I and A476V. This finding underscores the importance of protein surface on stability and is accord with the hypothesis that surface-located parts of protein are involved in initial steps of irreversible thermal deactivation (Johannes et al. 2005). As for changes of molecular forces, the mutation A117S and G225S form new hydrogen bonds, a key factor attributed to increased thermostability (Zhang et al. 2016). The A117 is adjacent to the N-terminus of α7. The substitution of alaine to serine in this position introduces a new hydrogen bond (3.1 Å) with the amine group of P118 (**Fig. 6a**), which strengthens the rigidity of the alpha helix. Similarly, mutation G225S creates a hydrogen bond (3.6 Å) with amide group of Q148, which might stabilize the surrounding surface region (**Fig. 6b**). Mutation Q324H and M381I

confer the improved thermostability through replacement of thermolabile amino acids (**Fig. 6c and d**). The Q324H and M381I are located in the protein surface and dimer interface, respectively. At high temperature, the glutamine and methionine are susceptible to deamidation and oxidization followed by the induction of enzyme destabilization (Liu et al. 2009). Replacmemt of glutamine to histidine might stabilize the enzyme by removing possible peptide backbone length change due to the deamidation (Daniel et al. 1996). Mutation of methionine to isoleucine might result in prolonged half-life times by contructing the tight and oxygen-resistant interface (Nomura et al. 2009). Introduction of favorable hydrophobic packing may also be helpful to stabilize *Zm*G6PDH at high temperatures. Mutation F277I changes the bulky phenylalanine residue to a smaller isoleucine residue, which might minimize possible streic clashes during conformation change at high temperature (**Fig. 6e**). Replacing alanine with valine at position 476 (**Fig. 6f**) could strengthen C-H/π interation between the prolonged alkane side chain and aromatic ring of Y329, resulting in a positive effect on protein stabilzation (Madhusudan Makwana and Mahalakshmi 2015). Given these observations, the *Zm*G6PDH could be further thermostablized by using iternative saturation mutagensis of each thermostablized residue and identifying new benefical sites for recombination (McLachlan et al. 2008).

In conclusion, this study improved the thermostability of ZmG6PDH from *Z. mobilis* by directed evolution without losing its naturally high specific activity. The Petri-dish-based double-layer screening, which was limited to use in thermophilic dehydrogenases previously, was adapted and applied to improve thermostability of this mesophilic G6PDH. The effectiveness of the thermostable mutant Mut-4 was demonstrated by the increased

productivity rate and yield of hydrogen from maltodextrin via the ivSB, suggesting the potential of thermostable *Zm*G6PDH mutants for high-temperature NAD(P)H regeneration in the *in vitro* synthetic biology platform.

Acknowledgments

This project could not have been carried out without the support of the Biological Systems Engineering Department, Virginia Polytechnic Institute and State University, Blacksburg, Virginia, USA and Tianjin Institute of Industrial Biotechnology, Chinese Academy of Sciences. This study was supported by the Department of Energy, Office of Energy Efficiency and Renewable Energy, Fuel Cell Technologies Office under Award Number DE-EE0006968. The manuscript was edited by Ryan S. Senger.

Compliance with ethical standards

Conflict of interest

The authors declare that they have no competing interests.

Ethical approval

This article does not contain any studies with human participants or animals performed by any of the authors.

References

Baik S-H, Ide T, Yoshida H, Kagami O, Harayama S (2003) Significantly enhanced stability of glucose dehydrogenase by directed evolution. Appl Microbiol Biotechnol 61:329-335. doi:https://doi.org/10.1007/s00253-002-1215-1

Chandrayan SK, Wu C-H, McTernan PM, Adams MWW (2015) High yield purification of a tagged cytoplasmic [NiFe]-hydrogenase and a catalytically-active nickel-free intermediate form. Protein Expr Purif 107:90-94. doi:10.1016/j.pep.2014.10.018

Charoensuk K, Sakurada T, Tokiyama A, Murata M, Kosaka T, Thanonkeo P, Yamada M (2017) Thermotolerant genes essential for survival at a critical high temperature in thermotolerant ethanologenic *Zymomonas mobilis* TISTR 548. Biotechnol Biofuels 10:204. doi:10.1186/s13068-017-0891-0

Conway T (1992) The Entner-Doudoroff pathway: history, physiology and molecular biology. FEMS Microbiol Rev 9:1-27. doi:10.1111/j.1574-6968.1992.tb05822.x

Daniel RM, Dines M, Petach HH (1996) The denaturation and degradation of stable enzymes at high temperatures. Biochem J 317:1-11. doi:10.1042/bj3170001

de Abreu M, Alvaro‐Benito M, Sanz‐Aparicio J, Plou FJ, Fernandez‐Lobato M, Alcalde M (2013) Synthesis of 6‐Kestose using an Efficient β‐Fructofuranosidase Engineered by Directed Evolution. Adv Synth Catal 355:1698-1702

Fuentealba M, Munoz R, Maturana P, Krapp A, Cabrera R (2016) Determinants of cofactor specificity for the glucose-6-phosphate dehydrogenase from *Escherichia coli*: simulation, kinetics and evolutionary studies. PLoS One 11(3):e0152403 doi:10.1371/journal.pone.0152403

Giver L, Gershenson A, Freskgard P-O, Arnold FH (1998) Directed evolution of a thermostable esterase. Proc Natl Acad Sci USA 95:12809-12813. doi:10.1073/pnas.95.22.12809

Gomez-Manzo S, Terron-Hernandez J, De la Mora-De la Mora I, Gonzalez-Valdez A, Marcial-Quino J, Garcia-Torres I, Vanoye-Carlo A, Lopez-Velazquez G, Hernandez-Alcantara G, Oria-Hernandez J, Reyes-Vivas H, Enriquez-Flores S (2014) The stability of G6PD is affected by mutations with different clinical phenotypes. Int J Mol Sci 15(11):21179-21201 doi:10.3390/ijms151121179

Hansen T, Schlichting B, Schönheit P (2002) Glucose-6-phosphate dehydrogenase from the hyperthermophilic bacterium *Thermotoga maritima*: expression of the *g6pd* gene and characterization of an extremely thermophilic enzyme. FEMS Microbiol Lett 216(2):249-253

Hasmann FA, Gurpilhares DB, Roberto IC, Converti A, Pessoa A (2007) New combined kinetic and thermodynamic approach to model glucose-6-phosphate dehydrogenase activity and stability. Enzyme Microb Technol 40(4):849-858

He MX, Wu B, Qin H, Ruan ZY, Tan FR, Wang JL, Shui ZX, Dai LC, Zhu QL, Pan K, Tang XY, Wang WG, Hu QC (2014) *Zymomonas mobilis*: a novel platform for future biorefineries. Biotechnol Biofuels 7:101. doi:10.1186/1754-6834-7-101

Huang R, Chen H, Zhong C, Kim JE, Zhang Y-HP (2016) High-throughput screening of coenzyme preference change of thermophilic 6-phosphogluconate dehydrogenase from $NADP^+$ to NAD^+. Sci Rep 6:32644. doi:10.1038/srep32644

Iyer RB, Wang J, Bachas LG (2002) Cloning, expression, and characterization of the *gsdA* gene encoding thermophilic glucose-6-phosphate dehydrogenase from *Aquifex aeolicus*. Extremophiles 6(4):283-289

Johannes TW, Woodyer RD, Zhao H (2005) Directed evolution of a thermostable phosphite dehydrogenase for NAD(P)H regeneration. Appl Environ Microbiol 71(10):5728-5734. doi:10.1128/AEM.71.10.5728-5734.2005

Kanji MI, Toews ML, Carper WR (1976) A kinetic study of glucose-6-phosphate dehydrogenase. J Biol Chem 251(8):2258-2262.

Kim EJ, Wu CH, Adams MW, Zhang Y-HP (2016) Exceptionally high rates of biological hydrogen production by biomimetic *in vitro* synthetic enzymatic pathways. Chem Eur J 22:16047-16051. doi:10.1002/chem.201604197

Kusumoto M, Kishimoto T, Nishiya Y (2010) Improvement of thermal stability of *Leuconostoc pseudomesenteroides* glucose-6-phosphate dehydrogenase. Journal of Analytical Bio-Science Vol 33(4):397-400

Lee WT, Levy HR (1992) Lysine‐21 of *Leuconostoc mesenteroides* glucose 6‐phosphate dehydrogenase participates in substrate binding through charge‐charge interaction. Protein Sci 1(3):329-334

Li G, Maria-Solano MA, Romero-Rivera A, Osuna S, Reetz MT (2017) Inducing high activity of a thermophilic enzyme at ambient temperatures by directed evolution. Chem Commun 53:9454-9457. doi:10.1039/C7CC05377K

Li Z, Jiang N, Yang K, Zheng J (2016) Cloning, expression, and characterization of a thermostable glucose-6-phosphate dehydrogenase from *Thermoanaerobacter tengcongensis*. Extremophiles 20(2):149-156 doi:10.1007/s00792-016-0808-z

Liu W, Hong J, Bevan DR, Zhang Y-HP (2009) Fast identification of thermostable beta-glucosidase mutants on cellobiose by a novel combinatorial selection/screening approach. Biotechnol Bioeng 103:1087-1094. doi:10.1002/bit.22340

Madhusudan Makwana K, Mahalakshmi R (2015) Implications of aromatic-aromatic interactions: From protein structures to peptide models. Protein Sci 24:1920-1933. doi:10.1002/pro.2814

Mayer KM, Arnold FH (2002) A colorimetric assay to quantify dehydrogenase activity in crude cell lysates. J Biomol Screen 7:135-140.

McLachlan MJ, Johannes TW, Zhao H (2008) Further improvement of phosphite dehydrogenase thermostability by saturation mutagenesis. Biotechnol Bioeng 99:268-274. doi:10.1002/bit.21546

Mercaldi GF, Dawson A, Hunter WN, Cordeiro AT (2016) The structure of a *Trypanosoma cruzi* glucose‐6‐phosphate dehydrogenase reveals differences from the mammalian enzyme. FEBS lett 590:2776-2786 doi:10.1002/1873-3468.12276

Nomura T, Kamada R, Ito I, Chuman Y, Shimohigashi Y, Sakaguchi K (2009) Oxidation of methionine residue at hydrophobic core destabilizes p53 tetrameric structure. Biopolymers 91:78-84 doi:10.1002/bip.21084

Rogers TA, Bommarius AS (2010) Utilizing simple biochemical measurements to predict lifetime output of biocatalysts in continuous isothermal processes. Chem Eng Sci 65:2118-2124 doi:10.1016/j.ces.2009.12.005

Rollin JA, del Campo JM, Myung S, Sun F, You C, Bakovic A, Castro R, Chandrayan SK, Wu C-H, Adams MWW, Senger RS, Zhang Y-HP (2015) High-yield hydrogen production from biomass by *in vitro* metabolic engineering: Mixed sugars coutilization and kinetic modeling. Proc Natl Acad Sci USA 112:4964-4969. doi:10.1073/pnas.1417719112

Roth T, Beer B, Pick A, Sieber V (2017) Thermostabilization of the uronate dehydrogenase from *Agrobacterium tumefaciens* by semi-rational design. AMB Express 7:103 doi:https://doi.org/10.1186/s13568-017-0405-2

Scopes RK (1997) Allosteric control of *Zymomonas mobilis* glucose-6-phosphate dehydrogenase by phosphoenolpyruvate. Biochem J 326:731-735.

Scopes RK, Testolin V, Stoter A, Griffiths-Smith K, Algar EM (1985) Simultaneous purification and characterization of glucokinase, fructokinase and glucose-6-phosphate dehydrogenase from *Zymomonas mobilis*. Biochem J 228(3):627-634

Sekar BS, Seol E, Park S (2017) Co-production of hydrogen and ethanol from glucose in *Escherichia coli* by activation of pentose-phosphate pathway through deletion of phosphoglucose isomerase (*pgi*) and overexpression of glucose-6-phosphate dehydrogenase (*zwf*) and 6-phosphogluconate dehydrogenase (*gnd*). Biotechnol Biofuels 10:85. doi:https://doi.org/10.1186/s13068-017-0768-2

Simon G, Mejean V, Jourlin C, Chippaux M, Pascal MC (1994) The *torR* gene of Escherichia coli encodes a response regulator protein involved in the expression of the trimethylamine N-oxide reductase genes. J Bacteriol 176:5601-5606

Wang Y, Huang W, Sathitsuksanoh N, Zhu Z, Zhang Y-HP (2011) Biohydrogenation from biomass sugar mediated by *in vitro* synthetic enzymatic pathways. Chem Biol 18:372-380. doi:https://doi.org/10.1016/j.chembiol.2010.12.019

Wu I, Arnold FH (2013) Engineered thermostable fungal Cel6A and Cel7A cellobiohydrolases hydrolyze cellulose efficiently at elevated temperatures. Biotechnol Bioeng 110:1874-1883

Xu B-L, Dai M, Chen Y, Meng D, Wang Y, Fang N, Tang X-F, Tang B (2015) Improving the thermostability and activity of a thermophilic subtilase by incorporating structural elements of its psychrophilic counterpart. Appl Environ Microbiol 81:6302-6313. doi:10.1128/AEM.01478-15

Yang S, Fei Q, Zhang Y, Contreras LM, Utturkar SM, Brown SD, Himmel ME, Zhang M (2016) *Zymomonas mobilis* as a model system for production of biofuels and biochemicals. Microb Biotechnol 9:699-717. doi:10.1111/1751-7915.12408

You C, Shi T, Li Y, Han P, Zhou X, Zhang Y-HP (2017) An *in vitro* synthetic biology platform for the industrial biomanufacturing of myo-inositol from starch. Biotechnol Bioeng 114:1855-1864. doi:10.1002/bit.26314

You C, Zhang X, Zhang Y-HP (2012) Simple cloning via direct transformation of PCR product (DNA Multimer) to *Escherichia coli* and *Bacillus subtilis*. Appl Environ Microbiol 78:1593-1595. doi:10.1128/AEM.07105-11

You C, Zhang Y-HP (2012) Easy preparation of a large-size random gene mutagenesis library in *Escherichia coli*. Anal Biochem 428:7-12. doi:10.1016/j.ab.2012.05.022

You L, Arnold FH (1996) Directed evolution of subtilisin E in *Bacillus subtilis* to enhance total activity in aqueous dimethylformamide. Protein Eng 9(1):77-83.

Zhang X-F, Yang G-Y, Zhang Y, Xie Y, Withers SG, Feng Y (2016) A general and efficient strategy for generating the stable enzymes. Sci Rep 6:33797. doi:10.1038/srep33797

Zhang Y-HP, Sun J, Zhong J-J (2010) Biofuel production by *in vitro* synthetic enzymatic pathway biotransformation. Curr Opin Biotechnol 21(5):663-669 doi:10.1016/j.copbio.2010.05.005

Zhao X, Shi F, Zhan W (2015) Overexpression of *ZWF1* and *POS5* improves carotenoid biosynthesis in recombinant

Saccharomyces cerevisiae. Lett Appl Microbiol 61:354-360. doi:10.1111/lam.12463

Zheng M, Chen K, Wang R-F, Li H, Li C-X, Xu J-H (2017) Engineering 7β-hydroxysteroid dehydrogenase for enhanced ursodeoxycholic acid production by multi-objective directed evolution. J Agric Food Chem 65:1178-1185. doi:10.1021/acs.jafc.6b05428

Zhu Z, Tam TK, Sun F, You C, Zhang Y-HP (2014) A high-energy-density sugar biobattery based on a synthetic enzymatic pathway. Nat Commun 5:3026. doi:10.1038/ncomms4026

Zhu Z, Zhang Y-HP (2017) *In vitro* metabolic engineering of bioelectricity generation by the complete oxidation of glucose. Metab Eng 39:110-116. doi:https://doi.org/10.1016/j.ymben.2016.11.002

Figure Legends

Fig. 1 The scheme of Petri-dish-based double-layer screening method for fast identification of thermostable *Zm*G6PDH mutants (a) and a photo of a typical screening plate (b), where positive mutants with darker colors are indicated by red arrows. G6P: glucose 6-phosphate; 6PGL: 6-phosphogluconolactone; PMS: phenazine methosulfate; TNBT: tetranitroblue tetrazolium

Fig. 2 Heat-inactivation of wild-type and mutated *Zm*G6PDHs. The half-life times ($t_{1/2}$) of enzymes (1 μg/mL) at 60°C were estimated by the semi-log plot of relative residual activity vs. indicated periods of time

Fig. 3 (a) DSC of wild-type and thermostable mutants of *Zm*G6PDHs from generation 1 (Mut 1-1), 2 (Mut 2-1), 3 (Mut 3-1) and 4 (Mut 4-1). As the thermostability of mutants increased, the transition peak moved to higher temperatures. The experiments were repeated three times independently. Data shown are for one of three representative experiments. (b) Activity of wild-type *Zm*G6PDH and final mutant Mut 4-1, as a function of temperature. The temperature of optimal activity increases with improved thermostability

Fig. 4 Hydrogen production from maltodextrin via *in vitro* synthetic biosystems. (a) Scheme of the *in vitro* synthetic biosystems for hydrogen production. αGP: α-glucan phosphorylase; PGM: Phosphoglucomutase; G6PDH: glucose 6-phosphate dehydrogenase; DI: diaphorase; SHI: [NiFe] hydrogenase; P_i: phosphate; G1P: glucose 1-phosphate; G6P: glucose 6-phosphate; 6PGL, 6-phosphogluconolactone; $BV_{(ox)}$: oxidized benzyl viologen; $BV_{(red)}$: reduced benzyl viologen. (b) H_2 evolution profiles at 60°C via the *in vitro* synthetic biosystems. The result of wild-type

*Zm*G6PDH and the thermostable Mut 4-1 are shown with black and red line, respectively. The experiments were repeated three times independently. Data shown are for one of three representative experiments

Fig. 5 Dimeric structure model of *Zm*G6PDH mutant Mut 4-2. The subunit A and B are colored gray and lightblue, respectively. Thermostabilized mutations and putative catalytic active sites are featured as red and yellow spheres, respectively. Substrate G6P and $NADP^+$ are depicted as sticks and colored according to the types: N, blue; O, red; C, green and P, orange

Fig. 6 Local environments of thermostablized mutations (a) A117S, (b) G225S, (c) Q324H, (d) M381I, (e) F277I and (f) A476V in Mut 4-1. The subunit A and B are shown as cartoon and colored gray and lightblue, respectively. The interested residues and $NADP^+$ are depicted as sticks. Native and mutated residues are colored blue and red, respectively. Thermolabile groups of glutamine and methionine are marked by red dashed circle. Distances to $NADP^+$, hydrogen bonds and CH-π interactions are indicated by cyan, yellow and magenta dashed line, respectively. The pseudoatom is featured as black sphere. Distances of molecular forces are labeled in blue. Other atoms are colored according to the types: N, blue; O, red; C, green, P, orange and S, yellow

Table 1. Comparison of enzymatic properties of characterized G6PDHs

Organism	GenBank Number	Sp. Act.[a] (U/mg)	Temp. (°C)	Half-life times	Reference
Mesophilic host					
Escherichia coli	APL65798.1	187	25	ND	(Fuentealba et al. 2016)
Homo sapiens	AH003054.2	224	25	20 min, 52°C	(Gomez-Manzo et al. 2014)
Leuconostoc mesenteroides	AAA25265.1	719	25	10 min, 50°C	(Kusumoto et al. 2010; Lee and Levy 1992)
Leuconostoc mesenteroides	AAA25265.1 (Mutant M5)	ND	ND	75 min, 50°C[b]	(Kusumoto et al. 2010)
Saccharomyces cerevisiae	X57336.1	400[c]	25	21 min, 45°C[d]	(Hasmann et al. 2007)
Zymomonas mobilis	AHJ70511.1	390	25	ND	(Scopes et al. 1985)
Zymomonas mobilis	AHJ70511.1	316	30	7 min, 60°C	In this study
Thermophilic host					
Aquifex aeolicus	AY218838.1	19	70	2,700 min, 70°C	(Iyer et al. 2002)
Geobacillus stearothermophilus	JQ040549.1	35	50	15 min, 65°C[e]	(Iyer et al. 2002; Rollin et al. 2015)
Thermoanaerobacter tengcongensis	AAM24260.1	262	70	900 min, 70°C	(Li et al. 2016)
Thermotoga maritima	AKE28931.1	20	80	20 min, 100°C	(Hansen et al. 2002)

[a] Sp. Act is the abbreviation of specific activity
[b] the half-life time of mutant was calculated based on residual activities at 50°C
[c] the specific activity of G6PDH from *Saccharomyces cerevisiae* was based on data of commercial enzyme from Sigma-Aldrich
[d] the half-life time of G6PDH from *Saccharomyces cerevisiae* was based on the residual activity of enzyme in cell free extract
[e] the G6PDH from *Geobacillus stearothermophilus* retained 60% retention of activity after 15 minutes incubation at 65°C

Table 2. The strains, plasmids, and oligonucleotides used in this study

Description	Contents	Sources
Strains		
E. coli BL21 star™ (DE3)	F- *omp*T *hsd*S_B (r_B-, m_B-) *galdcmrne*131 (DE3)	Invitrogen
E. coli TOP10	F- *mcr*A Δ(*mrr-hsd*RMS-*mcr*BC) Φ80*lac*Z ΔM15 Δ*lac*X74 *rec*A1 *ara*D139 Δ(*araleu*)7697 *gal*U *gal*K *rps*L (StrR) *end*A1 *nup*G	Invitrogen
Plasmids		
pET28a-P*tac-6pgdh*	dual promoter (P*T7* and P*tac*) and *Moth6pgdh*	(Huang et al. 2016)
pET28a-P*tac-g6pdh*	dual promoter (P*T7* and P*tac*) and *Zmg6pdh*	This study
Primers		
Vect_F	5'-CATCGTCGAAACGGTATTTGTCATATGTATATCTCCTTCTTAAAGTTAAAC-3'	
Vect_R	5'-GTGATGGAGTAACTTGGTATGACCACCACCACCACCACCACTGACTCGAGGATCCGGCTGCT-3'	
G6P_F	5'-GTTTAACTTTAAGAAGGAGATATACATATGACAAATACCGTTTCGACGATG-3'	
G6P_R	5'-AGCAGCCGGATCCTCGAGTCAGTGGTGGTGGTGGTGGTCATACCAAGTTACTCCATCAC-3'	

Table 3. Characterization of ZmG6PDH and mutants

Enzymes	Mutations	Specific activity (U/mg)		$t_{1/2}$ (h, 60°C)	Fold	T_m (°C)	dT_m (°C)
		30°C	60°C				
Wild-type	-	316.2 ± 5.4	852 ± 10	0.125 ± 0.004	1	67.3 ± 0.2	0
Mut 1-1	A117S/Q324H/V443I/S470I	326.9 ± 5.4	772 ± 33	1.69 ± 0.04	14	68.8 ± 0.1	1.5
Mut 2-1	A117S/Q324H/**M381I**/V443I/S470I	314.2 ± 4.3	850 ± 12	9.35 ± 0.31	75	69.7 ± 0.1	2.4
Mut 3-1	A117S/**F277I**/Q324H/M381I/V443I/S470I	269.7 ± 3.2	741 ± 20	11.82 ± 0.45	95	69.6 ± 0.2	2.3
Mut 4-1	**L99I**/A117S/**G225S**/F277I/Q324H/M381I/V443I/S470I/**A476V**	298.6 ± 3.3	847 ± 21	15.52 ± 0.49	124	70.7 ± 0.1	3.4

Additional mutations relative to their parent enzyme are highlighted in bold. The half-lives ($t_{1/2}$) were measured with 1 μg/mL G6PDHs at 60°C. Each value represents the average ± standard deviation of triplicate measurements.

Table 4. Enzyme kinetics for ZmG6PDH and mutants

Enzymes	K_M ($NADP^+$, μM)	K_M (G6P, μM)	K_{ia} ($NADP^+$, μM)	k_{cat} (s^{-1})
Wild-type	14.3 ± 0.4	78 ± 2	40 ± 4	305 ± 3
Mut 1-1	24.0 ± 0.7	151 ± 4	68 ± 7	329 ± 3
Mut 2-1	22.5 ± 0.6	99 ± 2	35 ± 3	306 ± 3
Mut 3-1	19.9 ± 0.4	73 ± 1	54 ± 4	261 ± 2
Mut 4-1	15.9 ± 0.5	81 ± 2	22 ± 3	288 ± 3

Specific activities of G6PDH and mutants are measured at 30°C. Data were collected from triplicate measurements and enzyme kinetic parameters are fit to the ordered bi-bi rate equation (Kanji et al. 1976).

Figure 1. The scheme of Petri-dish-based double-layer screening method for fast identification of thermostable ZmG6PDH mutants

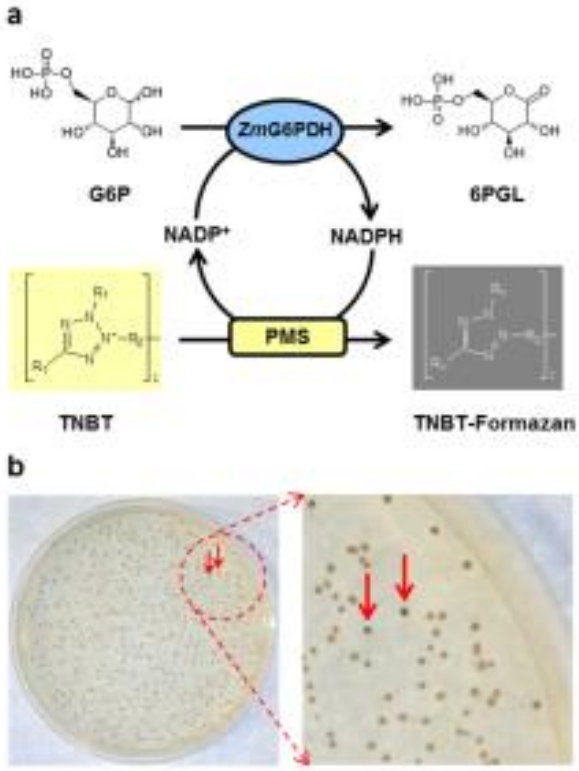

Figure 2. Heat-inactivation of wild-type and mutated ZmG6PDHs

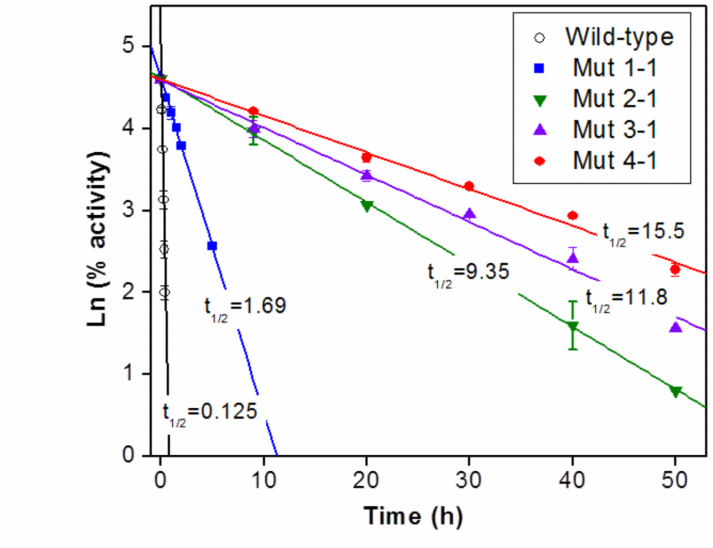

Figure 3. (a) DSC of wild-type and thermostable mutants of ZmG6PDHs from generation 1 (Mut

1-1), 2 (Mut 2-1), 3 (Mut 3-1) and 4 (Mut 4-1). As the thermostability of mutants increased, the transition peak moved to higher temperatures. The experiments were repeated three times independently. Data shown are for one of three representative experiments. (b) Activity of wild-type ZmG6PDH and final mutant Mut 4-1, as a function of temperature. The temperature of optimal activity increases with improved thermostability

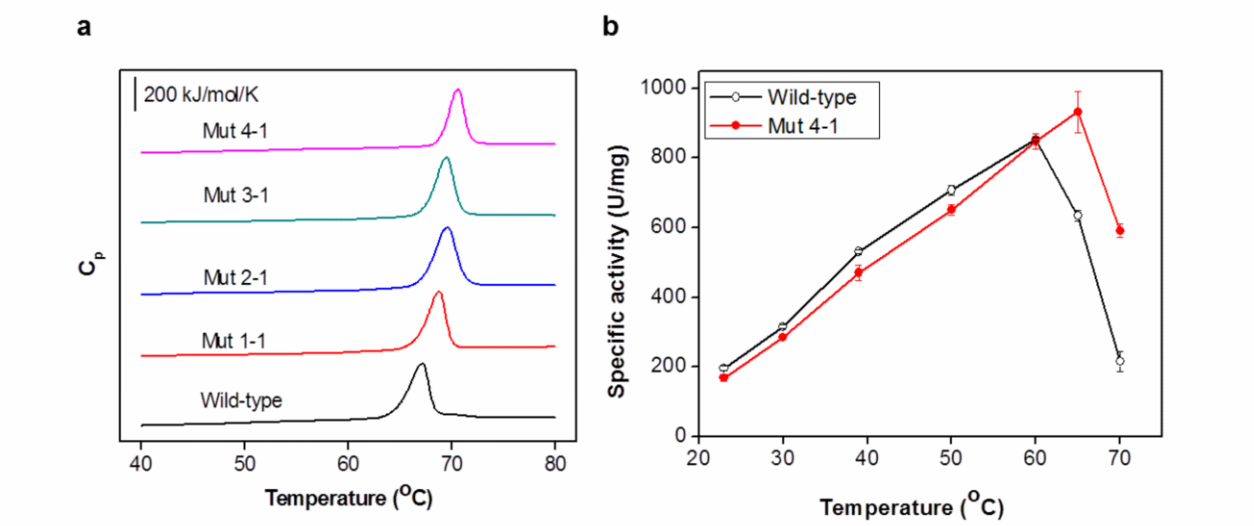

Figure 4. Hydrogen production from maltodextrin via *in vitro* synthetic biosystems

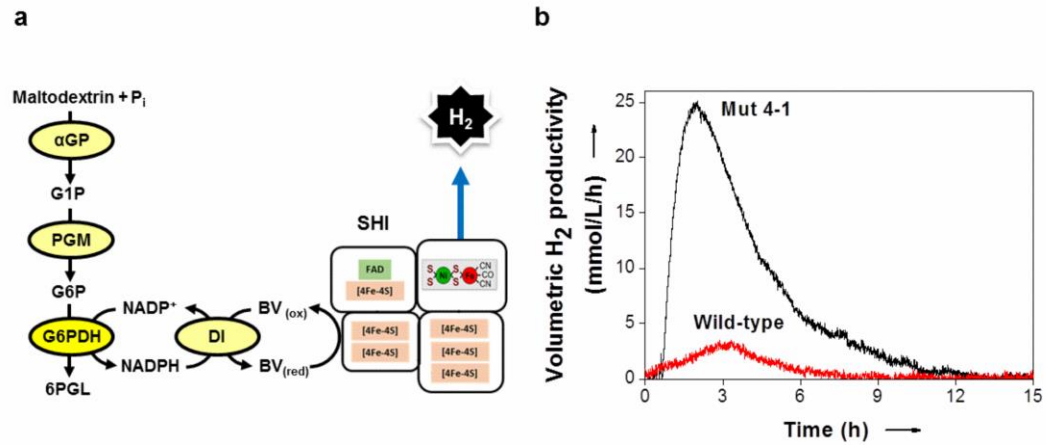

Figure 5. Dimeric structure model of ZmG6PDH mutant Mut 4-2

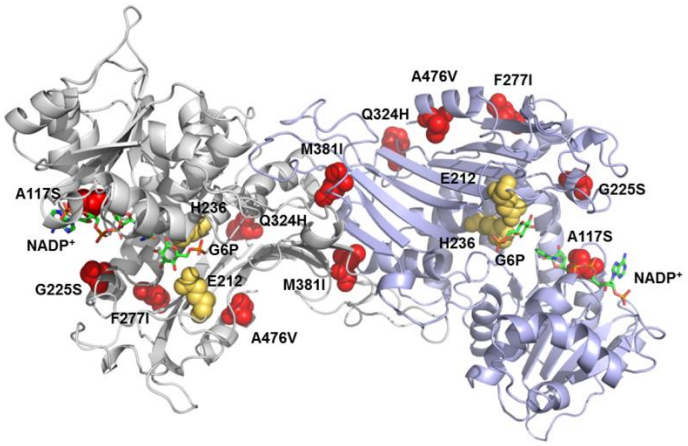

Figure 6. Local environments of thermostablized mutations

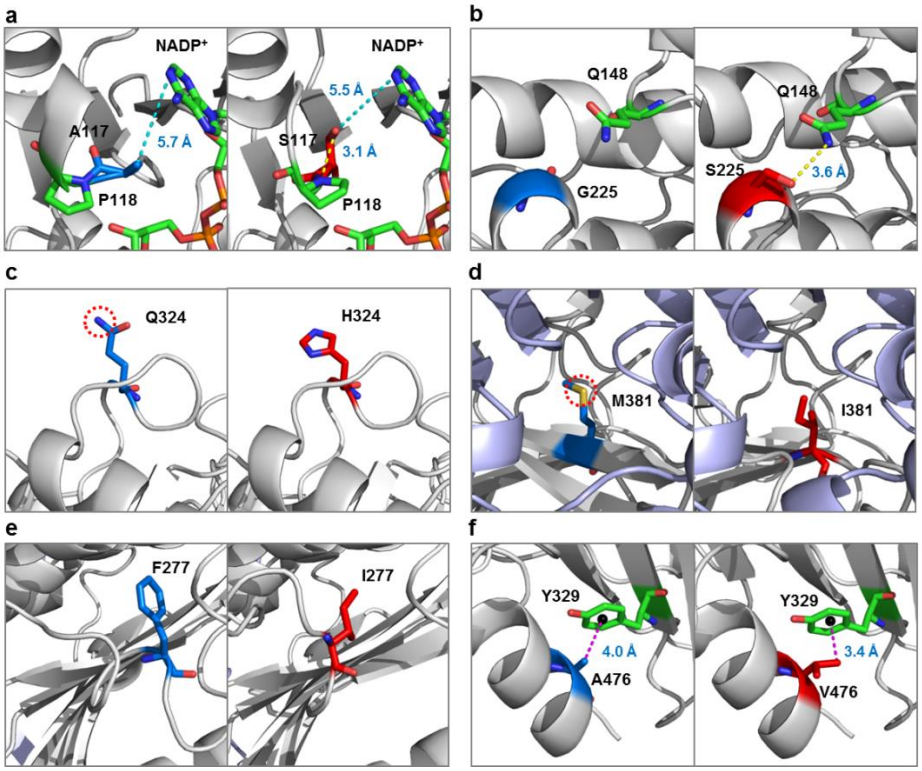

Chapter 5: Engineering a NADP-dependent dehydrogenase on nicotinamide mononucleotide: high-throughput screening and artificial electron transport chain

Rui Huang[1], Hui Chen[1], Ryan S. Senger[1,2], Yi-Heng Percival Zhang[1,3*]

[1] Department of Biological Systems Engineering, Virginia Tech, Blacksburg, Virginia 24061, USA

[2] Department of Chemical Engineering, Virginia Tech, Blacksburg, Virginia 24061, USA

[3] Tianjin Institute of Industrial Biotechnology, Chinese Academy of Sciences, 32 West 7th Avenue, Tianjin Airport Economic Area, Tianjin 300308, China

*Corresponding author

Email: yhzhang@vt.edu

Abstract

NAD(P)-dependent redox enzymes play a central role in transferring electrons among chemical compounds in metabolic pathways. Engineering of coenzyme preference of NAD(P)-dependent dehydrogenases from dinucleotide coenzyme NAD(P) to small-size mononucleotide biomimetic analogues is of importance to systems biocatalysis and synthetic biology. Here we developed a high-throughput screening method involving sequential steps of colony growth on Petri dishes, colony duplication on filter papers, colony lysis, and vacuum washing for identifying novel coenzyme preference of 6-phophogluconate dehydrogenase (6PGDH) on nicotinamide mononucleotide (NMN) while minimizing the background signal from intracellular coenzymes and other cellular reducing compounds. By using this method, we applied six-round directed evolution to improve its specific activity on NMN^+ by a factor of 50. The specific activity of the best engineered 6PGDH on NMN^+ was as high as 18 U/mg, comparable to that of the wild-type enzyme on its natural coenzyme $NADP^+$. Furthermore, we demonstrate the first NMN-based electron transport chain comprised of engineered 6PGDH, FMN-containing diaphorase, and NiFe-hydrogenase for *in vitro* biohydrogen production. These results suggest that engineered dehydrogenases could have the same activities on mononucleotide coenzymes as on dinucleotide coenzymes and costs of biomimetic coenzymes could be decreased greatly for systems biocatalysis.

Keywords: 6-phophogluconante dehydrogenase, biomimetic coenzyme, directed evolution, high-throughput screeening, NAD(P)-dependent dehydrogenase, nicotinamide mononucleotide, biohydrogen

Introduction

An electron transport chain (ETC) in living cells is comprised of a series of redox reactions that transfer electrons from electron donors to acceptors. ETCs play a central role in extracting energy from sunlight through photosynthesis and oxidation of carbohydrates for cellular respiration. Nicotinamide adenine dinucleotide (NAD, which includes NAD^+ and NADH) and nicotinamide adenine dinucleotide phosphate (NADP, which includes $NADP^+$ and $NADPH^,$) are the most important electron carriers, because two-thirds of redox enzymes use them to transfer electrons[1]. NAD(P)-dependent redox enzymes account for approximately 18% of 6,300 cataloged enzymes in the BRENDA database [2,3]. NAD and NADP play distinctive roles in catabolism and anabolism, respectively. NADH is usually produced from NAD^+ via the oxidation of organic substrates (e.g., glucose) followed by its oxidation for ATP generation, while NADPH is consumed for the synthesis of cellular macromolecules, such as proteins, lipids, and nuclear acids. NAD is a dinucleotide containing a nicotinamide riboside and an adenine linked by phosphate groups. NADP has an additional phosphate group esterified at the 2'-hydroxyl group of adenosine monophosphate moiety of NAD.NAD is synthesized from nicotinamide mononucleotide (NMN) and ATP catalyzed by nicotinamide nucleotide adenylyltransferase and NADP is synthesized from NAD at a cost of a second ATP (**Figure S1**).

Engineering of coenzyme preferences of NAD(P)-dependent redox enzymes from NADP to NAD [4-6], the reverse [7,8], and broadening of coenzyme selectivity [9] are important areas of research in protein engineering and are relevant in metabolic engineering and synthetic biology [1,10]. The Arnold group has developed the Cofactor Specificity Reversal–Structural Analysis and Library Design (CSR-SALAD) web application, an easy-to-use tool for reversing enzymatic

natural nicotinamide cofactor specificity [10]. This structure-guided, semi-rational strategy tool is based on comprehensive survey of previous studies of coenzyme engineering, a large number of protein crystal structures, and homogenous oxidoreductase sequences with different coenzyme preferences. However, this method cannot be applied to small-size non-natural biomimetic coenzymes. This is because structural similarities of biomimetic and natural derivatives are lacking. Appropriate coordination and binding of biomimetics in the coenzyme binding pocket require the introduction of novel hydrogen bond networks and van der Waals interactions, which might totally differ with those for NAD(P) [11]. Engineering redox enzymes to have activity with small nicotinamide-containing biomimetic coenzymes of less than half the size of NAD(P) is of significant scientific interest NAD(P) [12], as these would be important for *in vitro* biocatalysis systems that rsuffer from costly and degradable coenzymes [13] and for synthetic biology in developing bioorthogonal redox systems [14].It has proven difficult to engineer NAD(P)-dependent dehydrogenases to have activity with small-size less-costly and more stable nicotinamide-based biomimetic coenzymes; although, a few examples been demonstrated in recent literature, such as 1-benzyl-3-carbamoyl-pyridium chloride (BNA) [15], nicotinamide mononucleotide (NMN) [16], methyl-1,4-dihydronicotinamide (MNA), and 1-phenethyl-1,4-dihydropyridine-3-carboxamide [11]. However, nearly all reported redox enzymes with activity with nicotinamide biomimetics are flavin-dependent oxidoreductases, such as enoate reductases [17], cytochrome P450 BM3 [18], and DT diaphorase [19]. The (enzyme-bound) flavin prosthetic group can oxidize biomimetic coenzymes and then its reduced flavin can be oxidized with other compounds, such as oxygen. Hence, the role of the nicotinamide ring is limited to reducing the flavin prosthetic group and, in principle, can be substituted by a variety of reductants [19]. To our knowledge, the few examples of engineered NAD(P)-dependent (flavin-free) dehydrogenases with activity for NMN include horse

liver alcohol dehydrogenase [20], *Gaobacillus stearothermophilus* lactate dehydrogenase [21], and *Pyrococcus furiosus* alcohol dehydrogenase [16]. However, all these exhibit three-four orders of magnitude lower specific activity on NMN^+ than their natural coenzymes (**Table S1**). Thought, it raises the question whether NAD(P)-dependent dehydrogenase mutants can exhibit comparable activities with NMN^+.

Directed evolution is a powerful enzyme engineering method to improve and optimize wild-type enzymes in order to evolve robust biocatalysts for practical applications.. However, the challenge is to develop efficient high-throughput screening (HTS) methods that evaluate the performance of mutated enzymes [22]. For activity with NAD(P), the use of 96-well microplate screening based on the absorbency at 340 nm is straightforward [23]. Also, NAD(P)H can be monitored with a colorimetric redox indicator, such as nitroblue tetrazolium (NBT) [14,24]. Holbrook and coworkers [25] developed a method to transfer colonies from Petri dishes to nitrocellulose paper, followed by cell lysis and NBT assay [25]. Zhang and coworkers later developed an improved double-layer HTS by using a redox dye tetranitroblue tetrazolium [5]. However, these HTS assays cannot be applied to identify novel mutated dehydrogenases with activity for biomimetics due to the preference of a targeted dehydrogenase for its natural coenzyme and very high background signal caused by interaction of other intracellular reducing compounds with the redox dye [11,16,21]. Because of this, we sought to develop a novel HTS to identify dehydrogenase activity with biomimetic coenzymes while minimizing the background signal from the cell lysate.

6-phosphogluconate dehydrogenase (6PGDH, EC 1.1.1.44), the second dehydrogenase in the pentose phosphate pathway, converts the 6-phophogluconate (6PG) and $NADP^+$ to ribulose 5-phosphate, NADPH, and CO_2. This enzyme has been used to produce high-yield hydrogen [26],

generate bioelectricity [27], and regenerate reduced coenzymes for biohydrogenation [28]. The coenzyme preference of 6PGDH from *Moorella thermoacetica* [5] and *Thermotaga maritima* [6] have been changed from $NADP^+$ to NAD^+ via directed evolution and rational design, respectively. In this study, we developed a novel HTS for rapid identification of *T. maritima* 6PGDH mutants with activity forwith NMN^+, which is a precursor of NAD^+,with less than half the size of NAD. The best mutant after multiple rounds of evolution exhibited comparable activities on NMN^+ compared with the wild-type on $NADP^+$. Furthermore, we demonstrate in this article the artificial NMN-based ETC for *in vitro* hydrogen production.

Results

A novel HTS approach

Effective identification of desired mutants from a large mutant library is the most challenging task of coenzyme engineering. Because dehydrogenases have generally poor activity with biomimetic coenzymes, the resulting signal in a HTS can easily be overwhelmed by background signals from the reducing environment within cells or impaired by oxygen exposure. Moreover, natural dehydrogenases always exhibit several orders of magnitude higher activities on natural coenzymes than biomimetic ones. Up to mM levels of intracellular natural coenzyme can exist in cell lysate [29]. This can lead to significant interference when screening using cell lysate and biomimetics, resulting in a failure of the HTS.

We developed cycle integrating directed evolution followed by a novel HTS approach that effectively minimizes background signal from reducing cell lysates and intracellular coenzymes (e.g., NAD(P)) (**Figure 1b**). Two inducible promoters, P*tac* and P*T7*, were used for controlling modest expression of *Tm*6PGDH in *E.coli* TOP10 for screening and the high expression of *Tm*G6PGDH in *E. coli* BL21 (DE3) for enzyme characterization, respectively. The transformed *E.coli* TOP10 cells harboring mutant libraries were firstly grown on the solid agar LB kamamycin media in Petri dishes and then heat-treated at 70ºC for 1 hour to lyse the cells, deactivate natural *E. coli* dehydroegnases, and partially oxidize intracellular reducing compounds. Lysed colonies were transferred to the surface of a Whatman filter paper, which was put into a Buchner funnel. Washing buffer (50 mL each washing) was used to immerse the filter paper several minutes followed by vacuum filtration. The washed filter paper was put into another Petri-dish and overlaid by the melted agarose solution containing 6PG, NMN^+, WST-1, and diaphorase from *Geobacillus stearothermophilus* (*Gs*DI). In it, the *Tm*6PGDH catalyzed the

reduction of NMN^+ to NMNH by oxidizing the 6-phophogluconate to ribulose 5-phosphate while coproducing CO_2. The NMNH then reduced the colorless redox dye WST-1 in the presence of electron mediator *Gs*DI, yielding the yellow WST-1 formazan (**Figure 1a**). Following theincubation at room temperature, the positive mutants were identified based on their deeper yellow color. This was followed by plasmid extraction and transformation into *E. coli* BL21 (DE3) for characterization.

Optimization of the HTS approach

Critical was choosing the proper redox dye to react with the reduced NMNH generated by *Tm*6PGDH mutants (which have activity with oxidized NMN^+). Although intensive efforts have been conducted to determine NAD(P)-dependent dehydrogenase activities based on a chromogenic redox dye, such as NBT [14,24], 2,6-dichlorophenolindophenol (DCPIP), methylene blue, Alamar Blue (resazurin), and others, most of these are not suitable for HTS with NMN. We collected 24 redox dyes that change color based on oxidation/reduction state (**Table S2**) and screened them based on four criteria: (1) reduction potential of the dye, (2) oxygen tolerance, (3) dye sensitivity, and (4) mediator selectivity (**Figure 2a**). First, the redox potential of an ideal redox dye should be close to that of the reduced nicotinamide based coenzyme (i.e., NAD(P)H, -0.32 V) at a neutral pH, enabling generation of a color signal. The redox dyes with high redox potentials, such as iodine, potassium permanganate, potassium dichromate, were excluded because of potential to cross-react with other reductants (i.e., vitamin C, glutathione). Second, the reduced dye must be stable and cannot be re-oxidized by air. This eliminated seven dyes, including methyl viologen, benzyl viologen, neutral red, methylene blue, DCPIP, indigo carmine and phenazine methosulfate (PMS). Third, the extinction coefficient of the reduced dye should be

larger than that of the reduced conezyme. This means a signal is amplified and cannot be decolored by the over-reduction. This eliminated potassium ferricyanide and and Alamar Blue. Fourth, the mediator should have high selectivity between the reduced biomimic and oxidized dye and great stability for a long-term colorimetric reaction. Another nine redox dyes were eliminated due to uncoupling reactions (i.e., P450s) or poor thermostability (i.e., azoreductase from *E. coli*) of corresponding mediators. After careful selection and evalutation, the candidates selected for further analysis were: tetrazolium redox dye, NBT, XTT and WST-1 (**Figure 2b**).

Figures 2c,d show the results of colony colorimetric assay of *Tm*6PGDH with activity on NMN^+. All three dyes, including NBT, XTT and WST-1, generated expected color change catalyzed by enzyme-coupled reactions with NMN^+. With the dyes selected, the NMN signal comprised 55-59% of the total chromogenic signal. The background signals were generated by nonspecific reactions between redox dyes and reduced cell materials and *Tm*6PGDH activity on NAD(P) in cell lysate. Among these dyes,the WST-1 dye showed the lowest level of dye background signals (around 10% of the total chromogenic signal) and was selected as the optimal redox dye for further optimization of an HTS.

To minimize the background signal resulting from intracellular NAD(P) using the WST-1 dye, a immersion-filtration procedure was implemented where colonies on the filter paper were washed by 0, 100, 200 and 400 mL phosphate sodium buffer (**Figure 2e**). With the identical low dye background signal of the WST-1 dye, the noise from intracellular NAD(P) decreased from 35% to 4% of the total signal when washing buffer was added from 0 to 200 mL, and decreased slightly further when the washing volume was increased to 400 mL. With this washing method and the low background of the WST-1 dye, the signal of *Tm*6PGDH activity on NMN^+ was increased from 55% to 85% of the total chromogenic signal (**Figure 2f**). Given these

observations, the 400 mL washing volume was used throughout.

The selectivity and activity of the mediator was also a key determinant in developing the HTS for dehydrogenase activity with biomimetics.The highly selective and active mediators on NMNH is desirable because they ensure the effective hydride transfer from NMNH to WST-1 while minimize the background signals from reduced compounds or residual NAD(P) in the cell lysate. We tested three enzyme mediators (i.e., *Gs*DI, *Pfu*NROR and *Tm*DI) and one chemical mediator (PMS) for the colorimetric assay with NMN^+ (**Figure 2g**). The original *Gs*DI was the best mediator, showing the highest signal with the biomimetic and the lowest background signal produced by reducing biomolecules and NAD(P) in cell lysate. The other mediators *Pfu*NROR, *Tm*DI and PMS were limited by increased background signal from intracellular $NAD(P)^+$, low activity signal with NMN^+, and increased dye background noise. These led to a decrease of chromogenic signal of the biomimetic to 66%, 46% and 21% of total chromogenic signal, respectively (**Figure 2h**). After optimization of redox dyes, washing volume, and mediators, the dye background noise and intracellular NAD(P) noise was ultimately minimized to less than 10% and 4% of the total chromogenic signal, respectively, while the signal from activity on NMN^+ was increased from 55% to 85%. This improved the signal-to-noise ratio of the screening from 1.1 to 5.7, making it adequate for a HTS to discover mutated dehydrogenases with activity with NMN^+.

Validation of the HTS

The optimal HTS was carried-out to identify mutants of *Tm*6PGDH with activity for NMN^+ from libraries generated by three-rounds of saturation mutagenesis in positions in and around the NADP binding pocket and another three-rounds of random mutagenesis of the entire

gene. The screening conditions became more stringent (i.e., lower concentration of NMN^+, shorter reaction time) during later rounds of screening. In early screens (rounds 1-4), positive mutants (featuring stronger yellow color) were identified by adding 1 mM NMN^+ with 6 hours incubation. In later screens (rounds 5 and 6), 0.3 mM NMN^+ was added, and a 4-hour incubation was used (**Figure 3**). Approximately 20,000 mutants were screened and about 10-20 positive mutants were identified in each round. The most active characterized mutant in each round was chosen as the parental gene for the next round of directed evolution. The mutagenesis, HTS, and characterization were repeated six times, until no further improvement was observed.

Mutagenesis strategy

Residues wild-type *Tm*6PGDH involved in the binding of 2' phosphate (N32/R33/T34), pyrophosphate (A11/V12) and adenine moieties (D82/T83/Q86) of $NADP^+$ were the mutagenesis targets for constructing the first three rounds of mutant libraries (**Figure 4a**). Starting with the wild-type *Tm*6PGDH exhibiting low activity on NMN^+ (0.6 U/mg), the saturation mutagenesis of N32 with rational design of R33I and T34I, and screening created a mutant Mut 1-1 with slightly increased activity (0.68 U/mg) compared to the parent.. The next mutant Mut 2-1, generated from library of A11/V12 and HTS, exhibited a more than 8-fold improved activity on NMN^+ (4.66 U/mg). The saturation library of D82/T83/Q86 and screening evolved the 6PGDH to more active mutant Mut 3-1, which had a further 2-fold increase in activity on NMN^+ (9.19 U/mg). Using the mutant Mut 3-1 as template, we did another three rounds of random mutagenesis and screening, and identified three new mutants Mut 4-1, Mut 5-1 and Mut 6-1 with gradual increases in activity with NMN^+. The final mutant Mut 6-1, showed a more than 30-fold higher rate of desired reaction compared to wild-type enzyme, and reached a specific activity of 17.7 U/mg on NMN^+,

which was comparable to that of wild-type enzyme on natural coenzyme $NADP^+$ (18.0 U/mg) (**Figure 4b**).

Characterization of *Tm*6PGDH and its mutants

The mutation sites, specific activities, and apparent kinetic constants on $NADP^+$ and NMN^+ of *Tm*6PGDH and its mutants are given in **Table 1**. The wild-type *Tm*6PGDH had a k_{cat} of 1.3 s^{-1}, a K_M of 30.6 mM on NMN^+, resulting in a low catalytic efficiency of 0.043 mM^{-1} s^{-1}. As expected, the wild-type enzyme worked perfectly on natural coenzyme, showing a high k_{cat} (15.9 s^{-1}), a low K_M (0.0012 mM) and high catalytic efficiency (13394.5 mM^{-1} s^{-1}) on $NADP^+$.. The Mut 1-1carried two mutation sites R33I/T34I, which was introduced by designed mutations in the primer. The saturtion mutagenesis and screening of N32 found the orginal asparagine was found as the optimal residue in this position. The mutation change led to a increase in k_{cat} (1.7 s^{-1}), a increase in K_M (37.9 mM) and a slightly improved catalytic efficiency on NMN^+ (0.046 mM^{-1} s^{-1}) compared to those of parental enzyme, while the catalyctic efficiency on $NADP^+$ was greatly decreased to 1.3 mM^{-1} s^{-1} ,which was caused by the evaluated K_M (11.5 mM). An additional mutation site A11G and slient mutation of V12 were introduced into Mut 2-1. This new mutant exhibited a increased k_{cat} (10.2 s^{-1}), a decreased K_M (20.7 mM), resulting in a more than 12-fold increase in catalytic efficiency on NMN^+ (0.49 mM^{-1} s^{-1}) compared to those of wild-type enzyme. A similar enhancement of enzymatic performance on $NADP^+$ was aslo found in Mut 2-1 and the catalytic efficiency on $NADP^+$ was increased from 1.3 to 13.2 mM^{-1} s^{-1}. The Mut 3-1 harboring three new mutations D82L/T83L/Q86L showed a further increase in activity (k_{cat} = 19.3 s^{-1}) and catalytic efficiency (0.7 mM^{-1} s^{-1}) but lower affinity (K_M = 27.5 mM) on NMN^+. Its catalytic efficiency on $NADP^+$ was increased from 13.2 to 52.7 mM^{-1} s^{-1},which was caused by the

decreased K_M (0.39 mM) compared to Mut 2-1. Simultaneous improvement in activities and unchanged K_M on NMN^+ and $NADP^+$ was observed in the residual mutants generated by random mutagenesis. The final mutant Mut 6-1, which cotained 18 mutations, showed a k_{cat} of 27.4 s^{-1}on NMN^+, indicating a more than 20-fold and 1.5-fold higher maximum activity of wild-type enzyme on NMN^+ and $NADP^+$, respectively. With the decreased K_M (13.5 mM), the catalytic effiicency of Mut 6-1 on NMN^+ was increased to 2.04 mM^{-1} s^{-1}, giving a a more than 50-fold improvement comparing with that of wild-type enzyme. As for the properties on $NADP^+$, the k_{cat} of Mut 6-1 was increased to 28.9 s^{-1}, while its K_M was 0.19 mM, resulting in a more than 90-fold lower catalytic efficiency (148.6 mM^{-1} s^{-1}) compared to that of wild-type enzyme. The apparent kinetic constants of wild-type enzyme and mutants toward NAD^+ were also determined. A gradual increase of catalytic efficiency on NAD^+ was observed accompanied with the evolutionary progression from the wild-type enzyme to the final mutant (**Table S3**).

To evaluate coenzyme scope change of *Tm*6PGDHs, we tested the specific activities of wild-type enzyme and newly optimized mutant Mut 6-1 against a range of nicotinamide based coenzymes (**Table 2**). We were pleased to find that the engineered enzyme Mut 6-1 was able to utilize all these coenzymes. As expected, the greatest change in specific activity was observed in the case of NMN^+. The Mut 6-1 had the specific activity of 17.7 U/mg, resulting in a more than 30-fold improvement compared to wild-type enyzme. The engineered enzyme also exhibited high activity on $NAD(P)^+$ (>27 U/mg), showing a more than 1.5 and 5.8-fold higher activity of wild-type enzyme on $NADP^+$ and NAD^+, respectively. Nicotinamide riboside (NR^+) is the truncated percusor of NMN^+ without the phosphate linked with the ribose ring. Suprisingly, The engineered enzyme Mut 6-1 had a specific activity of 0.014 U/mg on NR^+, 7-fold higher than that of wild-type enzyme. This level of activity, however, was still a more than 200-fold lower than that of

wild-type enzyme on natural coenzyme and more protein engineering works need to be done for its practical application. BNA^+ is a common synthetic coenzyme cotaining a hydrophilic benzyl group. In contrast to the previous observations, the engineered enzyme showed a 2.5-fold decreased activity (0.006 U/mg) on BNA^+ compared to that of wild-type enzyme.

In vitro hydrogen generation via an NMN-dependent ETC

The low-cost and stable biomimetic coenzyme is a long sought candidate to substitute the costly NAD(P) for the *in vitro* hydrogen generation [30]. Here we constructed a NMN-dependent ETC by consolidating the wild-type *Tm*6PGDH or the most active mutant Mut 6-1 with two thermophilic enzymes: (1) diaphorase from *Geobacillus stearothermophilus* and (2) Ni-Fe hydrogenase I from *Pyrococcus furiosus* (SHI), the biomimetic coenzyme NMN^+ and electron mediator benzyl viologen (BV^{2+}), to generate hydrogen (H_2) from 6PG at 60ºC. **Fig. 5a** shows the mechanism of the enzymatic pathway, which includes three sequential cascade reactions: (1) regeneration of NMNH from NMN^+ with concomitant oxidation of 6PG to Ru5P and release of CO_2 catalyzed by *Tm*6PGDHs; (2) Reduction of BV^+ from BV^{2+} and oxidation of NMNH catalyzed by *Gs*DI; (3) Generation of hydrogen and oxidation of BV^+ catalyzed by SHI.

When the wild-type *Tm*6PGDH was used for hydrogen generation, only a small amount of hydrogen was obtained after 6.2 hours of reaction, and the corresponding maximum hydrogen productivity was 2 mmole H_2 /L/h. However, when the wild-type enzyme was replaced by the most active mutant Mut 6-1 in the ETC, the *in vitro* hydrogen productivity was enhanced greatly. The maximum hydrogen productivity improved to 12 mmole H_2 /L/h (reached after 5.3 hours of reaction), resulting in a more than 6-fold improvement in productivity rate compared to that of wild-type enzyme.

Methods

Chemicals and Media

All chemicals, including nicotinamide adenine dinucleotide phosphate ($NADP^+$), Nicotinamide adenine dinucleotide (NAD^+), nicotinamide mononucleotide (NMN^+), 1-Benzyl-3-carbamoylpyridinium chloride (BNA^+), 6-phophogluconate (6PG), and benzyl viologen (BV^{2+}), were reagent grade or higher and purchased from Fisher Scientific (Pittsburgh, PA, USA) or Sigma-Aldrich (St. Louis, MO, USA), unless otherwise noted. Nicotinamide riboside (NR^+) was purchased from CTMedChem (Bronx, NY, USA). Redox dye 3,3'-[3,3'-Dimethoxy-(1,1'-biphenyl)-4,4'-diyl]-bis[2-(4-nitrophenyl)-5-phenyl-2H-tetrazolium chloride (NBT), 2-(4-Iodophenyl)-3-(4-nitrophenyl)-5-(2,4-disulfophenyl)-2H-tetrazolium, monosodium salt (WST-1) were purchased from Dojindo Molecular Technologies, Inc (Rockville, MD, USA). The 2,3-bis(2-methoxy-4-nitro-5-sulfophenyl)-2H-tetrazolium-5-carboxanilide (XTT) was purchased from Cayman Chemical Company Inc (Ann Arbor, MI, US). The genomic DNA of *Thermotoga maritima* and *Pyrococcus furiosus* were purchased from the American Type Culture Collection (Manassas, VA, USA). Primers were synthesized from Integrated DNA Technologies (Coralville, IA, USA). All enzymes for molecular biology experiments were purchased from New England Biolabs (NEB, Ipswich, MA, USA). Strains, plasmids are listed in **Table S4** and primers are listed in **Table S5**.

Preparation of plasmid pET28a-P_{tac}-*Tm6pgdh*

Plasmid pET28a-P_{tac}-*Tm6pgdh* contains 1.4-kb codon optimized *Tmg6pgdh* under control of dual promoter P_{T7}-P_{tac}. The parental *Tm6pgdh* gene was amplified from pET-ci-co*6pgdh* with a pair of primers Tm_6PG_F/Tm_6PG_R, and the linearized vector backbone was amplified

from pET28a-P_{tac}-*6pgdh* with a pair of primers Tm_6PGvect_F/Tm_6PGvect_R using the NEB Phusion® high-fidelity DNA polymerase. The two PCR fragments were assembled by prolonged overlap extension PCR (POE-PCR) [31]. The POE-PCR product was transformed into *E.coli* TOP10, yielding the plasmid pET28a-P_{tac}-*Tm6pgdh*.

Preparation of plasmid pET20b-*Tmdi*

The plasmid pET20b-*Tmdi* was constructed as follows. The gene encoding *T. maritima* diaphorase (*Tm*DI) was amplified from genomic DNA of *T. maritima* MSB8 with a pair of primers Tm_DI_F/Tm_DI_R, and the linearized vector backbone was amplified from pET20b with a pair of primers Tm_DIvect_F/Tm_DIvect_R using the NEB Phusion® high-fidelity DNA polymerase. The two PCR products were assembled by prolonged overlap extension PCR (POE-PCR) [31] and transformed into *E.coli* BL21(DE3) to obtain plasmid pET20b-*Tmdi*.

Preparation of plasmid pET20b-*Pfunror*

The plasmid pET20b- *Pfunror* was constructed as follows. The gene encoding *P. furiosus* NAD(P)H: rubredoxin oxidoreductase (*Pfu*NROR) was amplified from genomic DNA of *P. furiosus* DSM 3638 with a pair of primers Pfu_NROR_F/Pfu_NROR_R, and the linearized vector backbone was amplified from pET20b with a pair of primers Pfu_NRORvect_F/Pfu_NRORvect_R using the NEB Phusion® high-fidelity DNA polymerase. The two PCR products were assembled by prolonged overlap extension PCR (POE-PCR) [31] and transformed into *E.coli* BL21(DE3) to obtain plasmid pET20b-*Pfunror*.

Saturation mutagenesis and mutant library construction

Three successive rounds of saturation mutagenesis of *Tm6pgdh* were created using QuickChange Site-directed mutagenesis Kit, digested by *Dpn*I, and transformed into *E.coli* TOP10 for screening as previously described [5]. The library N32/R33/T34 was chosen for the first round saturation mutagenesis and amplified from pET28a-P_{tac}-*tmg6pdh-di* by a pair of primes of 32,33,34_F/32,33,34_R. The positive mutant Mut 1-1 was used as template for the saturation mutagenesis of library A11/V12 and amplified by a pair of primes of 11,12_F/11,12_R. The positive mutant Mut 2-1 generated from second round mutagenesis and screening was used for the construction of mutant library of D81/T82/Q86 and amplified by a pair of primes 81,82,86_F/81,82,86_R. The positive mutant Mut 3-1 selected from this library was chosen as parental gene for creating mutant library of random mutagenesis.

Random mutagenesis and mutant library construction

A random mutant library encoding mutant Mut3-1 of *Tm6pgdh* was generated by error-prone PCR with an estimated average of five mutations per gene. The reaction solution with a total volume of 50 μL was comprised of 5 ng/μL plasmid, 0.2 mM dATP, 0.2 mM dGTP, 1 mM dCTP, 1 mM dTTP, 5 mM $MgCl_2$, 0.004 mM $MnCl_2$, 0.05 U/μL the NEB regular Taq polymerase and 0.4 μM primer pairs (Tm_6PG_F/Tm_6PG_R). The PCR reaction was conducted as follows: 1 cycle of 94ºC for 2 min; 16 cycles of 94ºC for 30 s, 60ºC for 30 s, 68ºC for 1.5 min; and a final extension cycle of 68ºC for 5 min. The linearized vector backbone was amplified as described above. The two PCR products were digested by *Dpn*I, purified and assembled into DNA multimers by POE-PCR. The PCR product after digestion by *Xho*I was purified, ligated and transformed into *E. coli* TOP10 competent cell for screening [32]. The identified positive mutants

from each round library were purified and characterized. The most active mutant on NMN^+ was selected as the template for the next round error-prone PCR.

Optimization of HTS

The redox dye, washing volume of colonies and mediators were sequentially optimized to find the optimal conditions for HTS. Colonies of *E. coli* TOP10 carrying the plasmid pET28a-P_{tac}-*Tm6pgdh* were grown on 15 mL of 1.5% LB agar medium with 50 μg/mL kanamycin and incubated at 37ºC for 2 days. The colonies were treated to 70ºC for 1 hour, cooled down to the room temperature, duplicated on the surface of sterile qualitative filter paper (Whatman 410, size 7.5 cm) and placed into the new Petri-dish (size 9 cm).

To select the optimal redox dye, 20 mL of 0.5% agarose (60ºC) containing 150 μM tetrazolium dye (i.e., NBT, XTT, WST-1), 0.13 μM GsDI (2.8 ug/mL), 2 mM 6PG, 1 mM NMN^+, 50 mM Tris-HCl (pH 7.5), 50 μg/mL chloramphenicol and 0.1% sodium azide, were applied to the colonies and incubated at room temperature for 3 days. The control groups with agarose solution excluding coenzyme NMN^+ (6PG only) or both substrates 6PG and NMN^+ (No substrate) were constructed to test the background caused by redox dyes and intracellular NAD(P).

To minimize the inference of intracellular NAD(P), the colonies duplicated on the filter paper were placed in the 47 mm filter and immersed in 50 mL of 50 mM phosphate-buffered saline (PBS) buffer (pH 7.5) for 3 minutes. The buffer was then drawn into the flask by vacuum filtration. The immersion-filtration procedure was repeated, and colonies were washed by 100, 200 and 400 mL PBS buffer, respectively. The washed filter paper was put into another Petri-dish, overlaid by 0.5% melted agarose solution containing 150 μM WST-1, 0.13 μM GsDI (2.8

ug/mL), 2 mM 6PG, 1 mM NMN^+, 50 mM Tris-HCl (pH 7.5), 50 μg/mL chloramphenicol and 0.1% sodium azide, and incubated at room temperature for 3 days. The control groups were constructed as described above.

To determine the optimal mediator for the colorimetric assay, colonies duplicated on the filter paper were washed by 400 mL PBS buffer as described above. The colonies were placed into new Petri-dishes and overlaid by 0.5% melted agarose solution containing 150 μM WST-1, 2 mM 6PG, 1 mM NMN+, 50 mM Tris-HCl (pH 7.5), 50 μg/mL chloramphenicol and 0.1% sodium azide with 0.13 μM different enzyme mediator (i.e., GsDI, TmDI, PfuNROR) or 0.5 μM chemical mediator phenazine methosulfate (PMS). The agarose covered colonies were incubated at room temperature for 3 days. The control groups were constructed as described above.

The color changes of all colonies were measured by camera. The saturation of colony color was analyzed by uncalibrated OD function of imageJ (http: //rsb.info.nih.gov/ij). The color difference between group containing both substrate 6PG and NMN^+ and the group of 6PG only was defined as the signal of 6PGDH activity on NMN^+. The color difference between group of 6PG only and no substrate, and the color density of no substrate group were defined as the background noise of intracellular NAD(P) and unspecific reaction of redox dyes, respectively. The conditions showing highest signal-to-noise ratio were identified as optimal.

Screening of *Tm*6PGDH mutants with increased activity on NMN^+

The HTS method was established as follows. Transformed cells containing mutant plasmid libraries were spread on the 15 mL of 1.5% agar LB medium containing 50 μg/mL kanamycin to reach an expected colony number of 500–800 per Petri-dish. The colonies were incubated at 37ºC for 2 days to accumulate sufficient *Tm*6PGDHs for screening. The colonies

were treated to 70ºC for 1 h to lyse the cell, degrade reductants and deactivate mesophilic redox enzymes inside the cell, such as *E. coli* 6PGDH [5]. After cooling down to room temperature, the heat-treated colonies were duplicated on the surface of sterile qualitative filter paper (Whatman 410, size 7.5 cm). The colonies were placed in the filter and immersed in 50 mL of 50 mM PBS buffer (pH 7.5) for 3 min. After that, the waste buffer was withdrawn by vacuum filtration. The immersion-filtration procedure was repeated seven times, and colonies were washed by 400 mL PBS buffer. The washed colonies were put into the new Petri-dish (size 9 cm) and overlaid by 0.5% melted agarose solution containing 150 μM WST-1, 0.13 μM GsDI (2.8 ug/mL), 2 mM 6PG, 1 mM NMN^+(for the first four rounds of screening) or 0.1 mM NMN^+ (for the fifth and sixth rounds of screening), 50 mM Tris-HCl (pH 7.5), 50 μg/mL chloramphenicol and 0.1% sodium azide, and incubated at room temperature for 6 hours. Positive mutants of *Tm*6PGDH with improved activity for NMN^+ were identified by the deeper yellow color. The colony showing the greatest color change of each Petri-dish was taken out by sterile toothsticks and suspended in 200 μL of the P1 buffer of Zymo ZR Plasmid Miniprep™ kit followed by the plasmid purification and transformation into *E. coli* TOP10 for DNA sequencing and *E. coli* BL21(DE3) for protein purification and characterization. The mutants showing the highest activity on NMN^+ from each round of mutagenesis and screening were selected as the template for the next round of mutagenesis.

Protein overexpression and purification

The *E. coli* BL21 strains harboring the Tm6PGDH and its mutants were grown in the LB medium with 50 μg/mL kanamycin at 37ºC. The IPTG-inducible overexpression and Ni-NTA purification of targeted enzymes was conducted as described previously [5], where the 100 μM

IPTG was used for protein induction, 50 and 250 mM imidazole were used for washing and elution step of Ni-NTA purification, respectively . Likewise, the *E. coli* BL21 strains containing *Gs*DI, *Tm*DI and *Pfu*NROR were grown the LB medium with 100 μg/mL ampicillin at 37ºC, overexpressed by IPTG induction and purified by Ni-NTA column as described above. Mass concentrations of purified proteins were determined by the Bradford assay using bovine serum albumin (BSA) as the standard.

Activity assay of Tm6PGDH and mutants

The activities of *Tm*6PGDH and mutants were measured at 60ºC for 5 minutes in a buffer comprised of 100 mM HEPES buffer (pH 7.5), 2 mM 6PG, 2 mM $NADP^+$ or 20 mM NMN^+, 5 mM $MgCl_2$, and 0.5 mM $MnCl_2$. The formation of NADPH or NMNH were monitored at 340 nm by a UV/visible spectrophotometer (Beckman Coulter, Fullerton, CA, USA), where the millimolar extinction coefficients (ε) of NADPH and NMNH are 6.22 mM^{-1} cm^{-1}[116]. The enzyme unit was defined as one μmole of NADPH or NMNH produced per minute. The apparent Michaelis–Menten kinetic constants of *Tm*6PGDH for $NADP^+$ and NMN^+ were determined using 0.001-2 mM $NADP^+$ or 1-40 mM NMN^+ with 2 mM 6PG, respectively. The data were collected and regressed by using the nonlinear least squares regression of GraphPad Prism 5 (Graphpad Software Inc, La Jolla, CA). The activities of *Tm*6PGDH and mutants on NAD^+ and biomimetic coenzyme NR^+ and BNA^+ were measured in the same buffer by replacing the NADP to 2 mM NAD^+, 20 mM NR^+ and 1 mM BNA^+, respectively. The formations of reduced coenzymes were monitored by using millimolar extinction coefficients (ε) of NADH (6.22 mM^{-1} cm at 340 nm), NRH (6.86 mM^{-1} cm at 336 nm) and BNAH (7.20 mM^{-1} cm at 360 nm). All runs were conducted in triplicate.

Conversion of NMNH via 6PGDH reaction

To measuring specific activity of *G. stearothermophilus* diaphorase (GsDI) on NMNH, The NMNH solution was prepared by the 6PGDH reaction with 6PG and NMN^+. In it, 1 U/mL Mut 6-1 was added in the degassed buffer containing 100 mM HEPES buffer (pH 7.5), 5 mM $MgCl_2$ and 0.5 mM $MnCl_2$, 10 mM NMN^+ and 10 mM 6PG followed by oxygen exclusion through argon gas. The reaction solution was incubated at 60ºC for 1 hour and then ultra-filtered by using 10,000 MWCO Amicon centrifugal filters from Milliporesigma (Bedford, MA, USA) to separate the protein and solution. The formation of NMNH in the solution was monitored at 340 nm by a UV/visible spectrophotometer (Beckman Coulter, Fullerton, CA, USA), where the millimolar extinction coefficients (ε) of NMNH is 6.22 mM^{-1} cm^{-1}[116]. Commonly, 1 mM NMNH could be obtained after the 6PGDH conversion and followed ultra-filtration.

Activity assay of diaphorase GsDI

The specific activities of *G. stearothermophilus* diaphorase (GsDI) on NMNH with oxidized benzyl viologen (BV^{2+}) were measured at 60ºC for 3 minutes. The enzyme reactions were carried out in an anaerobic screwcap IR quartz cuvette (Reflex Analytical Co., Ridgewood, NJ) with a degassed buffer containing 100 mM HEPES buffer (pH 7.5), 2 mM BV^{2+} , 1 mM NMNH, 5 mM $MgCl_2$ and 0.5 mM $MnCl_2$. The formation of reduced benzyl viologen was monitored 578 nm by a UV/visible spectrophotometer (Beckman Coulter, Fullerton, CA, USA), where the millimolar extinction coefficients (ε) of reduced benzyl viologen is 8.65 mM^{-1} cm^{-1} [33]. The specific activity of *Gs*DI on NADPH and NMNH with BV^{2+} are 4.2 and 2.9 U/mg at 60ºC, respectively.

Hydrogen production via *in vitro* artificial NMN-based ETC

The wild-type Tm6PGDH and the best mutant Mut 6-1 were used to produce hydrogen from 6PG via *in vitro* artificial NMN-based ETC. The enzyme cocktail was comprised of wild-type Tm6PGDH or Mut 6-1, diaphorase (DI) from *Geobacillus stearothermophilus*, and Ni-Fe hydrogenase I from *Pyrococcus furiosus* (SHI), which was kindly provided by Michael W. W. Adams [34]. The enzyme loadings are listed in **Table S6**. All enzymes were stored in 50% (wt/wt) glycerol at -80ºC. For removing the possible effect of glycerol on hydrogen production, all enzymes were diluted to 0.1% glycerol by using 100 mM HEPES buffer, and concentrated with 10,000 MWCO Amicon centrifugal filters from Milliporesigma (Bedford, MA, USA) before use. The final reagent solution was comprised of 100 mM HEPES buffer (pH 7.5), 50 mM 6PG, 20 mM NMN^+, 2 mM benzyl viologen (BV^{2+}), 5 mM $MgCl_2$, 0.5 mM $MnCl_2$, 56 μg /mL wild-type *Tm*6PGDH or Mut 6-1, 333 μg/mL of DI, and 147 μg/mL of SHI. 25 μg/mL of kanamycin and 0.01% (w/v) sodium azide were added to protect against the microbial contamination. Enzymatic H_2 reactions were conducted in a bioreactor at 60ºC. Continuous H_2 measurement was conducted in a continuous flow system with 50 mL/min ultrapure nitrogen (Airgas, Christiansburg, VA) as described below. The collected data were analyzed by Origin 8.0 (Northampton, MA, USA). All runs were conducted in triplicate.

Systems for continuous hydrogen measurement

Continuous hydrogen measurement was conducted in a continuous flow system purged with 50 mL/min ultrapure N_2 gas (Airgas, Christiansburg, VA). The hydrogen productivity was detected by a tin oxide thermal conductivity H_2 sensor (TGS 821, Figaro USA Inc., Arlington Heights, IL, USA) and equipped with a gas-tight flexible gas line. The temperature ranges of

reactor and condenser were set at 60°C and 21°C, respectively, which was under the control of refrigerated/heated circulating baths (NESLAB RTE7, Thermo Scientific; Isotemp 3016D, Fisher Scientific, USA). Data acquisition was exhibited with a USB-6210 device (National Instruments, Austin, TX, USA) and analyzed by Lab-View SignalExpress 2009 (National Instruments). The hydrogen signals were calibrated by in-line flow controllers and ultrapure H_2 gas (Airgas), as described previously [33].

Structural analysis of *Tm*6PGDH and mutants

The three-dimensional homology models of wild-type *Tm*6PGDH and mutants were constructed by SWISS-MODEL based on the cystral structure of *Lactococcus lactis* 6PGDH (PDB: 2IYP, 46.5% sequence identifiy). The structures of $NADP^+$ and NMN^+ were generated by using Chemdraw (PerkinElmer, Waltham, MA). The conformation space of the corresponding coenzyme binding area was analyzed using the Autodock program (Scripps Research Institute, La Jolla, CA). The results were presented and analyzed by by PyMOL (Schrödinger, Inc, Portland, OR, USA).

Discussion

Enzyme-based biocatalysis is becoming accepted as an alternative to whole-cell fermentation, but large-scale applications remain restricted to hydrolyases (e.g., amylase, protease, cellulase) and isomerases (e.g., glucose isomerase), with limited involvement of redox reactions [35]. Beyond the third wave of biocatalysis [22], *in vitro* biosystems comprised of numerous enzymes and coenzymes can be used to produce a myriad of products from special proteins and polypeptides [36], oligosaccharides [37], nucleotides [38], fine chemicals [39], isoprene [40], bioelectricity [41], hydrogen [42], alcohols [43,44], organic acids [45], to synthetic starch [46]. However, high prices (e.g.,

thousands of dollars per kg) and less stability of natural NAD(P) prevent their potential applications in *in vitro* production of low-value biocommodities. Low-cost stable biomimetics are of importance to decrease coenzyme costs in *in vitro* cascade biocatalysis. For instance, NMN^+ is a biomimetic coenzyme with a less than half size of NAD(P), showing successes in the enzyme-catalyzed reduction of cyclohexanone and electricity generation [47]. The simple structure gives this coenzyme series of superior properties, such as shorter synthesis pathway (**Figure S1**), less fragile bonds [48], and faster mass-transfer rates [16], which can result in a decreased coenzyme cost in biocatalysis. However, wild-type dehydrogenases often work poorly with NMN^+ and exhibit three to four orders of magnitude lower specific activities on NMN^+ than those with natural coenzymes. Coenzyme engineering of dehydrogenases to increase activity with NMN^+ is essentially important for biocatalysis applications.

It is a great challenge to identify beneficial mutants from large enzymatic libraries. for coenzyme engineering on biomimetics. In this work, we developed an HTS application for identification of *Tm*6PGDH mutants with activity for NMN^+ and minimal background signal. The optimized HTS used a colorimetric assay, where the signal of reduced NMNH generated by *Tm*6PGDH mutants was generated using the redox dye WST-1 and mediator *Gs*DI. This HTS proved to be simple and effective for coenzyme engineering with biomimetics and includes several advantages over alternative methods. Compared to standard 96- or 384-well plate assays, our method has higher screening capacity (approximately 800 colonies per petri-dish), simpler operation steps, less reagent consumption, less time required of cell cultures, and no need of using costly automation. Moreover, we applied the dual promoter *T7-tac* to control overexpression of *Tm*6PGDH and deleted the subcloning step involving the pET plasmid between screening and protein characterization, which was typically required in the directed

evolution protocol. The HTS detected dehydrogenase activity with biomimetic NMN^+ with precision, and the background signals in the colorimetric assay, such as inference of mesophilic redox enzymes and reduced coenzymes in the cell lysate, activity on intracellular NAD(P), and unspecific reactions between redox dyes and cell reduced materials were minimized by colony heat treatment, cell washing and the use of an optimal redox dye and mediator pair. Furthermore, because of the broad specificity of the mediator *Gs*DI to accept different biomimetic coenzymes, such as NMNH, NRH, BNAH (unpublished), the screening method showed great potential in the coenzyme engineering of dehydrogenases for a series of biomimetic analogs. Although this method is designed for the coenzyme engineering of thermophilic dehydrogenase, this Petri-dish based screening is also suitable to evolve mesophilic dehydrogenases, such as glucose 6-phosphate dehydrogenase from *Zymomonas mobilis* (unpublished), to the thermostable mutants. The engineered enzymes were then enabled to use as the template for the coenzyme engineering on biomimetics by using this method.

Because of the low activity of wild-type enzymes with biomimetic coenzymes, the colorimetric assay used in the HTS is needed urgently in the fields of enzyme engineering and biocatalysis. The living cell, which contains a highly reducing environment, contributed the major proportion of background signal. The NAD(P), reduced compounds (i.e., vitamin C, glutathione, cysteine) [49,50] and mesophilic redox enzymes [51] inside the cell can generate or regenerate strong reducing power and overwhelm the signal of reduced biomimetic coenzymes. Also, the integrated cell membrane can inhibit the mass transfer of extracellular substrates from entering the cell, which further decreases the dehydrogenase activity on biomimetic coenzymes. To minimize background signals from a cellular environment, we applied heat treatment to break cell membrane, denature mesophilic enzymes, and partially oxidize reduced compounds. This

was followed by cell washing to lower the concentration of intracellular NAD(P). Because lysed cells contain nutrients that can support the growth of a small number surviving cells following heat treatment, growth inhibitors, such as sodium azide and antibiotics, were added to melted the agarose solution to stop colony regrowth and retain low background signal. The redox dye, itself, was identified as another significant source of background signal. Three tetrazolium based redox dyes, NBT, XTT and WST-1, were chosen from 24 collected indicators due to their strong and stable coenzyme dependent color development.

Although sharing the same tetrazole core, these dyes were observed to have different levels of background noises. The NBT, which had protein binding affinity [52], may react with free cysteine residues in the heat-deactivated proteins and result in strong false positive signal [49]. XTT, was also reported to have modest reaction with reduced glutathionine and cause the background noise [53]. The WST-1, which showed stable color change with the lowest noise of redox dye, was chosen as the optimal redox dye. The mediator can be the chemical or enzyme which facilitates the electron transfer from electron donor (i.e., NMNH) to corresponding redox dyes. Due to the poor enzymatic performance of wild-type enzyme on biomimetics and possible noises, the mediator used for the coenzyme engineering on NMN^+ is required to have both selectivity and activity on NMNH. Although it is often used as coupled electron mediator with tetrazolium dyes, the chemical PMS is shown as a weaker mediator to oxidize NMNH compared to GsDI, no matter the catalyst units are calculated based on the molar concentration ((10 μM of PMS vs. 0.125 μM of *Gs*DI) or mass concentration (3.08 μg/mL of PMS vs. 2.88 μg/mL of *Gs*DI). Moreover, its inherent yellow color and unspecific reactions with reduced cell materials result in a strong background noise, which minimize the specificity of the colorimetric assay (**Figure S2**). The enzyme mediator *Pfu*NROR showing strong preference of NADPH [33], and the

*Tm*DI showing low activity on NMNH could not meet the both requirements at the same time and generated different levels of noises. Only the *Gs*DI which exhibited preference and high activity of smaller coenzymes [33] was chosen as the optimal mediator. Through iterative optimization of interested parameters, we finally minimize the background noise to less than 14% of whole chromogenic signal.

Molecular modeling of wild-type *Tm*6PGDH and Mut 6-1 were performed in order to shed light on the mechanism of substrate recognition. Seven amino acid substitutions (A11G, R33I, T34I, D82L, T83L, Q86L, A447V) from total 18 mutation sites of Mut 6-1 were predicted to confer the increased activity on NMN^+. More than half of beneficial mutation sites were located in the coenzyme binding pocket. The mutations occurred here greatly change the hydrophobicity of coenzyme binding pocket (**Figure 6a, 6c**), which may force the truncated coenzyme to adopt a favorable conformation for catalysis. The mutation A11G contributed the majority of activity increase on NMN^+. The A11 lies in the fingerprint motif (GxAxxG) of 6PGDH and protrudes into the coenzyme binding pocket (**Figure 6b**), which restricts the binding depth of coenzyme [54]. The incorporation of the smaller glycine residue in this position (**Figure 6d**) increase the distance between hydrophobic side chain and the phosphate group of NMN^+ (from 3.4 Å to 4.4 Å), which may introduce less repulsion interaction with coenzyme [54] and lead to an increased affinity in NMN^+. The R33I and T34I are introduced by designed mutations in the primer. Previous results showed these two mutations increased the catalytic efficiency of *Tm*6PGDH on NAD^+, a less complex coenzyme than $NADP^+$ [6]. We hypothesized these replacements would be also beneficial for accepting smaller coenzyme NMN^+. Indeed, these mutations introduce a strong steric exclusion effect on accepting $NADP^+$ [6]. These mutations, however, might minimize the possible attraction towards the phosphate group of NMN^+ and

increase the activity in NMN^+. The D82, T83, Q86 are three residue close proximity to the adenine moiety of $NADP^+$. Suprisingly, all these three residues were replaced to the same leucine in the mutant. Although they are far away from the binding site of NMN^+ (>10 Å), the strong hydrophobicity in this area might also prohibit the wrong allocation of the biomimetic coenzyme, generating a beneficial effect on NMN-dependent catalysis. Alanine at position 447 is the adjacent residue to the H448, which is responsible for interacting with 4-OH of 6PG in the homogenous 6PGDH from *Lactococcus lactis* [54]. The mutation from alanine to valine (A447V) might contribute a better acceptance of 6PG and facilitate the electron transfer from 6PG to the nicotinamide ring. Other mutations generated by the random mutagenesis, do not directly interact with both 6PG and NMN^+. The possible beneficial effects of these mutations are likely due to subtle reshaping of the active sites of enzyme for catalysis [55].

The efficient use of thermophilic enzymes plus economically advantageous and stable biomimetic coenzymes are critical to produce the low price hydrogen (~$1.5 per kg) via the *in vitro* synthetic enzymatic pathway [30]. We created an NMN-dependent ETC containing engineered 6PGDH, FMN-containing diaphorase, and NiFe-hydrogenase and electron carrier BV^{2+} for hydrogen production and demonstrated the effectiveness of engineered mutants on increased hydrogen productivity rate. To achieve complete conversion of starch to hydrogen by using an NMN-dependent *in vitro* synthetic enzymatic pathway [56], we are preparing to evolve two other redox enzymes involved in this pathway, glucose 6-phosphate dehydrogenase and diaphorase, and create the preferred mutants on this biomimetic coenzyme.

In conclusion, a novel HTS was developed to identify mutants of *Tm*6PGDH with activity with biomimetic coenzymes. Background signal in the colorimetric assay were greatly decreased by heat treatment, cell washing and the use of optimal redox dyes and enzyme mediators. The

best mutant Mut 6-1 showed a great increased catalytic efficiency, a comparable activity on NMN^+ compared to wild-type enzyme on $NADP^+$ as well as higher activity on natural coenzyme NAD(P) and NMN precursor nicotinamide riboside (NR^+). Based on the engineered enzyme, a novel NMN-dependent ETC was created for hydrogen production, demonstrating the effectiveness of engineered enzyme on improved hydrogen productivity rate. Coenzyme engineering along with the use of biomimetic coenzymes would break the last obstacle to industrial biomanufacturing catalyzed by *in vitro* synthetic enzymatic biosystems in biomanufacturing 4.0.

Acknowledgments

This project could not have been carried out without the support of the Biological Systems Engineering Department, Virginia Polytechnic Institute and State University, Blacksburg, Virginia, USA and Tianjin Institute of Industrial Biotechnology, Chinese Academy of Sciences. This study was supported by the Department of Energy, Office of Energy Efficiency and Renewable Energy, Fuel Cell Technologies Office under Award Number DE-EE0006968.

Contributions

RH, HC, and YHPZ conceived the project, performed experiments, and analyzed data. RSS contributed to the writing and editing of the manuscript.

Conflict of interest

The authors declare that they have no competing interests.

References

1 You, C., Huang, R., Zhu, Z. & Zhang, Y.-H. P. Protein engineering of oxidoreductases on nicotinamide-based coenzymes with the applications to synthetic biology. *Syn. Syst. Biotechnol.* (2017).

2 Schomburg, I., Chang, A. & Schomburg, D. BRENDA, enzyme data and metabolic information. *Nucleic Acids Res.* **30**, 47-49 (2002).

3 Schomburg, I. *et al.* The BRENDA enzyme information system–From a database to an expert system. *J. Biotechnol.* **261**, 194-206 (2017).

4 Scrutton, N. S., Berry, A. & Perham, R. N. Redesign of the coenzyme specificity of a dehydrogenase by protein engineering. *Nature* **343**, 38-43 (1990).

5 Huang, R., Chen, H., Zhong, C., Kim, J. E. & Zhang, Y.-H. P. High-throughput screening of coenzyme preference change of thermophilic 6-phosphogluconate dehydrogenase from $NADP^+$ to NAD^+. *Sci. Rep.* **6**, 32644., doi:10.1038/srep32644 (2016).

6 Chen, H., Zhu, Z., Huang, R. & Zhang, Y.-H. P. Coenzyme engineering of a hyperthermophilic 6-phosphogluconate dehydrogenase from $NADP^+$ to NAD^+ with its application to biobatteries. *Sci. Rep.* **6**, 36311, doi:10.1038/srep36311 (2016).

7 Hoelsch, K., Sührer, I., Heusel, M. & Weuster-Botz, D. Engineering of formate dehydrogenase: synergistic effect of mutations affecting cofactor specificity and chemical stability. *Appl. Microbiol. Biotechnol.* **97**, 2473-2481 (2013).

8 Brown, S. D. *et al.* Mutant alcohol dehydrogenase leads to improved ethanol tolerance in *Clostridium thermocellum*. *Proc. Natl. Acad. Sci. USA*, 13752-13757, doi:10.1073/pnas.1102444108 (2011).

9 Woodyer, R. D., van der Donk, W. A. & Zhao, H. Relaxing the nicotinamide cofactor specificity of phosphite dehydrogenase by rational design. *Biochemistry* **42**, 11604-11614 (2003).

10 Cahn, J. K. B. *et al.* A general tool for engineering the NAD/NADP cofactor preference of oxidoreductases. *ACS Syn. Biol.* **7**, 326–333, doi:10.1021/acssynbio.6b00188 (2017).

11 Nowak, C., Pick, A., Lommes, P. & Sieber, V. Enzymatic reduction of nicotinamide biomimetic cofactors using anengineered glucose dehydrogenase: providing a regeneration system for artificial cofactors. *ACS Catal.* **7**, 5202-5208 (2017).

12 Paul, C. E., Arends, I. W. C. E. & Hollmann, F. Is simpler better? synthetic nicotinamide cofactor analogues for redox chemistry. *ACS Catal.* **4**, 788-797, doi:10.1021/cs4011056 (2014).

13 Rollin, J. A., Tam, W. & Zhang, Y.-H. P. New biotechnology paradigm: cell-free biosystems for biomanufacturing. *Green Chem.* **15**, 1708-1719, doi:10.1039/C3GC40625C (2013).

14 Ji, D. *et al.* Creation of bioorthogonal redox systems depending on nicotinamide flucytosine dinucleotide. *J. Am. Chem. Soc.* **133**, 20857-20862, doi:10.1021/ja2074032 (2011).

15 Lo, H. C. & Fish, R. H. Biomimetic NAD^+ models for tandem cofactor Regeneration, Horse Liver Alcohol Dehydrogenase Recognition of 1,4-NADH Derivatives, and Chiral Synthesis. *Angew. Chem. Int. Ed.* **41**, 478-481 (2002).

16 Campbell, E., Meredith, M., Minteer, S. D. & Banta, S. Enzymatic biofuel cells utilizing a biomimetic cofactor. *Chem. Commun.* **48**, 1898-1900 (2012).

17 Paul, C. E. *et al.* Mimicking nature: synthetic nicotinamide cofactors for C=C

bioreduction using enoate reductases. *Org. Lett.* **15**, 180-183, doi:10.1021/ol303240a (2013).
18 Ryan, J. D., Fish, R. H. & Clark, D. S. Engineering cytochrome P450 enzymes for improved activity towards biomimetic 1,4-NADH cofactors. *Chembiochem : a European journal of chemical biology* **9**, 2579-2582, doi:10.1002/cbic.200800246 (2008).
19 Paul, C. E. & Hollmann, F. A survey of synthetic nicotinamide cofactors in enzymatic processes. *Appl. Microbiol. Biotechnol.* **100**, 4773–4778, doi:10.1007/s00253-016-7500-1 (2016).
20 Sicsic, S., Durand, P., Langrene, S. & Le Goffic, F. Activity of NMN^+, nicotinamide ribose and analogs in alcohol oxidation promoted by horse-liver alcohol dehydrogenase. Improvement of this activity and structural requirements of the pyridine nucleotide part of the NAD^+ coenzyme. *Eur. J. Biochem.* **155**, 403-407 (1986).
21 Flores, H. & Ellington, A. D. A modified consensus approach to mutagenesis inverts the cofactor specificity of *Bacillus stearothermophilus* lactate dehydrogenase. *Protein Eng. Des. Sel.* **18**, 369-377, doi:10.1093/protein/gzi043 (2005).
22 Bornscheuer, U. T. *et al.* Engineering the third wave of biocatalysis. *Nature* **485**, 185-194 (2012).
23 Brinkmann-Chen, S. *et al.* General approach to reversing ketol-acid reductoisomerase cofactor dependence from NADPH to NADH. *Proc. Natl. Acad. Sci. USA* **110**, 10946-10951, doi:10.1073/pnas.1306073110 (2013).
24 Mayer, K. M. & Arnold, F. H. A colorimetric assay to quantify dehydrogenase activity in crude cell lysates. *J. Mol. Screen.* **7**, 135-140 (2002).
25 El Hawrani, A. S., Sessions, R. B., Moreton, K. M. & Holbrook, J. J. Guided evolution of enzymes with new substrate specificities. *J. Mol. Biol.* **264**, 97-110 (1996).
26 Rollin, J. A. *et al.* High-yield hydrogen production from biomass by *in vitro* metabolic engineering: Mixed sugars coutilization and kinetic modeling. *Proc. Natl. Acad. Sci. USA* **112**, 4964-4969, doi:10.1073/pnas.1417719112 (2015).
27 Zhu, Z. G. & Zhang, Y.-H. P. *In vitro* metabolic engineering of bioelectricity generation for the complete oxidation of glucose. *Metab. Eng.* **39**, 110-116 (2017).
28 Wang, Y., Huang, W., Sathitsuksanoh, N., Zhu, Z. & Zhang, Y.-H. P. Biohydrogenation from biomass sugar mediated by *in vitro* synthetic enzymatic pathways. *Chem. Biol.* **18**, 372-380 (2011).
29 Bennett, B. D. *et al.* Absolute Metabolite Concentrations and Implied Enzyme Active Site Occupancy in *Escherichia coli*. *Nat. chem. biol.* **5**, 593-599, doi:10.1038/nchembio.186 (2009).
30 Zhang, Y.-H. P., Sun, J. & Zhong, J.-J. Biofuel production by *in vitro* synthetic enzymatic pathway biotransformation. *Curr. Opin. Biotechnol.* **21**, 663-669, doi:10.1016/j.copbio.2010.05.005 (2010).
31 You, C., Zhang, X. & Zhang, Y.-H. P. Simple cloning via direct transformation of PCR product (DNA Multimer) to *Escherichia coli* and *Bacillus subtilis*. *Appl. Environ. Microbiol.* **78**, 1593-1595., doi:10.1128/AEM.07105-11 (2012).
32 You, C. & Zhang, Y.-H. P. Easy preparation of a large-size random gene mutagenesis library in *Escherichia coli*. *Anal. Biochem.* **428**, 7-12., doi:10.1016/j.ab.2012.05.022 (2012).
33 Kim, E. J., Wu, C. H., Adams, M. W. & Zhang, Y.-H. P. Exceptionally high rates of biological hydrogen production by biomimetic *in vitro* synthetic enzymatic pathways.

Chem. Eur. J. **22**, 16047-16051., doi:10.1002/chem.201604197 (2016).
34 Chandrayan, S. K., Wu, C.-H., McTernan, P. M. & Adams, M. W. W. High yield purification of a tagged cytoplasmic [NiFe]-hydrogenase and a catalytically-active nickel-free intermediate form. *Protein Expr. Purif.* **107**, 90-94., doi:10.1016/j.pep.2014.10.018 (2015).
35 Straathof, A. J. J. Transformation of Biomass into Commodity Chemicals Using Enzymes or Cells. *Chem. Rev.*, doi:10.1021/cr400309c (2013).
36 Carlson, E. D., Gan, R., Hodgman, C. E. & Jewett, M. C. Cell-free protein synthesis: Applications come of age. *Biotechnol. Adv.* **30**, 1185-1194, doi:10.1016/j.biotechadv.2011.09.016 (2012).
37 Xu, Y. *et al.* Chemoenzymatic synthesis of homogeneous ultralow molecular weight heparins. *Science* **334**, 498-501, doi:10.1126/science.1207478 (2011).
38 Hennig, M., Scott, L. G., Sperling, E., Bermel, W. & Williamson, J. R. Synthesis of 5-fluoropyrimidine nucleotides as sensitive NMR probes of RNA structure. *J. Am. Chem. Soc.* **129**, 14911-14921, doi:10.1021/ja073825i (2007).
39 Bujara, M., Schümperli, M., Pellaux, R., Heinemann, M. & Panke, S. Optimization of a blueprint for *in vitro* glycolysis by metabolic real-time analysis. *Nat. Chem. Biol.* **7**, 271-277 (2011).
40 Korman, T. P. *et al.* A synthetic biochemistry system for the *in vitro* production of isoprene from glycolysis intermediates. *Protein Science* **25**, 576–585, doi:10.1002/pro.2436 (2014).
41 Zhu, Z., Tam, T. K., Sun, F., You, C. & Zhang, Y.-H. P. A high-energy-density sugar biobattery based on a synthetic enzymatic pathway. *Nat. Commun.* **5**, 3026., doi:10.1038/ncomms4026 (2014).
42 Martín del Campo, J. S. *et al.* High-Yield Production of Dihydrogen from Xylose by Using a Synthetic Enzyme Cascade in a Cell-Free System. *Angew. Chem. Int. Ed.* **52**, 4587-4590, doi:10.1002/anie.201300766 (2013).
43 Guterl, J.-K. *et al.* Cell-free metabolic engineering - Production of chemicals via minimized reaction cascades. *ChemSusChem* **5**, 2165-2172 (2012).
44 Krutsakorn, B. *et al. In vitro* production of n-butanol from glucose. *Metab. Eng.* **20**, 84-91 (2013).
45 Ye, X. *et al.* Synthetic metabolic engineering-a novel, simple technology for designing a chimeric metabolic pathway. *Microb. Cell Fact.* **11**, 120 (2012).
46 You, C. *et al.* Enzymatic transformation of nonfood biomass to starch. *Proc. Natl. Acad. Sci. USA* **110**, 7182-7187, doi:10.1073/pnas.1302420110 (2013).
47 Paul, C. E., Arends, I. W. & Hollmann, F. Is simpler better? Synthetic nicotinamide cofactor analogues for redox chemistry. *ACS Catal.* **4**, 788-797 (2014).
48 Hofmann, D., Wirtz, A., Santiago-Schübel, B., Disko, U. & Pohl, M. Structure elucidation of the thermal degradation products of the nucleotide cofactors NADH and NADPH by nano-ESI-FTICR-MS and HPLC-MS. *Anal. Bioanal. Chem.* **398**, 2803-2811, doi:10.1007/s00216-010-4111-z (2010).
49 Funk, D., Schrenk, H. H. & Frei, E. Serum albumin leads to false-positive results in the XTT and the MTT assay. *BioTechniques* **43**, 178, 180, 182 passim (2007).
50 Chakrabarti, R., Kundu, S., Kumar, S. & Chakrabarti, R. Vitamin A as an enzyme that catalyzes the reduction of MTT to formazan by vitamin C. *J. Cell Biochem.* **80**, 133-138 (2000).

51 Berridge, M. V., Herst, P. M. & Tan, A. S. Tetrazolium dyes as tools in cell biology: new insights into their cellular reduction. *Biotechnol. Annu. Rev.* **11**, 127-152, doi:10.1016/s1387-2656(05)11004-7 (2005).
52 Letinsky, M. S. & Decino, P. A. Histological staining of pre- and postsynaptic components of amphibian neuromuscular junctions. *J. Neurocytol.* **9**, 305-320 (1980).
53 Berridge, M. V., Tan, A. S., McCoy, K. D. & Wang, R. The biochemical and cellular basis of cell proliferation assays that use tetrazolium salts. *Biochemica* **4**, 14-19 (1996).
54 Sundaramoorthy, R. *et al.* Crystal structures of a bacterial 6-phosphogluconate dehydrogenase reveal aspects of specificity, mechanism and mode of inhibition by analogues of high-energy reaction intermediates. *Febs j.* **274**, 275-286, doi:10.1111/j.1742-4658.2006.05585.x (2007).
55 Romney, D. K., Murciano-Calles, J., Wehrmüller, J. E. & Arnold, F. H. Unlocking reactivity of TrpB: a general biocatalytic platform for synthesis of tryptophan analogs. *J. Am. Chem. Soc.* **139**, 10769 (2017).
56 Kim, J.-E. *et al.* Advanced water splitting for green hydrogen gas production through complete oxidation of starch by *in vitro* metabolic engineering. *Metab. Eng.* (2017).

Supporting information

Supporting information includes coenzyme synthesis pathway in vivo from NMN^+ to $NADP^+$, the structure analysis of individual mutation site conferring increased activity on NMN^+, comparisons of activities of redox enzymes on NMN^+, the analysis of 24 collected redox dyes, enzyme loading in hydrogen production experiments, details in apparent kinetics of mutants on $NAD(P)^+$ and NMN^+, and the information of strains, plasmid and primers.

Figure legend

Figure 1. Principles of high-throughput screening for coenzyme engineering on NMN^+. (a) The colorimetric assay for *Tm*6PGDH activity on NMN^+. The *Tm*6PGDH cleaves the 6-phophogluconate into ribulose 5-phosphate and CO_2, and reduces NMN^+ to NMNH. The enzyme mediator *Gs*DI catalyzes the consequent reduction of colorless WST-1 to yellow WST-1 formazan by oxidizing the NMNH. (b) The Schematic of high-throughput screening for identification of positive mutants on NMN^+. In this work, (1) the DNA mutations were introduced by saturation mutagenesis of coenzyme binding pocket and random mutagenesis of entire gene. (2) The DNA mutation library was transformed into *E. coli* TOP10 competent cell with high transformation efficiency, yielding the cell mutant library. (3) The colonies grown on the LB agar plate were heat-treated to deactivate the mesophilic enzymes and reduced compounds inside the cell followed by the duplication of colonies on the surface of filter paper. (4) The colonies on the filter paper were placed into a Buchner funnel and washed by several hundred mL of phosphate sodium buffer in order to decrease the concentration of intracellular NAD(P). (5) The washed colonies were overlaid by melted agaroase solution containing 6PG, a biomimetic (NMN^+), a mediator (*Gs*DI) and a redox dye (WST-1), and (6) incubated at room

temperature for color development. (7) The positive mutants featuring deeper yellow colors were identified from Petri-dish. The corresponding colonies were isolated for plasmid extraction followed by transformation into *E. coli* cells for characterization. The most active mutant on NMN^+ was selected as the parent for the next round of mutagenesis.

Figure 2. Iterative optimization of high-throughput screening. (a) Schematic of down-selection of candidate redox dyes for screening. The 24 redox dyes contained derivatives of (1) indophenol, (2) indigo dye, (3) azo dye, (4) permanganate ion, (5) tetrazolium, (6) viologen, (7) heterocyclic quinoneimine and other uncategorized compounds. The redox dyes was then down-selected to find out the promising candidate molecules based on redox potential change, O_2 tolerance, dye sensitivity and mediator selectivity. (b) Candiated redox dyes for detection of *Tm*6PGDH on NMN^+. The structure of these three redox dyes had the same tetrazolium core with different modified groups linked with benzyl rings. The color change from oxidized form to reduced form of NBT, XTT and WST-1 were colorless to purple, colorless to orange and colorless to yellow, respectively. (c) Optimization of redox dyes for screening. The heat-treated colonies were overlaid by melted agarose solution containing tetrazolium redox dyes (i.e., NBT, XTT, WST-1), 6PG, NMN^+ and mediator *Gs*DI and incubated at room temperature for color development. Two control groups with agarose solution excluding coenzyme NMN^+ (6PG only) or both substrates 6PG and NMN^+ (No substrate) were prepared to test background noise resulted from redox dyes and intracellular NAD(P). (d) Analysis of color change of heat-treated colonies. The saturation of colony color was analyzed by uncalibrated OD function of imageJ (http: //rsb.info.nih.gov/ij). (e) Optimization of washing volume for screening. In order to minimize the background noise of intracellular NAD(P), the heat-treated colonies were washed by 0, 100, 200 and 400 mL of phosphate sodium buffer, respectively, followed by overlay of melted agarose solution containing

reagents and incubation for color development. (f) Analysis of color change of colonies. The pictures were analyzed as described above. (g) Optimization of mediators for screening. In order to find the mediator with high selectivity and activity on NMNH, The heat-treated colonies was washed and overlaid by the melted agarose solution containing different mediators (i.e., *Gs*DI, *Tm*DI, *Pfu*NROR, PMS) for color development. (h) Analysis of color change of colonies. The pictures were analyzed as described above.

Figure 3. Pictures of high-throughput screening to identify active mutants on NMN^+. (a) An example of Petri-dish result of first 4 rounds of screening. The colonies were overlaid by the melted agarose solution containing 1 mM NMN^+ and incubated at room temperature for 6 hours. The positive mutants showing stronger yellow color were identified with red arrows. (b) An example of Petri-dish result of fifth-sixth rounds of screening. The colonies were overlaid by the melted agarose solution containing 0.3 mM NMN^+ and incubated at room temperature for 4 hours. The positive mutants showing stronger yellow color were identified with red arrows

Figure 4. Directed evolution of Tm6PGDH for increasing activity on NMN^+. (a) Structure model of wild-type *Tm*6PGDH in complex with $NADP^+$. Residues in close proximity (< 5 Å) to the 2' phosphate, pyrophosphate and adenine moieties of $NADP^+$ are colored red, blue and magenta, respectively, and chosen as interested target for saturation mutagenesis. (b) The evolutionary progression of mutants with increased activities on NMN^+.

Figure 5. Hydrogen production via *in vitro* artificial NMN-based ETC. (a) Schematic of synthetic enzymatic pathway for hydrogen production. (b) H_2 evolution profiles at 60°C via *in vitro* artificial NMN-based ETC. The result of wild-type *Tm*6PGDH (WT) and the most active mutant Mut 6-1 of are shown with black and red line, respectively. The experiments were

repeated three times independently; data shown are for one of three representative experiments.

Figure 6. Hydrophobicity change of coenzyme binding pocket of wild-type Tm6PGDH (a) and mutant 6-1 (c). The interactions between NMN^+ and A11 and mutation A11G were shown in b and d, respectively. The corresponding distances were indicated as yellow dashed line with yellow label. The hydrophobicity scale of individual residue was estimated based on Normalized consensus hydrophobicity scale. The deeper red color indicated a higher scale of hydrophobicity. The original interested residues were labeled as black and the replacements were marked as orange. The biomimetic coenzyme NMN^+ was depicted as sticks. Atoms were colored according to the types: N, blue; O, red; P, orange; C, green.

Table 1. Apparent kinetic constants of *Tm*6PGDHs for NMN^+ and $NADP^+$

Enzyme	Mutations	$NADP^+$				NMN^+			
		Sp. Act. (U/mg)	k_{cat} (s^{-1})	K_M (mM)	k_{cat}/K_M ($mM^{-1}.s^{-1}$)	Sp. Act. (U/mg)	k_{cat} (s^{-1})	K_M (mM)	k_{cat}/K_M ($mM^{-1}.s^{-1}$)
WT	-	18.0 ± 0.8	15.9± 0.2	0.0012 ± 0.0001	13394.5	0.60 ± 0.01	1.3 ± 0.1	30.6 ± 1.7	0.04
Mut 1-1	R33I/T34I	1.2 ± 0.2	14.8 ± 0.7	11.5 ± 1.1	1.3	0.68 ± 0.01	1.7 ± 0.1	37.9 ± 3.6	0.04
Mut 2-1	**11G**/R33I/T34I	10.2 ± 0.7	28.3 ± 0.6	2.1 ± 0.1	13.2	4.66 ± 0.02	10.2 ± 0.2	20.7 ± 0.7	0.49
Mut 3-1	11G/R33I/T34I/ **D82L**/**T83L**/**Q86L**	16.4 ± 0.1	21.1 ± 0.3	0.39 ± 0.02	53.7	9.19 ± 0.09	19.3 ± 0.4	27.5 ± 1.2	0.70
Mut 4-1	11G/**K27R**/R33I/T34I/D82L/T83L/Q86L/**I120F**/**D294V**/**Y383C**/**N387S**/**A447V**	20.0 ± 0.3	21.9 ± 0.2	0.22 ± 0.01	101.0	12.31 ± 0.14	18.9 ± 0.4	15.1 ± 0.6	1.25
Mut 5-1	11G/K27R/R33I/T34I/**F60Y**/D82L/T83L/Q86L/K118N/**I120F**/D294V/**F326S**/Y383C/N387S/A447V	20.6 ± 0.4	23.6 ± 0.3	0.21 ± 0.01	113.0	16.40 ± 0.40	25.8 ± 0.8	16.0 ± 1.1	1.62
Mut 6-1	11G/K27R/R33I/T34I/F60Y/D82L/T83L/Q86L/K118N/I120F/**D251E**/D294V/F326S/**F329Y**/Y383C/N387S/**V390G**/A447V	27.1 ± 0.8	28.9 ± 0.3	0.19 ± 0.01	148.6	17.7 ± 0.35	27.4± 0.5	13.5 ± 0.5	2.04

Table 2. Activities of wild-type *Tm*6PGDH and Mut 6-1 for coenzymes

Enzymes	Specific activity (U/mg)				
	NMN^+	$NADP^+$	NAD^+	NR^+	BNA^+
WT	0.60 ± 0.01	18.0 ± 0.8	4.9 ± 0.2	0.0020 ± 0.0001	0.00035 ± 0.00006
Mut 6-1	17.7 ± 0.35	27.1 ± 0.8	28.5 ± 0.2	0.014± 0.001	0.0031 ± 0.002

Figure 1. Principles of high-throughput screening for coenzyme engineering on NMN^+

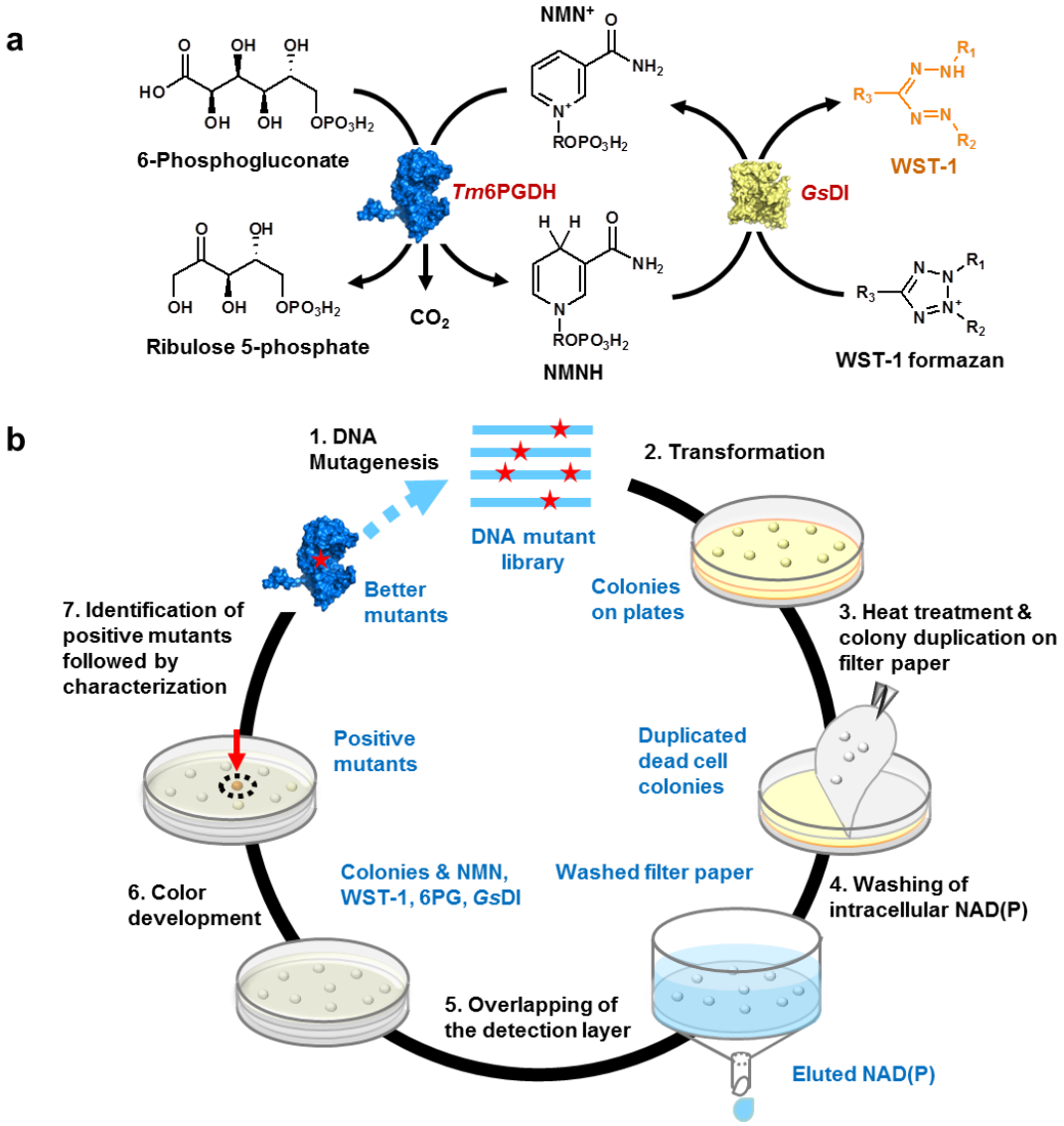

Figure 2. Iterative optimization of high-throughput screening

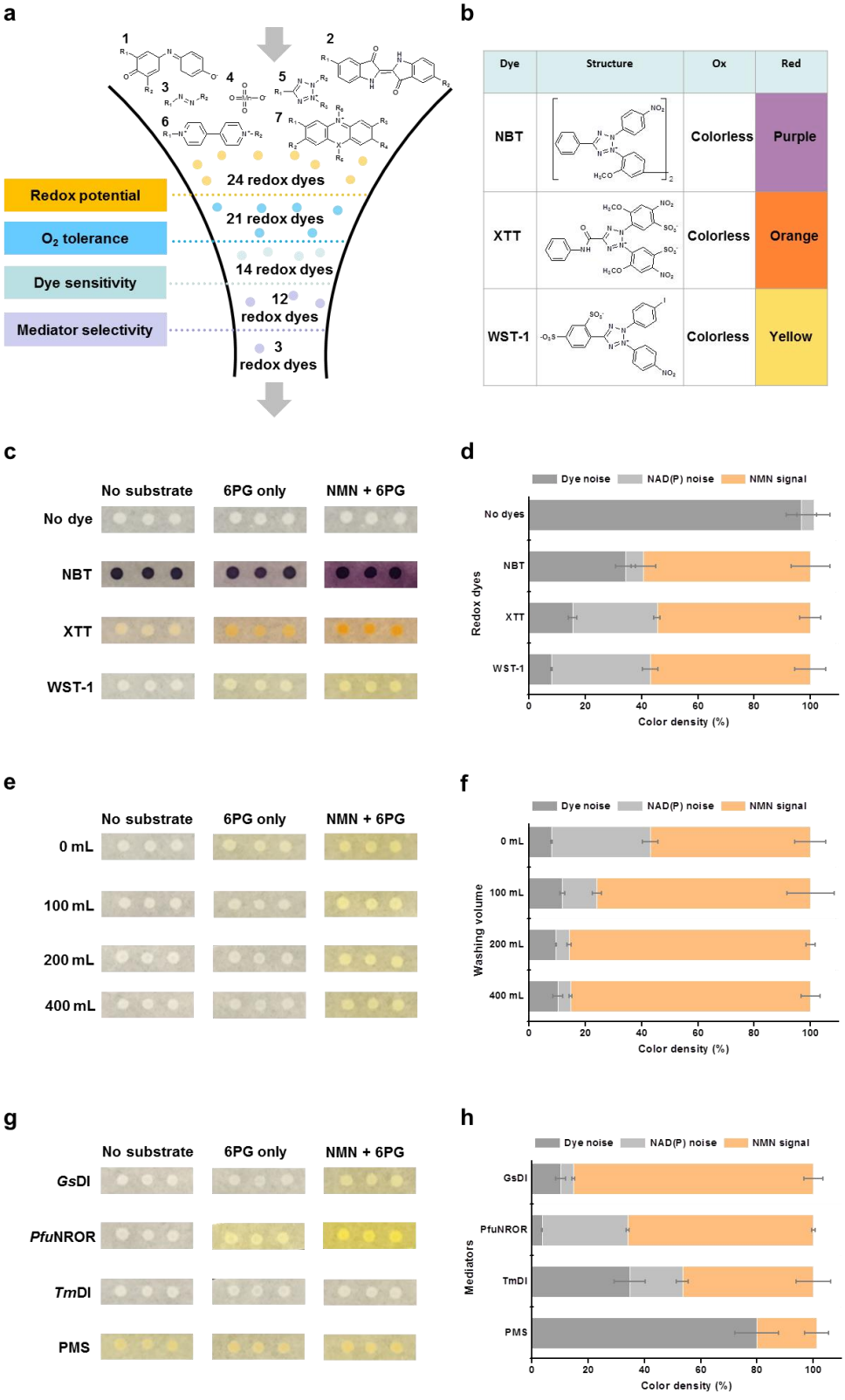

Figure 3. Pictures of high-throughput screening to identify active mutants on NMN^+

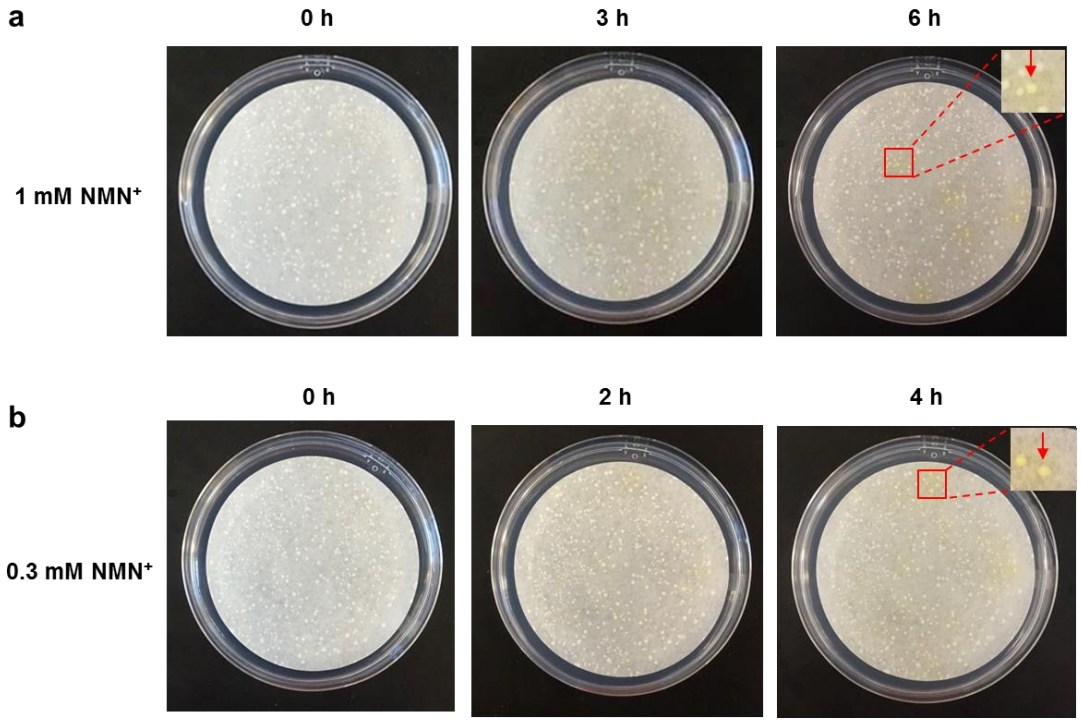

Figure 4. Directed evolution of *Tm*6PGDH for increasing activity on NMN^+

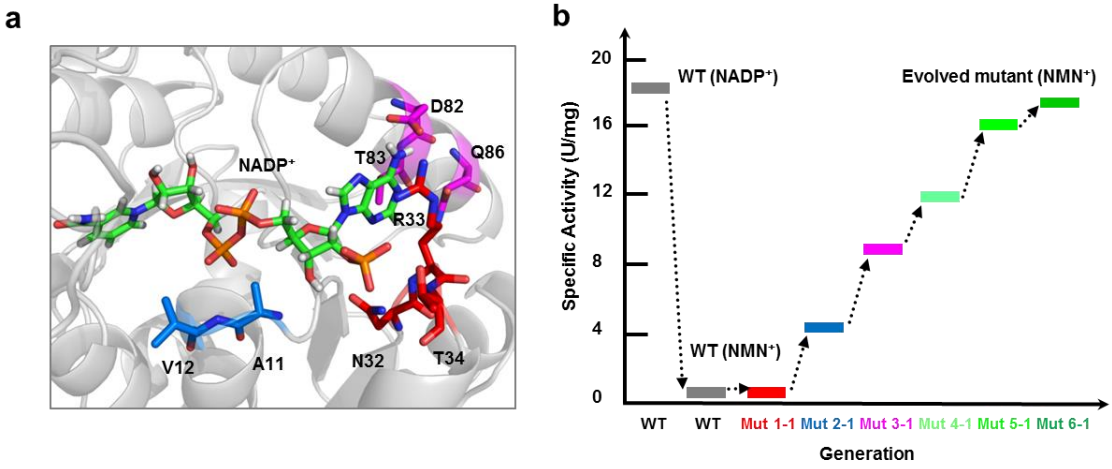

Figure 5. Hydrogen production via *in vitro* artificial NMN-based ETC

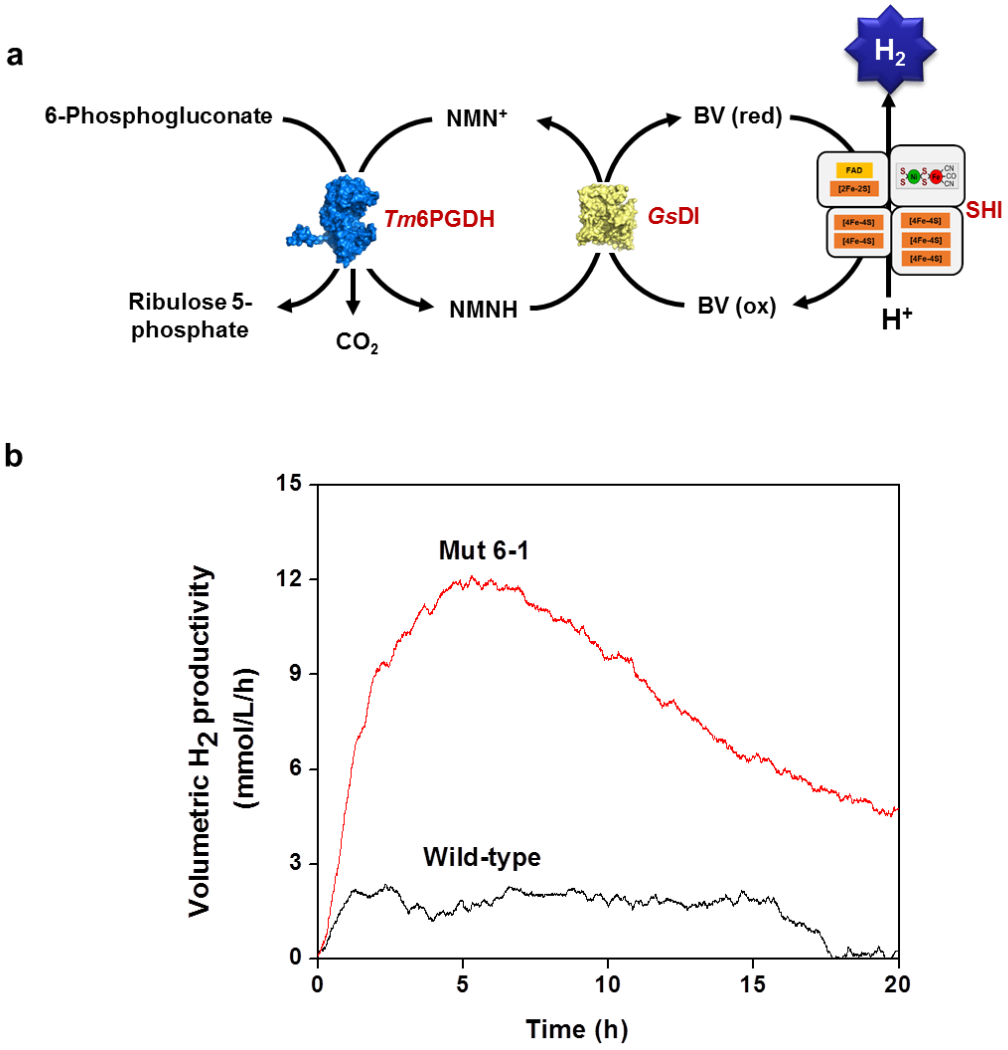

Figure 6. Hydrophobicity change of coenzyme binding pocket of wild-type Tm6PGDH and mutant 6-1

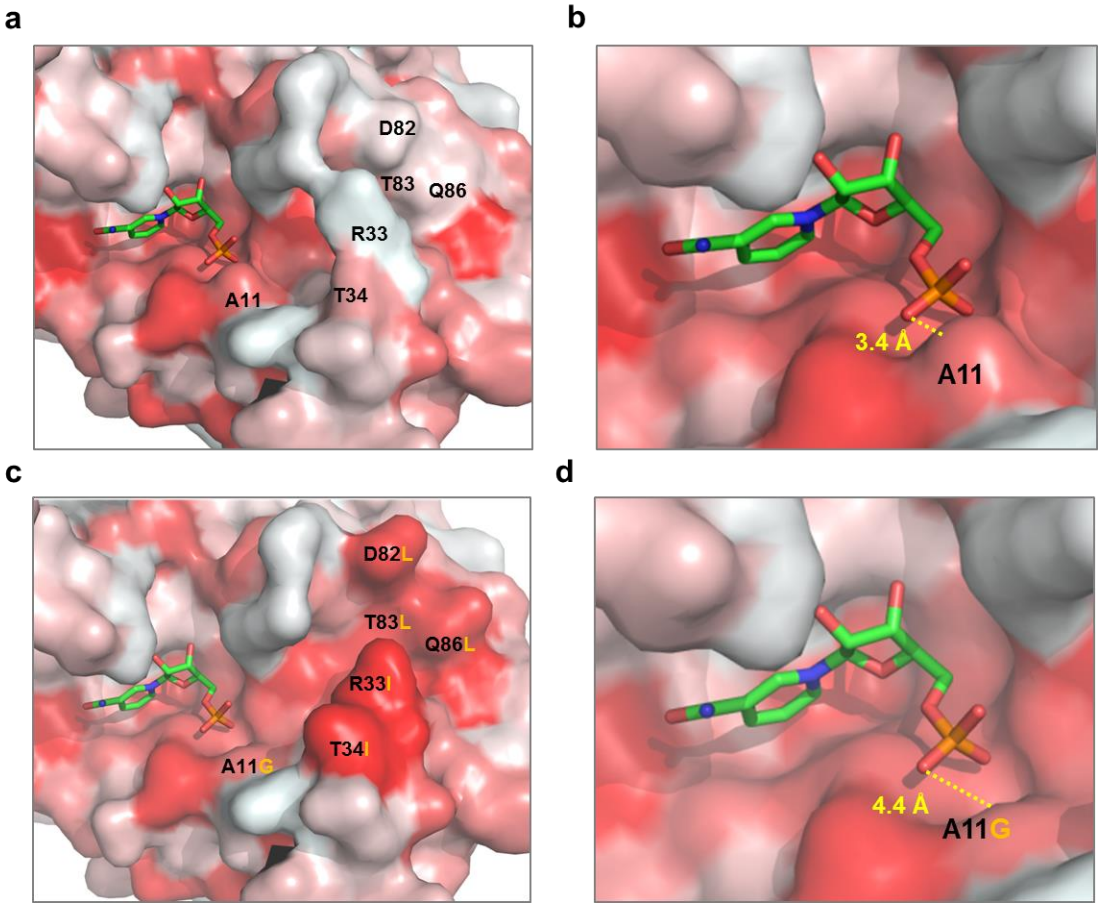

Chapter 6: General Conclusions and Future Work

The coenzyme engineering of NAD(P)-dependent dehydrogenases is of importance for biocatalysis and synthetic biology in vivo and *in vitro*. The coenzyme engineering of 6PGDH on unnatural coenzymes, such as NAD^+ and biomimetic coenzyme NMN^+, is critical for efficient use of these less costly coenzymes in the *in vitro* synthetic biosystem for hydrogen production and facilitates the production of low-cost hydrogen. In this dissertation, we developed a HTS for coenzyme engineering of 6PGDH on NAD^+ and produced an engineered 6PGDH with a 4,278 fold reversal of coenzyme selectivity from $NADP^+$ to NAD^+. This method was also used to screen the mutant of highly active G6PDH with improved thermostability. The evolved mutant exhibited a more than 124-fold improvement in the half-life time at 60ºC without losing its specific activity, and showed a more than 7-fold increased productivity rate and yield of hydrogen production from starch via the *in vitro* enzymatic pathway. With this method, we further added the novel cell washing step and used the optimal redox dyes and diaphorase to decrease the background signals coming from $NADP^+$ and reduced biomolecules in the cell lysate, and developed a new screening method for coenzyme engineering of 6PGDH for activity with the biomimetic coenzyme NMN^+. By using six-rounds of directed evolution and screening, we gained a more active mutant, which showed a more than 50-fold increase in catalytic efficiency on the NMN^+. Consolidated with two other thermophilic redox enzymes, diaphorase from *Geobacillus stearothermophilus* and Ni-Fe hydrogenase I from Pyrococcus furiosus , the engineered enzyme was used to

create a novel biomimetic coenzyme dependent ETC for hydrogen production, which showed a more than 6-fold increased productivity rate compared to the wild-type enzyme. These results demonstrated the effectiveness of new HTS in coenzyme engineering of NAD(P)-dependent dehydrogenases.

To construct the whole biommetic coenzyme dependent *in vitro* synthetic biosystem for hydrogen production, activities on NMN^+ of three NAD(P)-dependent redox enzymes including glucose 6-phosphate dehydrogenase, diaphorase and hydrogenase, must be improved by coenzyme engineering. The efficient use of engineered dehydrogenases along with the biomimetic coenzymes would break the last obstacle to industrial biomanufacturing for hydrogen production catalyzed by *in vitro* synthetic enzymatic biosystems in biomanufacturing 4.0.

Appendix. Supporting information for engineering a NADP-dependent dehydrogenase on nicotinamide mononucleotide: high-throughput screening and artificial electron transport chain

Rui Huang[1], Hui Chen[1], Ryan S. Senger[1,2], Yi-Heng Percival Zhang[1,3*]

[1] Department of Biological Systems Engineering, Virginia Tech, Blacksburg, Virginia 24061, USA

[2] Department of Chemical Engineering, Virginia Tech, Blacksburg, Virginia 24061, USA

[3] Tianjin Institute of Industrial Biotechnology, Chinese Academy of Sciences, 32 West 7th Avenue, Tianjin Airport Economic Area, Tianjin 300308, China

*Corresponding author

Email: yhzhang@vt.edu

Supporting information

Engineering a NADP-dependent dehydrogenase on nicotinamide mononucleotide: high-throughput screening and artificial electron transport chain

Rui Huang[1], Hui Chen[1], Ryan S. Senger[1,2], Yi-Heng Percival Zhang[1,3*]

[1] Department of Biological Systems Engineering, Virginia Tech, Blacksburg, Virginia 24061, USA

[2] Department of Chemical Engineering, Virginia Tech, Blacksburg, Virginia 24061, USA

[3] Tianjin Institute of Industrial Biotechnology, Chinese Academy of Sciences, 32 West 7th Avenue, Tianjin Airport Economic Area, Tianjin 300308, China

*Corresponding author

Email: yhzhang@vt.edu

SI Figures

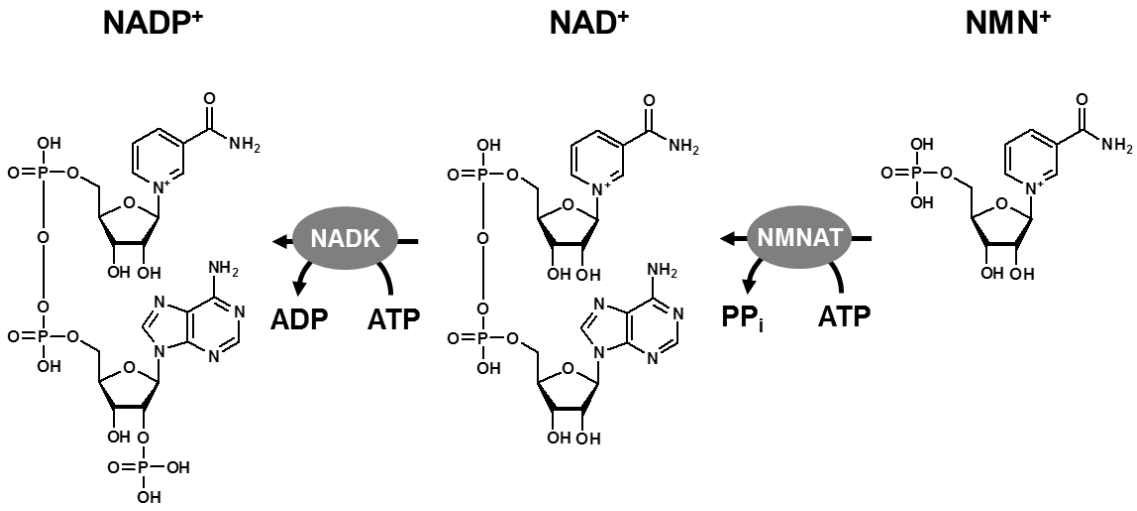

Figure S1. The Enzymatic pathway for NAD(P) synthesis. The NAD is synthesized from nicotinamide mononucleotide (NMN) and ATP catalyzed by nicotinamide nucleotide adenylyltransferase (NMNAT), and NADP is synthesized from NAD and ATP catalyzed by NAD kinase (NADK)

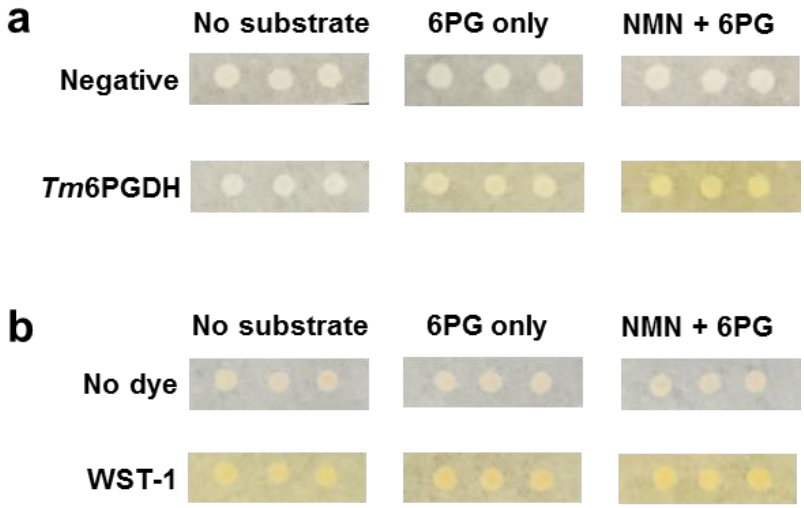

Figure S2. Test of background signals from mesophilic redox enzyme and PMS. (a) Test of background signals from mesophilic redox enzymes in the heat-treated colonies. The *E. coli* TOP10 (pET28a-P*tac*) was a negative control while *E. coli* TOP10 (pET28a-P*tac*-*Tm6pgdh*) was a positive control. Colonies were treated at 70 for 1 h and duplicated on the filter paper. The heat-treated cells were then overlaid by the melted agarose solution containing substrates and mediator *Gs*DI followed by incubation at room temperature for 3days for color development. Two control groups with agarose solution excluding coenzyme NMN^+ (6PG only) or both substrates 6PG and NMN^+ (No substrate) were prepared to test background noise resulted from redox dyes and intracellular NAD(P). The pale colony color in negative groups suggested the deactivation of mesophilic redox enzymes, while the strong color change between NMN+6PG group and no substrate group of *Tm*6PGDH indicated that the targeted thermophilic 6PGDH remains active after the heat treatment. (b) Test of background noise of PMS in the colorimetric assay. The colonies of *E. coli* TOP10 (pET28a-P*tac*-*Tm6pgdh*) were heat-treated and operated as described as above. The treated colonies were overlaid by the melted agarose with WST-1 or without WST-1 (No dye)

SI tables

Table S1. Apparent kinetic parameters of dehydrogenases on NMN^+

Enzyme	Mutation	Host	Coenzyme	Other coenzymes	Sp. Act (U/mg)	Temp (^oC)	k_{cat} (s^{-1})	K_M (mM)	k_{cat}/K_M ($mM^{-1}. s^{-1}$)	Ref.
Lactate dehydrogenase	P16Q/C81S/N85R	*Bacillus stearothermophilus*	NMN^+	No	$5.01\text{-}5.72*10^{-6}$ [a]	25	ND	ND	ND	[1]
Alcohol dehydrogenase	-	*Equus caballus*	NMN^+	Zn^{2+}	ND	37	0.024	10	0.0024	[2-4]
Alcohol dehydrogenase	-	*Pyrococcus furiosus*	NMN^+	No	ND	45	0.0005	2.5	0.0002	[5]
Alcohol dehydrogenase	K249G/H255R	*Pyrococcus furiosus*	NMN^+	No	ND	45	0.026	2.6	0.010	[5]
Tm6PGDH	-	*Thermotoga maritima*	NMN^+	No	0.047	60	1.3	30.6	0.04	This study
Tm6PGDH	K27R/F60Y/K118N/I120F/D251E/D294V/F326S/F329Y/Y383C/N387S/V390G/A447V	*Thermotoga maritima*	NMN^+	No	17.7	60	27.4	13.5	2.04	This study

a, the specific activity of lactate dehydrogenase on NMN^+ is calculated one the basis of the absorbance change of NNMNH vs time plot from corresponding reference, where the mole extinction coefficient of NMNH is 6,220 at 340 nm.

Table S2. Characterization of redox dye for screening

Compound	Group	Structure	Color (ox)	Color (re)	E^0 (V, pH 7)	O_2 inference	Extinction coefficient (mM)	Mediator properties	Others	Ref.
Methyl viologen	Bipyridinium	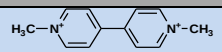	Colorless	Blue	-0.45	Yes[a]	9.8 (reduced, 578 nm)	NAD(P)H:rubredoxin oxidoreductase (NROR) from *Pyrococcus furiosus* , reaction with NMNH (ND), no uncoupling reaction, thermophilic	Cell toxicity	6-10
Benzyl viologen	Bipyridinium	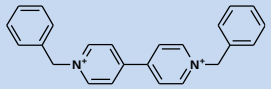	Colorless	Blue	-0.36	Yes	8.7 (reduced, 578 nm)	Diaphorase from *Geobacillus stearothermophilus* (GsDI), react with NMNH (Yes), no uncoupling reaction, thermophilic	Cell toxicity	6,9,11-13
Neutral red	Phenazine	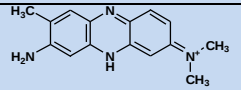	Red	Colorless	-0.33	Yes	7.12 (oxidized, 540 nm)	No need	Red (pH <6.8); Yellow (pH >8.0)	6,14-17
WST-1	Tetrazolium	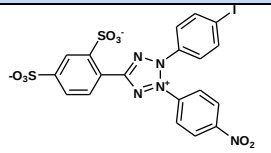	Colorless	Yellow	-0.14	No	37.0 (reduced, 433 nm)	GsDI, react with NMNH (Yes), no uncoupling reaction, thermophilic. 1-m PMS is another mediator	No	18-20
XTT	Tetrazolium	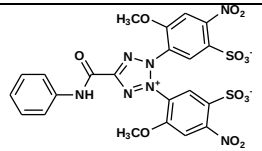	Colorless	Orange	-0.14[b]	No	23.6 (reduced, 450 nm)	GsDI, react with NMNH (Yes), no uncoupling reaction, thermophilic. PMS is another mediator	No	20-24
NBT	Tetrazolium	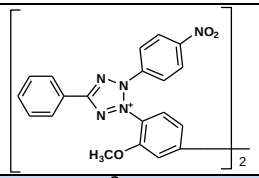	Colorless	Dark blue	-0.13[b]	No	30.0 (reduced diformazan, 560 nm)	GsDI, react with NMNH (Yes), no uncoupling reaction, thermophilic. PMS is another mediator	No	20,21,25,26
Indigo carmine	Indigo dye	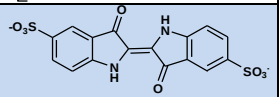	Blue	Red (partially reduced), Yellow (reduced)	-0.13	Yes[c]	19.4 (oxidized, 610 nm)	Azoreductase from *Bacillus cereus*, reaction with NMNH (ND), no uncoupling reaction, mesophilic	Light sensitive, Yellow (pH >13)	27-32

Methylene blue	Phenothiazin	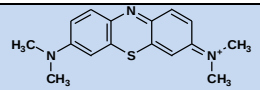	Blue	Colorless	+0.071	Yes[d]	40.0 (oxidized, 613 nm)	No need	No	[33-35]
Phenazine methosulfate (PMS)	Phenazine	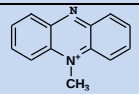	Green	White (precipitation)	+0.080	Yes	26.3 (oxidized, 387 nm)	No need	Light sensitive	[36-39]
2,6-Dichlorophenolindophenol	Indophenol	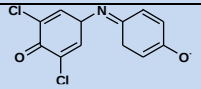	Blue	colorless	+0.22	Yes[e]	19.0 (oxidized, 600 nm)	No need	Red (pH< 5.7)	[27,40-43]
Potassium ferricyanide	Coordinated complex		Yellow	Green	+0.36	ND	1.0 (oxidized, 420 nm)	P450 CYP175A1 from *Thermus thermophilus*, reaction with NMNH (ND), uncoupling reaction (ND), thermophilic	No	[44-46]
Alamar Blue	Phenoxazin	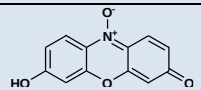	Blue	Pink (fluorescence)	+0.38	No	73 (reduced 572 nm)	PMS, react with NMNH, no uncoupling reaction	Affected by fluorescent material. Over-reduction produces colorless byproduct	[19,47-51]
Azo-rhodamine derivative 9	Azo dye	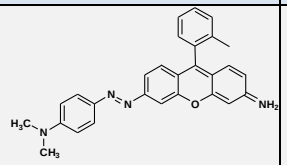	Colorless	Green (fluorescence)	ND	ND	82	Azoreductase from *E.coli*, react with NMNH (ND), no uncoupling reaction, mesophilic	Radioactive substances required.	[52,53]
Carmoisine	Azo dye	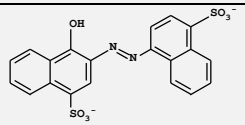	Red	Colorless	ND	ND	ND	Azoreductase from *Bacillus lentus* BI377, react with NMNH (ND), uncoupling reaction (ND), thermophilic	The reduced product amine can be toxic	[54]

1-Methoxynaphthalene	Naphthalene		Blue (dimer)	Colorless	ND	No	ND	P450BSβ (CYP152A1) mutant from *Bacillus subtilis*, reaction with NMNH (ND), uncoupling reaction (ND), mesophilic	H_2O_2 required, which may react with NMNH	[55]
2-Substituted phenols	Phenol		Red or Brown (polymer)	Colorless	ND	No	ND	2-hydroxybiphenyl 3-monooxygenase from *Pseudomonas azelaica* HBP1, react with NMNH (ND), uncoupling reaction, mesophilic	No	[56]
7-Ethoxycoumarin	Coumarin	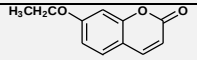	Blue (fluorescence)	colorless	ND	No	ND	P450 from *Rhodococcus sp*, reaction with NMNH (ND), uncoupling reaction, mesophilic	O_2 required, low enzymatic activity	[57]
7-Ethoxyresorufin	Phenoxazin	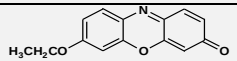	Pink (fluorescence)	Orange	ND	No	73 (oxidized, 572 nm)	P450s, reaction with NMNH (ND), uncoupling reaction, commonly mesophilic	O_2 required	[50]
Indole	Indole		Blue (indigo)	Colorless	ND	No	19.4 (oxidized, 610 nm)	P450CAM mutant from *Pseudomonas putida*, reaction with NMNH (ND), uncoupling reaction, mesophilic	O_2 required	[29,58-60]
Styrene	Styrene		Purple (final product)	Colorless	ND	No	ND	P450 BM-3 139-3 mutant from *Bacillus megaterium*, reaction with NMNH (ND), uncoupling reaction, mesophilic	O_2 required, final color of product fades with time	[61]
Para-Nitrophenoxy analog (pNA)	p-Nitrophenol	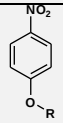	Yellow	colorless	ND	No	17.5 (oxidized, 400 nm)	P450 BM-3 mutant from *Bacillus megaterium*, reaction with NMNH (ND), uncoupling reaction (ND), mesophilic	O_2 required, esterase may result in false positive	[62,63]

Iodine	Halogen	I_2	Purple	Colorless	+0.54	Poor	ND	No need	Protein oxidation	[44,64,65]
Potassium permanganate	Metal ion		Violet	Black (MnO_2)	+0.60	No	2.5 (oxidized, 525 nm)	No need	DNA and protein oxidation	[44,66-69]
Potassium dichromate	Metal ion		Orange	green (Cr^{3+})	+1.36	No	Interfered by concentration	No need	DNA and protein oxidation	[44,66,70,71]

a, the reaction rate of reduced methyl viologen with oxygen is $6*10^6$ mol/L/min. b, the standard potential of NBT and XTT are calculated on the basis of rate constant between superoxide and NBT/XTT ,where the $E_0(O_2/O_2^-)$ is -0.15 V. c, the reaction rate of reduced Indigo carmine with oxygen is $2*10^{-4}$ mol/L/min. d, the reaction rate of reduced methylene blue with oxygen is $1*10^4$ mol/L/min by using NADH as reducing power. e, the reaction rate of reduced 2,6-dichlorophenolindophenol with oxygen is predicted as $8*10^{-6}$ mol/L/min based on reaction of phenol indophenol with oxygen. Dyes with high redox potential, high oxygen sensitivity, low or unstable absorptivity change, dependence on low specificity mediators were shaded as orange, blue, light blue and gray, respectively.

Table S3. Apparent kinetic constants and activities of *Tm*6PGDHs for NAD(P)$^+$ and NMN$^+$

Enzyme	NADP$^+$				NAD$^+$				NMN$^+$			
	Sp. Act. (U/mg)	k_{cat} (s^{-1})	K_M (mM)	k_{cat}/K_M ($mM^{-1}.s^{-1}$)	Sp. Act. (U/mg)	k_{cat} (s^{-1})	K_M (mM)	k_{cat}/K_M ($mM^{-1}.s^{-1}$)	Sp. Act. (U/mg)	k_{cat} (s^{-1})	K_M (mM)	k_{cat}/K_M ($mM^{-1}.s^{-1}$)
WT	18.0 ± 0.8	15.9± 0.2	0.0012 ± 0.0001	13394.5	4.9 ± 0.2	55.9 ± 2.9	14 ± 1	4.1	0.60 ± 0.01	1.3 ± 0.1	30.6 ± 1.7	0.04
Mut 1-1	1.2 ± 0.2	14.8 ± 0.7	11.5 ± 1.1	1.3	6.2 ± 0.2	48.8 ± 1.3	7.9 ± 0.5	6.2	0.68 ± 0.01	1.7 ± 0.1	37.9 ± 3.6	0.04
Mut 2-1	10.2 ± 0.7	28.3 ± 0.6	2.1 ± 0.1	13.2	21.2 ± 0.1	29.8 ± 0.5	0.57 ± 0.02	52.6	4.66 ± 0.02	10.2 ± 0.2	20.7 ± 0.7	0.49
Mut 3-1	16.4 ± 0.1	21.1 ± 0.3	0.39 ± 0.02	53.7	15.5 ± 0.3	22.0 ± 0.4	0.46 ± 0.03	47.8	9.19 ± 0.09	19.3 ± 0.4	27.5 ± 1.2	0.70
Mut 4-1	20.0 ± 0.3	21.9 ± 0.2	0.22 ± 0.01	101.0	21.5 ± 0.2	24.6 ± 0.3	0.27 ± 0.01	90.1	12.31 ± 0.14	18.9 ± 0.4	15.1 ± 0.6	1.25
Mut 5-1	20.6 ± 0.4	23.6 ± 0.3	0.21 ± 0.01	113.0	25.5 ± 0.4	29.3 ± 0.5	0.24 ± 0.01	122.6	16.40 ± 0.40	25.8 ± 0.8	16.0 ± 1.1	1.62
Mut 6-1	27.1 ± 0.8	28.9 ± 0.3	0.19 ± 0.01	148.6	28.5 ± 0.2	29.8 ± 0.4	0.22 ± 0.01	138.0	17.7 ± 0.35	27.4± 0.5	13.5 ± 0.5	2.04

Table S4. List of Strains and Plasmids

Strain/plasmids	Genotype	Reference
Strain		
E. coli Bl21^{star}(DE3)	B F$^{–}$ *ompT gal dcm lon hsdS$_B$*($r_B^- m_B^-$) *rne131* (DE3)	Invitrogen
E. coli TOP10	F– *mcr*A cr*mrr-hsd*RMS-*mcr*BC) Φ80*lac*Zac80 Δ*lac*X74 *rec*A1 *ara*D139 Δ(*ara leu*) 7697 *gal*U *gal*K *rps*L (StrR) *end*A1 *nup*G	Invitrogen
Plasmid		
pET-ci-co*6pgdh*	codon optimized *Tm6pgdh*	[72]
pET28a-P$_{tac}$-*6pgdh*	dual promoter (P$_{T7}$ and P$_{tac}$) and *Moth6pgdh*	[73]
pET28a-P$_{tac}$-*tm6pgdh*	dual promoter (P$_{T7}$ and P$_{tac}$) and *Tm6pgdh*	This study
pET20b-*Gsdi*	*Gsdi*	[74]
pET20b-*Tmdi*	*Tmdi*	This study
pET20b-*Pfunror*	*Pfunror*	This study

Table S5. All Oligonucleotides Are Listed from 5' to 3' End

Primers	Sequence (5'→3')
Tm_6PG_F	CTTTAAGAAGGAGATATACATATGAAATCTCATATTGGTCTCATCGGTC
Tm_6PG_R	GTGGTGGTGGTGGTGGTGCTCGAGTCCTATCTCTCCTTCCTCCCAG
Tm_6PGvect_F	GACCGATGAGACCAATATGAGATTTCATATGTATATCTCCTTCTTAAAG
Tm_6PGvect_R	CTGGGAGGAAGGAGAGATAGGACTCGAGCACCACCACCACCACCAC
11,12_F	TGGTCTCATCGGTCTG**NNKNNK**ATGGGTCAGAATCTGGCGCTGAATATT
11,12_R	CAGACCGATGAGACCAATATGAGATTTCAT
32,3,34_F	TAAAGTGAGCGTGTAT**NNKATTATT**GCCCAGCGTACAGAAGAATTCGT
32,33,34_R	ATACACGCTCACTTTATAGCCTTTACGGGCAATATTCAG
81,82,86_F	GGTAAACCTGTTGAC**NNKNNK**ATTAGT**NNK**CTGCTGCCACATCTGGAGCCTG
81,82,86_R	GTCAACAGGTTTACCGGCTTTCACCATCAGGATGATTTTACGAG
Pfu_NROR_F	CTTTAAGAAGGAGATATACATATGAAGGTAGTTATTGTTGGAAACG
Pfu_NROR_R	CAGTGGTGGTGGTGGTGGTGCTCGAGGGAGTAGAAATCTAAGATCTC
Pfu_NRORvect_F	CGTTTCCAACAATAACTACCTTCATATGTATATCTCCTTCTTAAAG
Pfu_NRORvect_R	GAGATCTTAGATTTCTACTCCCTCGAGCACCACCACCACCACCACTG
Tm_DI_F	CTTTAAGAAGGAGATATACATGTGAAAGTAGTGATCGTTGGAAAC
Tm_DI_R	CAGTGGTGGTGGTGGTGGTGCTCGAGTCGCGTGCTTCTTAGTCTTTCC
Tm_DIvect_F	GTTTCCAACGATCACTACTTTCACATGTATATCTCCTTCTTAAAG
Tm_DIvect_R	GGAAAGACTAAGAAGCACGCGACTCGAGCACCACCACCACCACCACTG

The mutation sites of saturation mutagenesis were marked as bold

Table S6. Enzyme loadings for hydrogen production

Enzyme	Abbrev.	E.C. #	Source	Purification	Spc. Act at 60ºC (U/mg)	Mass loading (mg/mL)	Units (U/mL)	Reference
6-phosphogluconate dehydrogenase	*Tm*6PGDH	1.1.1.44	*T. maritima*	His/NTA	0.6 (17.7)[a]	55.6	0.03 (0.98)	This study
Diaphorase	*Gs*DI	1.6.99.3	*G. stearothermophilus*	His/NTA	2.9	333	1	This study
[NiFe]-hydrogenase SH1	SH1	1.12.1.3	*P. furiosus*	His/NTA	6.8[b]	147	1	[9]

a, specific activities of wild-type *Tm*6PGDH and Mut 6-1 on 20 mM NMN^+ at 60ºC were shown in regular form and parentheses, respectively. b, the specific activity of H_2ase at 60ºC was anticipated by using its activity at 50ºC (3.4U/mg) and Q10 rule.

References

1 Flores, H. & Ellington, A. D. A modified consensus approach to mutagenesis inverts the cofactor specificity of *Bacillus stearothermophilus* lactate dehydrogenase. *Protein. Eng. Des. Sel.* **18**, 369-377 (2005).

2 Sicsic, S., Durand, P., Langrene, S. & Le Goffic, F. Activity of NMN^+, nicotinamide ribose and analogs in alcohol oxidation promoted by horse-liver alcohol dehydrogenase. Improvement of this activity and structural requirements of the pyridine nucleotide part of the NAD^+ coenzyme. *Eur. J. Biochem.* **155**, 403-407 (1986).

3 Green, R. W. & McKay, R. H. The behavior of horse liver alcohol dehydrogenase in guanidine hydrochloride solutions. *J. Biol. Chem.* **244**, 5034-5043 (1969).

4 Eklund, H. *et al.* The structure of horse liver alcohol dehydrogenase. *FEBS Lett.* **44**, 200-204 (1974).

5 Campbell, E., Meredith, M., Minteer, S. D. & Banta, S. Enzymatic biofuel cells utilizing a biomimetic cofactor. *Chem. Commun.* **48**, 1898-1900 (2012).

6 PUEYO, J. J., GOMEZ-MORENO, C. & Mayhew, S. G. Oxidation-reduction potentials of ferredoxin-$NADP^+$ reductase and flavodoxin from *Anabaena* PCC 7119 and their electrostatic and covalent complexes. *FEBS J.* **202**, 1065-1071 (1991).

7 Bird, C. & Kuhn, A. Electrochemistry of the viologens. *Chem. Soc. Rev.* **10**, 49-82 (1981).

8 Bus, J. S., Aust, S. D. & Gibson, J. E. Superoxide- and singlet oxygen-catalyzed lipid peroxidation as a possible mechanism for paraquat (methyl viologen) toxicity. *Biochem. Biophys. Res. Commun.* **58**, 749-755 (1974).

9 Kim, E. J., Wu, C. H., Adams, M. W. & Zhang, Y.-H. P. Exceptionally high rates of biological hydrogen production by biomimetic *in vitro* synthetic enzymatic pathways. *Chem. Eur. J.* **22**, 16047-16051., doi:10.1002/chem.201604197 (2016).

10 Lin, Q., Li, Q., Batchelor-McAuley, C. & Compton, R. G. Methyl viologen mediated oxygen reduction in ethanol solvent: the electrocatalytic reactivity of the radical cation. *J. Electrochem. Soc.* **4**, 71-80 (2013).

11 Jones, R. W. & Garland, P. B. Sites and specificity of the reaction of bipyridylium compounds with anaerobic respiratory enzymes of *Escherichia coli*. Effects of permeability barriers imposed by the cytoplasmic membrane. *Biochem. J.* **164**, 199-211 (1977).

12 Mills, A., McFarlane, M. & Schneider, S. A viologen-based UV indicator and dosimeter. *Anal. Bioanal. Chem.* **386**, 299-305, doi:10.1007/s00216-006-0605-0 (2006).

13 Lewinsohn, E. & Gressel, J. Benzyl viologen-mediated counteraction of diquat and paraquat phytotoxicities. *Plant Physiol.* **76**, 125-130 (1984).

14 Ausländer, W. & Junge, W. Neutral red, a rapid indicator for pH-changes in the inner phase of thylakoids. *FEBS Lett.* **59**, 310-315 (1975).

15 Park, D. H. & Zeikus, J. G. Electricity generation in microbial fuel cells using neutral red as an electronophore. *Appl. Environ. Microbiol.* **66**, 1292-1297 (2000).

16 V, T. F. & T, S. C. New approach to biosensing of co-enzyme nicotinamide adenine dinucleotide (NADH) by incorporation of neutral red in aluminum doped nanostructured ZnO thin films. *Biochim. Biophys. Acta.*, doi:10.1016/j.bbagen.2017.01.001 (2017).

17 Park, D. H. & Zeikus, J. G. Utilization of electrically reduced neutral red by *Actinobacillus succinogenes*: physiological function of neutral red in membrane-driven fumarate reduction and energy conservation. *J. Bacteriol.* **181**, 2403-2410 (1999).

18 Rish, K. R., Swartzlander, R., Sadikot, T. N., Berridge, M. V. & Smith, A. Interaction of heme and heme-hemopexin with an extracellular oxidant system used to measure cell growth-associated plasma membrane electron transport. *Biochim. Biophys. Acta.* **1767**, 1107-1117, doi:10.1016/j.bbabio.2007.06.003 (2007).

19 Zhu, A., Romero, R. & Petty, H. R. An enzymatic colorimetric assay for glucose-6-phosphate. *Anal. Biochem.* **419**, 266-270, doi:10.1016/j.ab.2011.08.037 (2011).

20 Berridge, M. V., Herst, P. M. & Tan, A. S. Tetrazolium dyes as tools in cell biology: new insights into their cellular reduction. *Biotechnol. Annu. Rev.* **11**, 127-152, doi:10.1016/s1387-2656(05)11004-7 (2005).

21 Rao, P. S. & Hayon, E. Experimental determination of the redox potential of the superoxide radical O_2. *Biochem. Biophys. Res. Commun.* **51**, 468-473 (1973).

22 Sutherland, M. W. & Learmonth, B. A. The tetrazolium dyes MTS and XTT provide new quantitative assays for superoxide and superoxide dismutase. *Free Radic. Res.* **27**, 283-289 (1997).

23 Johnson, S. M., Doherty, S. J. & Croy, R. R. Biphasic superoxide generation in potato tubers. A self-amplifying response to stress. *Plant Physiol.* **131**, 1440-1449, doi:10.1104/pp.013300 (2003).

24 Lechpammer, S. *et al.* Development of an XTT tetrazolium salt-based assay for detection of specific

hyperthermia sensitizers in a high-flux screening programme. *Int. J. Hyperthermia.* **18**, 203-215 (2002).
25 Bielski, B. H., Cabelli, D. E., Arudi, R. L. & Ross, A. B. Reactivity of HO_2/O_2^- radicals in aqueous solution. *J. Phys. Chem. Ref. Data* **14**, 1041-1100 (1985).
26 Miller, R. W. & Kerr, C. T. Dihydroorotate dehydrogenase. 3. Interactions with substrates, inhibitors, artificial electron acceptors, and cytochrome c. *J. Biol. Chem.* **241**, 5597-5604 (1966).
27 Barron, E. G. The rate of autoxidation of oxidation-reduction systems and its relation to their free energy. *J. Biol. Chem.* **97**, 287-302 (1932).
28 Pricelius, S. *et al.* Enzymatic reduction of azo and indigoid compounds. *Appl. Microbiol. Biotechnol.* **77**, 321-327, doi:10.1007/s00253-007-1165-8 (2007).
29 Sousa, M. M. *et al.* A photochemical study on the blue dye indigo: from solution to ancient Andean textiles. *Photochem. Photobiol. Sci.* **7**, 1353-1359 (2008).
30 Tedeschi, G., Chen, S. & Massey, V. DT-diaphorase. Redox potential, steady-state, and rapid reaction studies. *J. Biol. Chem.* **270**, 1198-1204 (1995).
31 Cohn, D. J. & Levinson, A. Indigo carmine for the quantitative determination of glucose in cerebrospinal fluid. *J. Pediatr.* **8**, 20IN123-122 (1936).
32 Ramesh, T. N., Kirana, D. V., Ashwini, A. & Manasa, T. Calcium hydroxide as low cost adsorbent for the effective removal of indigo carmine dye in water. *J. Saudi Chem. Soc.* **21**, 165-171 (2015).
33 Fletcher, J. & Wilson, M. The effect of methylene blue, a redox agent, on the viability of *Fusobacterium nucleatum*. *Microbios* **80**, 181-188 (1994).
34 Buchholz, K. *et al.* Interactions of methylene blue with human disulfide reductases and their orthologues from *Plasmodium falciparum*. *Antimicrob. Agents Chemother.* **52**, 183-191 (2008).
35 Sevcik, P. & Dunford, H. B. Kinetics of the oxidation of NADH by methylene blue in a closed system. *J. Phys. Chem.* **95**, 2411-2415 (1991).
36 Zaugg, W. S. Spectroscopic characteristics and some chemical properties of N-methylphenazinium methyl sulfate (phenazine methosulfate) and pyocyanine at the semiquinoid oxidation level. *J. Biol. Chem.* **239**, 3964-3970 (1964).
37 Rotsaert, F. A., Covian, R. & Trumpower, B. L. Mutations in cytochrome b that affect kinetics of the electron transfer reactions at center N in the yeast cytochrome bc 1 complex. *Biochim. Biophys. Acta.* **1777**, 239-249 (2008).
38 Nishikimi, M., Appaji, N. & Yagi, K. The occurrence of superoxide anion in the reaction of reduced phenazine methosulfate and molecular oxygen. *Biochem. Biophys. Res. Commun.* **46**, 849-854 (1972).
39 Butcher, R. G. Oxygen and the production of formazan from neotetrazolium chloride. *Histochemistry* **56**, 329-340 (1978).
40 Cabello, C. M., Bair, W. B., 3rd, Bause, A. S. & Wondrak, G. T. Antimelanoma activity of the redox dye DCPIP (2,6-dichlorophenolindophenol) is antagonized by NQO1. *Biochem. Pharmacol.* **78**, 344-354, doi:10.1016/j.bcp.2009.04.016 (2009).
41 Smith, M. D. & Olson, C. L. Differential amperometric determination of alcohol in blood or urine using alcohol dehydrogenase. *Anal. Chem.* **47**, 1074-1077 (1975).
42 Dupuy, C. *et al.* Nonenzymatic NADPH-dependent reduction of 2,6-dichlorophenol-indophenol. *Anal. Biochem.* **191**, 16-20 (1990).
43 Eröss, K., Svehla, G. & Erdey, L. The use of 2, 6-dichlorophenolindophenol as indicator in acid-base titrations. *Anal. Chim. Acta.* **31**, 246-250 (1964).
44 Vanýsek, P. *In CRC Handbook of Chemistry and Physics, 87th edition*. (CRC press Boca Raton, FL, 2006).
45 Mandai, T., Fujiwara, S. & Imaoka, S. A novel electron transport system for thermostable CYP175A1 from *Thermus thermophilus* HB27. *FEBS J.* **276**, 2416-2429 (2009).
46 Richardson, M. R. & Bryson, A. A critical examination of the ferrocyanide determination of zinc. *Analyst* **78**, 291-299 (1953).
47 O'Brien, J., Wilson, I., Orton, T. & Pognan, F. Investigation of the Alamar Blue (resazurin) fluorescent dye for the assessment of mammalian cell cytotoxicity. *Eur. J. Biochem.* **267**, 5421-5426 (2000).
48 Rampersad, S. N. Multiple applications of Alamar Blue as an indicator of metabolic function and cellular health in cell viability bioassays. *Sensors* **12**, 12347-12360 (2012).
49 Goegan, P., Johnson, G. & Vincent, R. Effects of serum protein and colloid on the alamarBlue assay in cell cultures. *Toxicol. In vitro* **9**, 257-266 (1995).
50 Klotz, A. V., Stegeman, J. J. & Walsh, C. An alternative 7-ethoxyresorufin O-deethylase activity assay: a continuous visible spectrophotometric method for measurement of cytochrome P-450 monooxygenase activity. *Anal. Biochem.* **140**, 138-145 (1984).

51 Candeias, L. *et al.* The catalysed NADH reduction of resazurin to resorufin. *J. Chem. Soc. Perkin Trans. 2*, 2333-2334 (1998).
52 Shin, N. *et al.* Development of an Azoreductase-based Reporter System with Synthetic Fluorogenic Substrates. *ACS Chem. Biol.* **12**, 558-563, doi:10.1021/acschembio.6b00852 (2017).
53 Piao, W. *et al.* Development of azo-based fluorescent probes to detect different levels of hypoxia. *Angew. Chem. Int. Ed. Engl.* **52**, 13028-13032, doi:10.1002/anie.201305784 (2013).
54 Oturkar, C. C., Othman, M. A., Kulkarni, M., Madamwar, D. & Gawai, K. R. Synergistic action of flavin containing NADH dependant azoreductase and cytochrome P450 monooxygenase in azoaromatic mineralization. *RSC Adv.* **3**, 3062-3070 (2013).
55 Shoji, O. *et al.* Aromatic C-H bond hydroxylation by P450 peroxygenases: a facile colorimetric assay for monooxygenation activities of enzymes based on Russig's blue formation. *J. Biol. Inorg. Chem.* **15**, 1109-1115, doi:10.1007/s00775-010-0671-9 (2010).
56 Meyer, A. *et al.* Changing the substrate reactivity of 2-hydroxybiphenyl 3-monooxygenase from *Pseudomonas azelaica HBP1* by directed evolution. *J. Biol. Chem.* **277**, 5575-5582, doi:10.1074/jbc.M110018200 (2002).
57 Roberts, G. A. *et al.* A self-sufficient cytochrome P450 with a primary structural organization that includes a flavin domain and a [2Fe-2S] redox center. *J. Biol. Chem.* **278**, 48914-48920 (2003).
58 Celik, A., Speight, R. E. & Turner, N. J. Identification of broad specificity P450CAM variants by primary screening against indole as substrate. *Chem. Commun. (Camb).* 3652-3654, doi:10.1039/b506156c (2005).
59 Kadkhodayan, S., Coulter, E. D., Maryniak, D. M., Bryson, T. A. & Dawson, J. H. Uncoupling oxygen transfer and electron transfer in the oxygenation of camphor analogues by cytochrome P450-CAM. Direct observation of an intermolecular isotope effect for substrate C-H activation. *J. Biol. Chem.* **270**, 28042-28048 (1995).
60 Mouri, T., Kamiya, N. & Goto, M. New strategy to enhance catalytic performance of *Escherichia coli* whole cell biocatalysts harboring P450cam mutants. *Biochem. Eng. J.* **53**, 229-233 (2011).
61 Alcalde, M., Farinas, E. T. & Arnold, F. H. Colorimetric high-throughput assay for alkene epoxidation catalyzed by cytochrome P450 BM-3 variant 139-3. *J. Biomol. Screen.* **9**, 141-146 (2004).
62 Bessey, O. A. & Love, R. H. Preparation and measurement of the purity of the phosphatase reagent, disodium p-nitrophenyl phosphate. *J. Biol. Chem.* **196**, 175-178 (1952).
63 Farinas, E. T., Schwaneberg, U., Glieder, A. & Arnold, F. H. Directed evolution of a cytochrome P450 monooxygenase for alkane oxidation. *Adv. Synth. Catal.* **343**, 601-606 (2001).
64 Ramachandran, L. Protein-iodine interaction. *Chem. Rev.* **56**, 199-218 (1956).
65 Hogg, D. M. & Jago, G. The oxidation of reduced nicotinamide nucleotides by hydrogen peroxide in the presence of lactoperoxidase and thiocyanate, iodide or bromide. *Biochem. J.* **117**, 791-797 (1970).
66 Hopwood, D. Fixation of proteins by osmium tetroxide potassium dichromate and potassium permanganate. *Histochemie* **18**, 250-260 (1969).
67 Kahl, B. F. & Paule, M. R. The use of diethyl pyrocarbonate and potassium permanganate as probes for strand separation and structural distortions in DNA. *Methods Mol. Biol.* **543**, 73-85, doi:10.1007/978-1-60327-015-1_6 (2009).
68 Kumar, N. V. & Varshney, U. Contrasting effects of single stranded DNA binding protein on the activity of uracil DNA glycosylase from Escherichia coli towards different DNA substrates. *Nucleic Acids Res.* **25**, 2336-2343 (1997).
69 Kalbus, G. E., Lieu, V. T. & Kalbus, L. H. A Spectrophotometric Study of the Permanganate–Oxalate Reaction: An Analytical Laboratory Experiment. *J. Chem. Educ.* **81**, 100 (2004).
70 Mattagajasingh, S. N., Misra, B. R. & Misra, H. P. Carcinogenic chromium(VI)-induced protein oxidation and lipid peroxidation: implications in DNA-protein crosslinking. *J. Appl. Toxicol.* **28**, 987-997, doi:10.1002/jat.1364 (2008).
71 Wiberg, K. B. & Mill, T. The kinetics of the chromic acid oxidation of benzaldehyde. *J. Am. Chem. Soc.* **80**, 3022-3029 (1958).
72 Wang, Y. & Zhang, Y. P. Overexpression and simple purification of the *Thermotoga maritima* 6-phosphogluconate dehydrogenase in *Escherichia coli* and its application for NADPH regeneration. *Microb. Cell Fact.* **8**, 30 (2009).
73 Huang, R., Chen, H., Zhong, C., Kim, J. E. & Zhang, Y.-H. P. High-throughput screening of coenzyme preference change of thermophilic 6-phosphogluconate dehydrogenase from $NADP^+$ to NAD^+. *Sci. Rep.* **6**, 32644., doi:10.1038/srep32644 (2016).
74 Zhu, Z., Tam, T. K., Sun, F., You, C. & Zhang, Y.-H. P. A high-energy-density sugar biobattery based on a

synthetic enzymatic pathway. *Nat. Commun.* **5**, 3026., doi:10.1038/ncomms4026 (2014).